FORM UPR16

Research Ethics Review Checklist

Please include this completed form as an appendix to your thesis (see the Research Degrees Operational Handbook for more information

UNIVERSITY OF PORTSMOUTH

Postgraduate Research Student (PGRS) Information			**Student ID:**	802166
PGRS Name:	Abdulrahman Ali Alsolami			
Department:	SCHOOL OF MATHEMATICS AND PHYSICS	**First Supervisor:**	Dr . James Burridge	
Start Date: (or progression date for Prof Doc students)	1/2/2016			
Study Mode and Route:	Part-time ☐	MPhil ☐	MD ☐	
	Full-time ☑	PhD ☑	Professional Doctorate ☐	

Title of Thesis:	Spatial effects in random walks
Thesis Word Count: (excluding ancillary data)	40,000

If you are unsure about any of the following, please contact the local representative on your Faculty Ethics Committee for advice. Please note that it is your responsibility to follow the University's Ethics Policy and any relevant University, academic or professional guidelines in the conduct of your study

Although the Ethics Committee may have given your study a favourable opinion, the final responsibility for the ethical conduct of this work lies with the researcher(s).

UKRIO Finished Research Checklist:
(If you would like to know more about the checklist, please see your Faculty or Departmental Ethics Committee rep or see the online version of the full checklist at: http://www.ukrio.org/what-we-do/code-of-practice-for-research/)

a)	Have all of your research and findings been reported accurately, honestly and within a reasonable time frame?	YES ☑ NO ☐
b)	Have all contributions to knowledge been acknowledged?	YES ☑ NO ☐
c)	Have you complied with all agreements relating to intellectual property, publication and authorship?	YES ☑ NO ☐
d)	Has your research data been retained in a secure and accessible form and will it remain so for the required duration?	YES ☑ NO ☐
e)	Does your research comply with all legal, ethical, and contractual requirements?	YES ☑ NO ☐

Candidate Statement:

I have considered the ethical dimensions of the above named research project, and have successfully obtained the necessary ethical approval(s)

Ethical review number(s) from Faculty Ethics Committee (or from NRES/SCREC):	

If you have *not* submitted your work for ethical review, and/or you have answered 'No' to one or more of questions a) to e), please explain below why this is so:

Signed *(PGRS)*:		**Date:** 1/8/2020

UNIVERSITY OF PORTSMOUTH

Spatial effects in random walks

ABDULRAHMAN ALI ALSOLAMI

A thesis presented for the degree of

Doctor of Philosophy

SCHOOL OF MATHEMATICS AND PHYSICS

University of Portsmouth

United Kingdom

31 January 2020

Abstract

In this thesis we investigate spatial effects in random walks by applying techniques from statistical physics. We first study a chase-capture model on a rectangular $L_1 \times L_2$ lattice with n hiding places. We derive an exact formula calculate the prey survival probability. We investigate the effects of the shape of the home range or the natural habitat of the prey (the lattice) on the prey survival probability and explore the optimal arrangement of hiding places. We show that the shape of home range does not have an effect on the prey survival probability unless the ratio L_2/L_1 (the width to the length of the home range) less than $\frac{1}{n}$. We give an approximation of the optimal arrangements of three, four and five holes inside different shapes of home range. We then investigate the average shape of the spatial memory of a foraging animal. The spatial memory is obtained by evaluating a two-dimensional Brownian motion at the arrival times of a non-homogeneous Poisson process. We obtain an analytic formula that measures how spherical this spatial memory is. We verify our analytic result by simulation, and show that a slower decaying memory leads to a more spherical shape. We then extend our work to the case where the walker repeatedly returns to a particular place. Rather thinking in the terms of memory, we consider the path to be tracked by an independent party at a time varying rate called the "tracking strategy". We derive an analytic expression which gives us the average size and elongation of the tracked Brownian bridge. We confirm our exact result by simulation and we give examples of different tracking strategies.

Dedication

To every member of my family, who has been my source of inspiration and strength to finish this thesis.

Declaration

Whilst registered as a candidate for the above degree, I have not been registered for any other research degree award. The results and conclusions embodied in this thesis are the work of the named candidate and have not been submitted for any other academic award.

Abdulrahman Alsolami

March 2020

Acknowledgements

First, I would like to express my deep thanks and appreciation to my supervisors Dr. James Burridge and Dr. Michał Gnacik for their support, knowledge, guidance and encouragement. Without your support and constant guidance this work would not have been achievable and I consider myself incredibly lucky to have worked with you both.

I am indebted to my parents, brothers and sisters for support and prayers that they have provided me during my studies. My heartfelt thanks are due to my wife, Rasha, for her prayers, encouragement and everything she has done to make this work possible.

Finally, I would like to thank the Department of Mathematics at King Abdulaziz University for their financial support.

Contents

List of Figures

List of Tables

Introduction

In this thesis we use techniques from statistical physics such as random walk, gyration tensor and some ideas from polymer physics to study spatial effects in random walks. We begin by studying the survival probability of a prey pursued by a predator on a two dimensional lattice in presence of hiding places. The predator always moves toward the prey whereas the prey preforms a simple random walk and heads towards the closest hiding place when the predator appears in its sighting range. The prey survives by reaching the hiding place before it is eaten. The prey is eaten when the predator jumps to the position occupied by the prey. The work done in this chapter is inspired by [2, 3]. The ecological study [3] found that hiding places created by prey animals were clustered within a distance about 25 meters and then regularly distributed at distances more than 40 meters. We used our model to study the effect of the shape of the home range (the natural habitat of the prey) on the prey survival probability, and then we investigate and quantify the advantages from regular holes arrangements.

Over the past few decades, there is considerable interest among scientists in studying the animal cognition [4, 5, 6, 7]. Primates have the mental abilities to know where [8, 9] and when [10] to look for food resources. An experimental study [11] examined the navigation efficiency of wild chimpanzees found that they possess detailed Euclidean maps which allow them to navigate between food sources efficiently. In the second part of the thesis, we study the shape of mental or Cognitive map [12, 13] of a foraging animal (the spatial area recalled by the forager). The path of a foraging animal, perhaps looking for food, is viewed as a two dimensional

random walk. While the forager is exploring its surroundings, a mental map is being formed. We model mental maps as the locations of a standard two-dimensional Brownian motion (a continuous random motion start from the origin) at the arrival times of a non-homogeneous Poisson process (a continuous random process we used here to model the observations occurred in a time-varying rate) with intensity function $c\mu(t)$, where c is a positive constant and $\mu(t)$ is a non-increasing density function of a continuous probability distribution which characterizes how the density of memory locations varies with time. We view $\mu(t)$ as measuring the typical amount of information retained from time t in the past. For this reason we refer to μ as the memory kernel. We investigate the relation between the way which the forager recalls information and the shape of the mental map. We derive an exact analytic formula linking the shape of spatial memory to the rate of memory decay [14]. We confirm our exact result by simulation and show that if a chosen memory kernel decays slower over time (that is, has a heavy tail when treated as a probability density function) then the corresponding mental map (modeled by the paths of our memorised random walk) is less elongated.

We extend our work to the case where the walker repeatedly returns to a certain location by modelling its trajectory as a Brownian bridge (a continuous-time stochastic process conditioned to start and terminate in the same location). Rather than thinking in terms of memory (memory locations are stored by the walker), we now consider the path to be "tracked" (by an independent party) at a time varying rate. We model the tracked path by evaluating a two-dimensional standard Brownian bridge at the arrival times of a non-homogeneous Poisson point process with intensity function $c\mu(t)$, where $c > 0$ and the function $\mu(t)$ is called the "tracking strategy"(characterize how the density of tracking points change with time), and is taken to be a probability density function supported on $[0, 1]$. We derive an exact formula relating the tracking strategy to the average shape of the tracked path. We verified our exact result by simulation and explore the influence of the number of the tracked locations on the average shape of the tracked path. We exploit exam-

ples of tracking strategies that lead to the 'tracked' walks having various aspherical shapes (we use the asphericity coefficient, that takes values in [0, 1], to measure the elongation ; close to zero meaning spherical and close to one meaning extremely elongated).

The function $\mu(t)$ in chapter 3 and chapter 4 may have other interpretations than memory kernel (as in chapter 3) and tracking strategy (as in chapter 4). For instance it may used for modelling the decay rates of scent [15] or the decay of disease particles [16, 17] left behind a forager (human or animal) in the environment. Consider a large group of foragers and suppose that some of the population are infected with an infectious disease such as norovirus [16] and respiratory infections such as influenza [17]. The infected foragers leave traces of disease particles in the environment while they move. If these traces decrease with time, then the density of active disease particles left behind the infected foragers will be higher in areas that visited more lately. Our results in chapter 3 and 4 allow us to analytically calculate, in terms of μ, the average size and shape (radius of gyration and asphericity) of the contaminated area. Predicting the average sizes and shapes of areas tainted by infected individuals may be beneficial for quantitatively understanding and controlling the spread of infectious diseases.

Chapter 1

Preliminaries

In this chapter, we introduce a brief background of stochastic processes that we use in the rest of the thesis. The first section covers the basic definitions and theorems for discrete-time Markov processes, whereas the second section covers the case of continuous-time stochastic processes and Itô's calculus.

1.1 Notation and conventions

- The set of the natural numbers, that is, the set of all positive integers is denoted by $\mathbb{N}$.
- The set of non-negative integers is denoted by $\mathbb{N}_0 = \mathbb{N} \cup \{0\}$.
- The notation $[P]_{ij}$ stands for the entry in i-th row and j-th column of matrix P.
- We will often denote the vectors in $\mathbb{R}^n$ as $\vec{x} = (x_1, x_2, ..., x_n)$; the arrows emphasis that we deal with vectors.

1.2 Discrete-time Markov chains

In this section we provide some basic definitions and properties of discrete-Markov chains with some examples. For an elaborate exposition of the theory of Markov

chains we refer the reader to [18, 19].

Definition 1.2.1. *A collection of random variables $\{X_n\}_{n\in\mathbb{N}}$, where X_n takes values in a countable set S is a discrete-time Markov chain (or has the Markov property) if*

$$\mathbb{P}(X_n = i_n | X_0 = i_0, X_1 = i_1, ..., X_{n-1} = i_{n-1}) = \mathbb{P}(X_n = i_n | X_{n-1} = i_{n-1}),$$

for any $n \in \mathbb{N}$ and $i_n \in S$.

The set S is called the state space and it consists all the possible states of the chain. A process is called a finite Markov chain if the state space S is finite. The notation

$$p_{ij} = \mathbb{P}(X_n = j | X_{n-1} = i) \qquad \text{for } n \in \mathbb{N} \tag{1.1}$$

represent a transition probability from state i to state j in one-step. If the transition probabilities do not depend on time, that is,

$$\mathbb{P}(X_n = j | X_{n-1} = i) = \mathbb{P}(X_1 = j | X_0 = i) \tag{1.2}$$

for all $n \in \mathbb{N}$, then the processes is called a time-homogeneous Markov chain. A time-homogeneous Markov chain can be represented by a matrix P called the transition matrix that is given by

$$P = [p_{ij}]_{i,j\in S}. \tag{1.3}$$

The transition matrix has to satisfy certain conditions given in the following definition.

Definition 1.2.2. *A transition matrix P is a square matrix that satisfies the following conditions:*

- $0 \leq p_{ij} \leq 1$ *for all* $i, j \in S$,
- $\sum_{j\in S} p_{ij} = 1$ *for all* $i \in S$.

A matrix that satisfies the two conditions in Definition 1.2.2 is called a stochastic matrix.

Definition 1.2.3. *Let $n \in \mathbb{N}$. The n-step transition probability is the probability of transitioning from one state to another in n-steps, that is,*

$$p_{ij}^{(n)} = \mathbb{P}(X_n = j | X_0 = i) \quad \text{for some } i, j \in S. \tag{1.4}$$

Theorem 1.2.1 (Chapman-Kolmogorov equation)**.** *For $i, j \in S$ and $m, n \in \mathbb{N}_0$, we have*

$$p_{ij}^{(n+m)} = \sum_{k \in S} p_{ik}^{(n)} p_{kj}^{(m)}. \tag{1.5}$$

Proof. For the proof please see [18] page 209.

Corollary 1.2.1. *If P is the transition matrix of a Markov chain, then*

$$p_{ij}^{(n)} = [P^n]_{ij} \quad \text{for all } i, j \in S. \tag{1.6}$$

Proof. The proof is by mathematical induction. For $n = 1$ the statement is true by (1.1) and (1.3), that is,

$$p_{ij} = [P]_{ij}. \tag{1.7}$$

For $n > 1$, we apply Theorem 1.2.1 so that

$$p_{ij}^{(n)} = \sum_{k \in S} p_{ik}^{(n-1)} p_{kj} \tag{1.8}$$

$$= [P^{n-1} P]_{ij} = [P^n]_{ij}. \tag{1.9}$$

□

Definition 1.2.4 (Initial Distribution)**.** *The initial probability distribution $\vec{\phi} = (\phi_i)_{i \in S}$ of a Markov chain with state space S satisfies the following conditions*

- $0 \leq \phi_i \leq 1$ *for all* $i \in S$
- $\sum_{i \in S} \phi_i = 1$.

The entry ϕ_i gives the probability that the chain starts in state i, that is,

$$\phi_i = \mathbb{P}(X_0 = i).$$

Corollary 1.2.2. *If P is the transition matrix and $\vec{\phi}$ is the initial distribution of a Markov chain, then the n-step distribution of the chain is $\vec{\phi}P^n$, that is,*

$$\mathbb{P}(X_n = j) = \sum_{i \in S} \phi_i (P^n)_{ij} = (\vec{\phi}P^n)_j, \tag{1.10}$$

where $(\vec{\phi}P^n)_j$ is the j-th entry of the vector $\vec{\phi}P^n$.

Proof. For the proof we refer the reader to [20] page 216.

Example 1.2.1. *Consider the Markov chain with three state as shown in figure 1.1.*

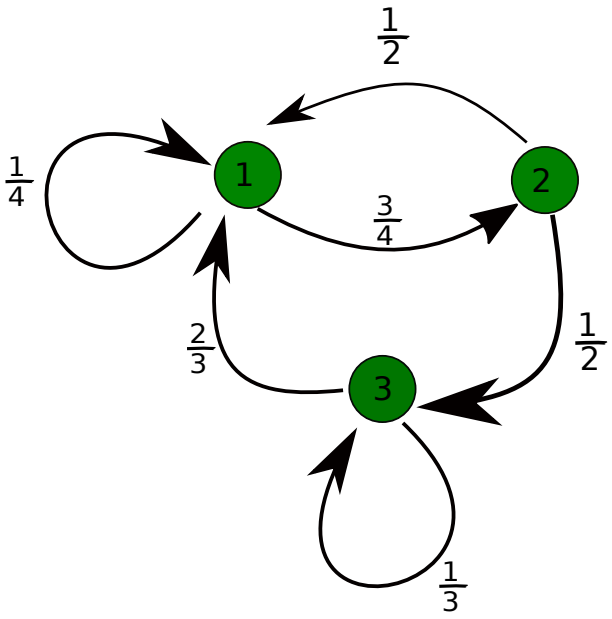

Figure 1.1: Three state transition diagram.

The transition matrix of the chain in figure 1.1 is

$$P = \begin{bmatrix} \frac{1}{4} & \frac{3}{4} & 0 \\ \frac{1}{2} & 0 & \frac{1}{2} \\ \frac{2}{3} & 0 & \frac{1}{3} \end{bmatrix}. \tag{1.11}$$

The transition matrix of the chain after 4-steps is given by

$$P^4 = \begin{bmatrix} 0.423177 & 0.339844 & 0.236979 \\ 0.437211 & 0.309896 & 0.252894 \\ 0.442515 & 0.315972 & 0.241512 \end{bmatrix}, \tag{1.12}$$

and probability that the chain is in state 3 after 4-steps starting from state 2 is obtained from the 2nd row and 3rd column of the matrix P^4, that is ,

$$\mathbb{P}(X_4 = 3|X_0 = 2) = 0.252894.$$

For initial distribution $\vec{\phi} = (0.2, 0.5, 0.3)$, the probability distribution of the chain after 10-steps is

$$\vec{\phi}P^{10} = \begin{pmatrix} 0.432439 & 0.324319 & 0.243241 \end{pmatrix}, \tag{1.13}$$

and the probability that the chain ends in state 1 after 10-steps is 0.432439.

1.2.1 Markov chain's long-run behaviour

One may ask what is the long-term behaviour of a Markov chain? Or does the chain converge to particular distribution after very large number of steps? To demonstrate that let us consider the following transition matrix for two states Markov chain

$$P = \begin{bmatrix} 0.3 & 0.7 \\ 0.8 & 0.2 \end{bmatrix}. \tag{1.14}$$

After large number of steps, we take the limit as $n \to \infty$, and obtain

$$\lim_{n\to\infty} P^n = \begin{bmatrix} 0.533333 & 0.466667 \\ 0.533333 & 0.466667 \end{bmatrix} = \begin{bmatrix} \vec{\pi} \\ \vec{\pi} \end{bmatrix}. \tag{1.15}$$

The limit exists and the $n-$th power of the transition matrix P converges to a matrix with identical rows $\vec{\pi}$. In this case the vector $\vec{\pi}$ is called the steady state distribution of the chain. Once the chain has reached the steady state distribution will stay there forever. For the transition matrix given in (1.14) and with any initial probability distribution $\vec{\phi} = (\phi_1, \phi_2)$, we can obtain the steady state distribution by taking the following limit

$$\lim_{n\to\infty} \vec{\phi} P^n = \vec{\pi}, \tag{1.16}$$

where $\vec{\pi} = (0.533333, 0.466667)$.

Another interesting question that would arise is: does every Markov chain have steady state distribution? In order to answer this question consider the following transition matrix for another Markov chain

$$P = \begin{bmatrix} 0 & 1 \\ 1 & 0 \end{bmatrix}. \tag{1.17}$$

For the initial probability distribution $\vec{\phi} = (0, 1)$,(i.e, the chain starts from state 2 with probability 1, we have

$$\vec{\phi} P^n = \begin{cases} (0,1) & \text{if } n \text{ even} \\ (1,0) & \text{if } n \text{ odd} \end{cases} \tag{1.18}$$

In this case $\lim_{n\to\infty} \vec{\phi} P^n$ does not exist, therefore, there is no steady state distribution.

Generally, for an initial probability distribution $\vec{\phi}$, suppose $\lim_{n\to\infty} \vec{\phi} P^n$ exits, then there exists a distribution $\vec{\pi}$ such that

$$\lim_{n\to\infty} \vec{\phi} P^n = \vec{\pi}.$$

We have

$$\vec{\pi} P = \left(\lim_{n\to\infty} \vec{\phi} P^n \right) P = \lim_{n\to\infty} \vec{\phi} P^{n+1} = \vec{\pi},$$

which means that the chain will stay in the steady state distribution $\vec{\pi}$ once it reached and stay forever.

Definition 1.2.5. *A Markov chain $\{X_n\}_{n\in\mathbb{N}_0}$ has a steady-state or equilibrium distribution $\vec{\pi}$ if the limit $\vec{\pi} = \lim_{n\to\infty} \vec{\phi}P^n$ exists.*

Remark 1.2.1. *From Definition 1.2.5, we note that the steady-state distribution is given by the solution of following linear system*

$$\vec{\pi}P = \vec{\pi},$$
$$\sum_{i\in S} \pi_i = 1.$$

1.2.2 Classification of states

In this section we introduce some classifications of states and classes in discrete-time Markov chains.

1) For any two states $i, j \in S$, we say that state j is accessible from state i, written as $i \to j$, if $p_{ij}^{(n)} > 0$ for some $n \in \mathbb{N}$.

2) The two states i and j, communicate if $i \to j$ and $j \to i$. In this case we write $i \leftrightarrow j$.

3) A state $i \in S$ is said to be absorbing if $p_{ii} = 1$.

4) A state $i \in S$ is said to be recurrent if

$$\mathbb{P}(X_n = i \text{ for some } n \in \mathbb{N} | X_0 = i) = 1,$$

otherwise, it is called transient.

5) Every absorbing state is a recurrent state.

6) A set of states, A , is called a communication class if every pair of states in A communicate and none of the states in the set communicate with any state outside A.

7) A Markov chain is said to be irreducible if the chain has only one communication class, otherwise, the chain is called reducible.

8) A communication class C_1 of a Markov chain is called a recurrent class if there is no state outside C_1 accessible from any state in C_1, otherwise the class is called transient.

Example 1.2.2. *Consider the Markov chain given by the following transition matrix*

$$P = \begin{bmatrix} 0 & \frac{1}{2} & \frac{1}{2} & 0 & 0 & 0 & 0 & 0 \\ \frac{1}{2} & \frac{1}{2} & 0 & 0 & 0 & 0 & 0 & 0 \\ 0 & 0 & 0 & \frac{1}{4} & 0 & 0 & 0 & \frac{3}{4} \\ 0 & 0 & \frac{1}{3} & 0 & \frac{2}{3} & 0 & 0 & 0 \\ 0 & 0 & 0 & 0 & 0 & 1 & 0 & 0 \\ 0 & 0 & 0 & 0 & 0 & 0 & 1 & 0 \\ 0 & 0 & 0 & 0 & 0 & \frac{1}{4} & 0 & \frac{3}{4} \\ 0 & 0 & 0 & 0 & 0 & 1 & 0 & 0 \end{bmatrix} \tag{1.19}$$

As we can see in the transition diagram of the given chain in figure (1.2) the chain has 4 communication classes. The three classes $\{1, 2\}, \{3, 4\}$ and $\{5\}$ are transient. The fourth class $\{6, 7, 8\}$ is recurrent.

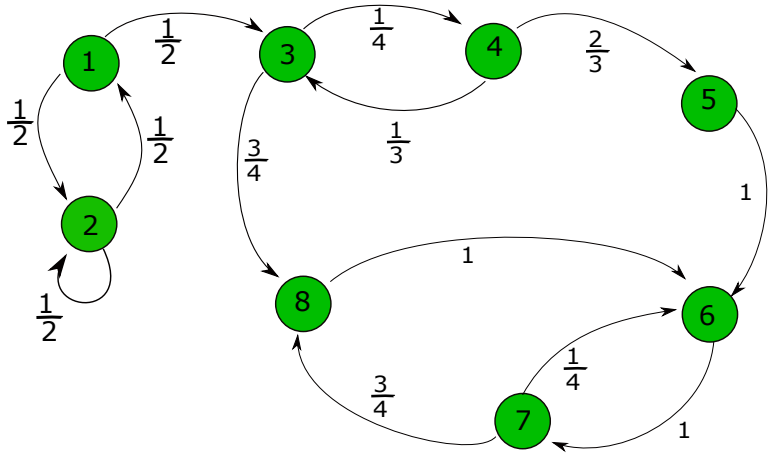

Figure 1.2: Markov chain with 8 states

1.2.3 Periodicity

Definition 1.2.6. *The period of a state $i \in S$, denoted by $d(i)$, is the greatest common divisor of the set $\{n \in \mathbb{N} : p_{ii}^{(n)} > 0\}$, that is,*

$$d(i) = GCD\{n \in \mathbb{N} : p_{ii}^{(n)} > 0\}, \tag{1.20}$$

where GCD is the greatest common divisor.

Definition 1.2.7. *If the period of a state is equal to one, then the state is called is aperiodic. Otherwise, it is called periodic.*

Theorem 1.2.2. *For any two states i and j are in the same communication class, then*

1) $d(i) = d(j)$.

2) The state i is recurrent if and only if the state j is recurrent .

Proof. For the proof please see [18] page 229.

Definition 1.2.8. *A finite Markov chain is said to be a ergodic if it is aperiodic and irreducible.*

Theorem 1.2.3. *An Ergodic Markov chain has unique steady-state distribution $\vec{\pi}$ which satisfies the equation $\vec{\pi}P = \vec{\pi}$.*

Proof. For the proof please see [21] page 139.

1.2.4 Mean hitting times

Definition 1.2.9. *For a finite Markov chain $\{X_n\}_{n\in\mathbb{N}}$ with state space $S = \{0, 1, 2, ..., m\}$, the first hitting time of $A \subset S$ is a random variable T_A which is defined by*

$$T_A = \min\{n \geq 0 | X_n \in A\}. \tag{1.21}$$

Definition 1.2.10. *The mean hitting time for the chain to reach the set A starting from the state $i \in S$ is defined by*

$$m_A(i) = \mathbb{E}[T_A | X_0 = i]. \tag{1.22}$$

When the set A is absorbing we refer to $m_A(i)$ as the mean absorption time into the set A starting from state i.

Theorem 1.2.4. *Let $i \in S$, the mean hitting time $m_A(i)$ is given by*

$$m_A(i) = \begin{cases} 0, & \text{if } i \in A \ , \\ 1 + \sum_{k \in S \setminus A} p_{ik}\, m_A(k), & \text{if } i \in S \setminus A \end{cases}$$

Proof. For the proof we refer the reader to [18] page 222.

1.2.5 Higher-order Markov chains

Definition 1.2.11. *For $k \in \mathbb{N}$, a stochastic process $\{X_n\}_{n \in \mathbb{N}}$ is called a Markov chain of order k if the future of the chain depends only on the last k states, namely,*

$$\begin{aligned} &\mathbb{P}(X_n = i_n | X_0 = i_0, X_1 = i_1, ..., X_{n-1} = i_{n-1}) \\ &\qquad = \mathbb{P}(X_n = i_n | X_{n-1} = i_{n-1}, ..., X_{n-k} = i_{n-k}), \end{aligned}$$

for any $k \leq n$ and $i_n \in S$.

Example 1.2.3. *Consider a walker placed uniformly in a two dimensional lattice $L \times L$ with periodic boundaries. Here, the absorbing state of a Markov chain is viewed as a hiding place for the walker represented by the letter H. Given the hiding place density $\rho = \frac{1}{L^2}$, what is the average time the walker requires until reaching the hiding place? Figure 1.3 gives visual illustration of the system when $L = 5$.*

Let $T_H(i, j)$ be the time before reaching the hiding place starting from site (i, j) and let $m_H(i, j) = \mathbb{E}[T_H(i, j)]$ for all $0 \leq i, j \leq L - 1$. By using Theorem 1.2.4, we

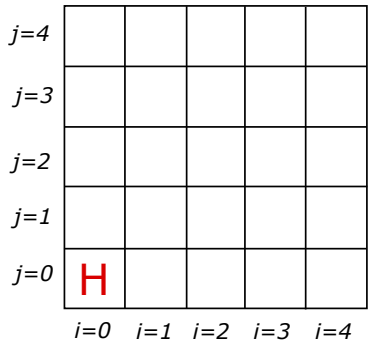

Figure 1.3: Two-dimensional system for $L = 5$. The letter H represent the hiding place

have

$$m_H(i,j) = \begin{cases} 0 & \text{if } (i,j) \text{ is a hiding place} \\ 1+ & \frac{1}{4}\Big(m_H(i+1,j) + m_H(i-1,j) + m_H(i,j+1) + m_H(i,j-1)\Big) \quad \text{otherwise.} \end{cases} \tag{1.23}$$

By solving the equations (1.23) simultaneously the average time τ for all sites in the system is obtained by

$$\tau = \frac{1}{L^2} \sum_{i=0}^{L-1} \sum_{j=0}^{L-1} m_H(i,j). \tag{1.24}$$

For $L = 9$, we found that the average time for the walker to reach the hiding place is $\tau = 128.992$ steps. Figure (1.4) gives a visual representation of the values of the expected time for each site in the system when $L = 9$ and hiding place is at the site $(1, 1)$. The darker colour means larger expected time to reach the hiding place.

1.2.6 Random walks

Random walks are fundamental stochastic processes. They have applications to many scientific fields such as modelling the motion of particle in physics [22, 23], epidemic spread [24, 25] and the search path of a foraging animal in ecology [26]. In this section, we will summarise the main concepts in random walks theory.

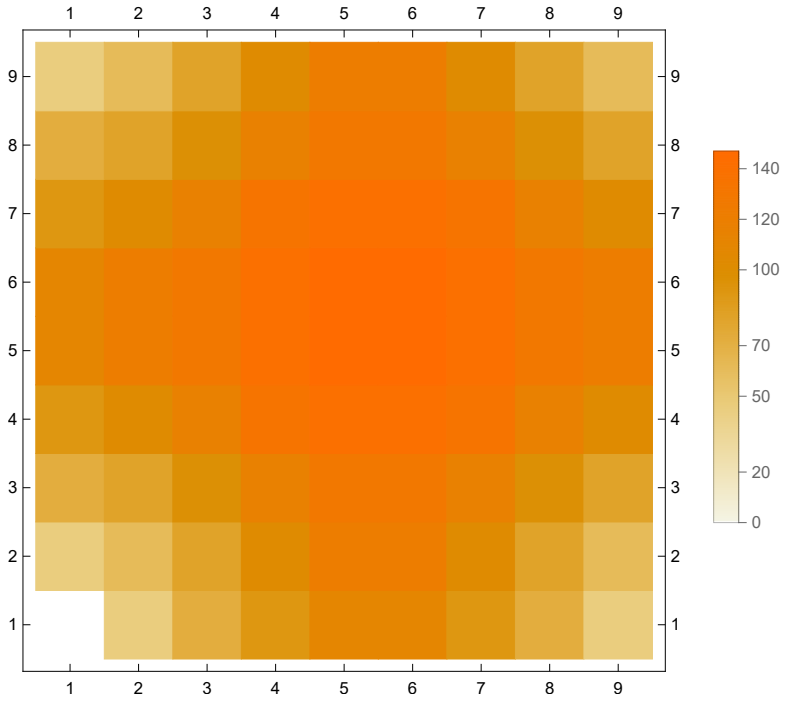

Figure 1.4: Visual illustration of the average time before hitting the hiding place for each site in the system when $L = 9$ and hiding place at $(1, 1)$. Darker colour indicate larger average time before reaching the hiding place.

Random walks on $\mathbb{Z}$

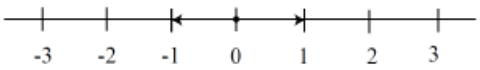

Figure 1.5: Integer Line $\mathbb{Z}$

Definition 1.2.12 (Simple random walk)**.** *A stochastic process* $\{S_n\}_{n\in\mathbb{N}_0}$ *is a simple random walk (also known as unrestricted random walk) if it satisfies the following conditions:*

- $S_0 = 0$,
- $S_n = \sum_{k=1}^{n} X_k \quad$ *for* $n \in \mathbb{N}$,

where the random walk increments $\{X_k : k \in \mathbb{N}\}$ *are independently and identically distributed random variables, each taking values in the set* $\{-1, 1\}$ *according to the*

following distribution for all $k \in \mathbb{N}$

$$\mathbb{P}(X_k = 1) = p, \tag{1.25}$$

$$\mathbb{P}(X_k = -1) = q = 1 - p. \tag{1.26}$$

When $p = \frac{1}{2}$ the walk is called symmetric simple random walk.

Lemma 1.2.1. *The mean and variance of the simple random walk* $\{S_n\}_{n\in\mathbb{N}_0}$ *are given by*

$$\mathbb{E}[S_n] = n(p - q),$$

and

$$\mathbb{V}[S_n] = 4npq. \tag{1.27}$$

Proof. From Definition 1.2.12, we have

$$S_n = \sum_{i=1}^{n} X_i \quad \text{for } n \in \mathbb{N}, \tag{1.28}$$

where X_i's are independent and identical Bernoulli random variables and its obvious that $\mathbb{E}[X_i] = p - q$ and $\mathbb{E}[X_i^2] = p + q = 1$. The expection of the random variable S_n is

$$\begin{aligned} \mathbb{E}[S_n] &= \mathbb{E}\left[\sum_{i=1}^{n} X_i\right] \\ &= \sum_{i=1}^{n} \mathbb{E}[X_i] = n(p - q). \end{aligned} \tag{1.29}$$

The variance of S_n is given by

$$\mathbb{V}[S_n] = \mathbb{E}[S_n^2] - (\mathbb{E}[S_n])^2. \tag{1.30}$$

In order to calculate the the variance of S_n we need to calculate the second moment $\mathbb{E}[S_n^2]$.

$$\begin{aligned}\mathbb{E}[S_n^2] &= \mathbb{E}\left[\left(\sum_{i=1}^{n} X_i\right)^2\right] \\ &= \mathbb{E}\left[\sum_{i=1}^{n} X_i^2 + 2\sum_{i=1}^{n}\sum_{j>i} X_i X_j\right] \\ &= \sum_{i=1}^{n}\mathbb{E}[X_i^2] + 2\sum_{i=1}^{n}\sum_{j>i}\mathbb{E}[X_i X_j]. \end{aligned} \tag{1.31}$$

For all $i \neq j$ we know that

$$\mathbb{E}[X_i X_j] = \mathbb{E}[X_i]\mathbb{E}[X_j] = (p-q)^2, \tag{1.32}$$

therefore

$$\begin{aligned}\mathbb{E}[S_n^2] &= n + 2\binom{n}{2}(p-q)^2 \\ &= n + n(n-1)(p-q)^2. \end{aligned} \tag{1.33}$$

By substituting (1.29) and (1.33) in(1.30) and simplifying, we have

$$\begin{aligned}\mathbb{V}[S_n] &= n - n(p-q)^2 \\ &= n[1-(p^2+q^2-2pq)] \\ &= n[1-(p^2+q^2+2pq-4pq)] \\ &= n\left[1-\left((p+q)^2-4pq\right)\right] \\ &= 4npq. \end{aligned}$$

□

Lemma 1.2.2 (General Distribution)**.** *Let $n \in \mathbb{N}$ and $k \in \mathbb{Z}$. The following probabilities are valid for any simple random walk $\{S_n\}_{n\in\mathbb{N}}$ (defined above)*

1) $\mathbb{P}(S_{2n} = 2k) = \binom{2n}{n+k} p^{n+k} q^{n-k}$ *for* $|k| \leq n$,

2) $\mathbb{P}(S_{2n+1} = 2k+1) = \binom{2n+1}{n+k+1} p^{n+k+1} q^{n-k}$ *for* $|k| \leq n$,

3) $\mathbb{P}(S_{2n} = 2k+1) = \mathbb{P}(S_{2n+1} = 2k) = 0$,

4) $\mathbb{P}(S_n = k) = 0$ *for all* $|k| > n$.

Proof. For the proof please see [18] page 169.

Theorem 1.2.5. *The probability that a simple walk returns to its starting point* $S_0 = 0$ *at some time* m *is given by*

$$\mathbb{P}(S_m = S_0) = 1 - |p - q|. \tag{1.34}$$

Proof. For the proof we refer the reader to [18] page 170.

In the simple random walk on integer line $\mathbb{Z}$ the next point or state of the walk depends on the current state and not on the history of the walk. Therefore, the simple random walk on integer line $\mathbb{Z}$ is a Markov chain with state space $\mathbb{Z}$. The transition probability from a state $i \in \mathbb{Z}$ to the next state on the integer line is given by

$$p_{i,i+1} = \mathbb{P}(S_n = i+1 | S_{n-1} = i) = p, \tag{1.35}$$

$$p_{i,i-1} = \mathbb{P}(S_n = i-1 | S_{n-1} = i) = q. \tag{1.36}$$

Random walk on $\mathbb{Z}^d$

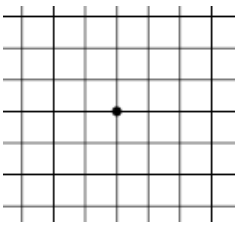

Figure 1.6: Integer Lattice $\mathbb{Z}^2$

The Points in $\mathbb{Z}^d$ are represented by vectors in $\mathbb{Z}^d = \{(x_1, ..., x_d) : x_i \in \mathbb{Z}\}$. We use superscripts to specify a point in $\mathbb{Z}^d$ and subscripts for components of a point

in $\mathbb{Z}^d$. For example the point x^i in the system $\mathbb{Z}^d$ can be written as $x^i = (x_1^i, ..., x_d^i)$. The unit vector in $\mathbb{Z}^d$ with one in the k-th component is denoted by e_k. In Chapter 2 we study a chase-capture problem which is modelled as a random walk on two dimensional lattice $\mathbb{Z}^2$.

Definition 1.2.13 (Random walk on $\mathbb{Z}^d$)**.** *The random process $\{S^n\}_{n\in\mathbb{N}_0}$ is a simple random walk on $\mathbb{Z}^d$ if $S^n = S^0 + \sum_{i=1}^n X^i$, where X^i is i.i.d. uniformly distributed over the set $\{e_1, -e_1, ..., e_d, -e_d\}$ for all $i \in \mathbb{N}$ and $S^0 \in \mathbb{Z}^d$.*

Definition 1.2.14. *A simple random walk on $\mathbb{Z}^d$ at each time step have $2d$ options to move, we say that the random walk is symmetric if all the $2d$ options are equally likely i.e. each option is with probability $\frac{1}{2d}$.*

Theorem 1.2.6. *If $\{S^n\}_{n\in\mathbb{N}_0}$ is a symmetric simple random walk on $\mathbb{Z}^d$ starting at $S^0 = \vec{0}$, then it is recurrent (returns to the origin with probability one infinitely many times) for $d = 1, 2$ and transient for $d \geq 3$.*

Proof. For the proof please see [18] page 218.

Theorem 1.2.7. *If $\{S^n\}_{n\in\mathbb{N}_0}$ is symmetric simple random walk on $\mathbb{Z}^d$ starting at $S^0 = \vec{0}$, then*

$$\mathbb{E}[S^n] = 0 \quad \textit{and} \quad \mathbb{E}[|S^n|^2] = n \tag{1.37}$$

Proof. For $1 \leq k \leq d$ and $1 \leq i \leq n$, X_k^i is the $k-$th entry of a uniformly distributed random variable on the set $\{e_1, -e_1, ..., e_d, -e_d\}$. We have

$$\mathbb{P}(X_k^i = 1) = \mathbb{P}(X_k^i = -1) = \frac{1}{2d} \quad \text{and} \quad \mathbb{P}(X_k^i = 0) = 1 - \frac{1}{d}, \tag{1.38}$$

this implies that

$$\mathbb{E}[X_k^i] = 0 \quad \text{and } \mathbb{E}[\big(X_k^i\big)^2] = \frac{1}{d}. \tag{1.39}$$

From Definition 1.2.13, X^i and X^j are independent for all $i \neq j$, so are X_k^i and X_k^j. For $i \neq j$, we have

$$\mathbb{E}[X_k^i X_k^j] = \mathbb{E}[X_k^i]\mathbb{E}[X_k^j] = 0$$

Therefore, for any $1 \leq k \leq d$, we have

$$\mathbb{E}[S_k^n] = \mathbb{E}\left[\sum_{i=1}^{n} X_k^i\right] = \sum_{i=1}^{n} \mathbb{E}[X_k^i] = 0,$$

this implies that $\mathbb{E}[S^n] = 0$. For $1 \leq k \leq d$, we have

$$\begin{aligned}
\mathbb{E}\left[(S_k^n)^2\right] &= \mathbb{E}\left[\left(\sum_{i=1}^{n} X_k^i\right)^2\right] \\
&= \mathbb{E}\left[\sum_{i=1}^{n} \left(X_k^i\right)^2 + 2\sum_{i=1}^{n}\sum_{j>i} X_k^i X_k^j\right] \\
&= \sum_{i=1}^{n} \mathbb{E}\left[\left(X_k^i\right)^2\right] + 2\sum_{i=1}^{n}\sum_{j>i} \mathbb{E}[X_k^i X_k^j] \\
&= \sum_{i=1}^{n} \mathbb{E}\left[\left(X_k^i\right)^2\right] = \sum_{i=1}^{n} \frac{1}{d} = \frac{n}{d},
\end{aligned}$$

implies that

$$\mathbb{E}\left[|S^n|^2\right] = \mathbb{E}\left[\sum_{k=1}^{d} (S_k^n)^2\right] = \sum_{k=1}^{d} \mathbb{E}\left[(S_k^n)^2\right] = \sum_{k=1}^{d} \frac{n}{d} = n. \qquad \square$$

A symmetric simple random walk on $\mathbb{Z}^d$ is a Markov chain on the state space $\mathbb{Z}^d$ and transition probabilities are given by

$$\mathbb{P}(S^n = \vec{y} | S^{n-1} = \vec{x}) = \begin{cases} \frac{1}{2d} & \text{if Taxi (Manhattan) distance between } \vec{x} \text{ and } \vec{y} \text{ is one} \\ 0 & \text{otherwise,} \end{cases} \tag{1.40}$$

for any $\vec{x}, \vec{y} \in \mathbb{Z}^d$ and the Taxi distance between the two states $\vec{x} = (x_1, x_2, ..., x_d)$

and $\vec{y} = (y_1, y_2, ..., y_d)$ defined as

$$d(\vec{x}, \vec{y}) = \sum_{i=1}^{d} |x_i - y_i|. \tag{1.41}$$

1.3 Continuous-time processes

1.3.1 Poisson process

Definition 1.3.1. *A stochastic process $\{N(t) : t \geq 0\}$ is called a homogeneous Poisson process if it satisfies the following conditions*

1) $N(0) = 0$.

2) The increments $N(t+s) - N(s) \in \mathbb{N}_0$ *for all* $s, t > 0$.

3) $N(t)$ *has independent increments, that is, the increments*

$$N(t_1), N(t_2) - N(t_1), ..., N(t_n) - N(t_{n-1}), \tag{1.42}$$

are independent random variables for any $0 < t_1 < t_2 < ... < t_n$.

4) $N(t)$ *has stationary increments, that is,*

$$N(t) - N(s) \text{ has the same distribution as } N(t-s), \text{for all } 0 < s < t. \tag{1.43}$$

5) For a constant λ*, called the intensity or the average arrival time rate, and for* $\delta t \to 0$*, we have*

$$\begin{aligned}
&\mathbb{P}(N(t+\delta t) = n+1 | N(t) = n) = \lambda \delta t + o(\delta t) \\
&\mathbb{P}(N(t+\delta t) = n+k | N(t) = n) = o(\delta t) \quad \text{for } k > 1 \\
&\mathbb{P}(N(t+\delta t) = n-k | N(t) = n) = 0 \quad \text{for } k > 0.
\end{aligned}$$

Poisson process is often called a counting process and $N(t)$ represents the total

number of events or arrivals that occurred up to time t since $t = 0$. The distribution of $N(t)$ is stated in the following theorem.

Theorem 1.3.1. *The number of events or arrivals in an interval of length $t > 0$ has Poisson distribution with parameter λt, that is,*

$$\mathbb{P}(N(t) = k) = \frac{(\lambda t)^k}{k!} e^{-\lambda t}, \text{ for all } k \in \mathbb{N}_0. \tag{1.44}$$

Proof (See [20], page 247). Let $p_k(t) = \mathbb{P}(N(t) = k)$. By applying the partitioning theorem [18] for $k \in \mathbb{N}$, we have

$$p_k(t + \delta t) = \sum_{i=0}^{k} \mathbb{P}(N(t + \delta t) = k | N(t) = k - i)\mathbb{P}(N(t) = k - i). \tag{1.45}$$

By using Definition 1.3.1, we have

$$p_k(t + \delta t) = [1 - \lambda\delta t + o(\delta t)]p_k(t) + [\lambda\delta t + o(\delta t)]p_{k-1}(t) + o(\delta t) \tag{1.46}$$

$$= [1 - \lambda\delta t]p_k(t) + [\lambda\delta t]p_{k-1}(t) + o(\delta t). \tag{1.47}$$

By rearranging and dividing by δt, we have

$$\frac{p_k(t + \delta t) - p_k(t)}{\delta t} = \lambda[p_{k-1}(t) - p_k(t)] + \frac{o(\delta t)}{\delta t}. \tag{1.48}$$

Taking the limit as $\delta t \to 0$ results in the following infinite set of coupled ordinary differential equations (ODEs)

$$p_k'(t) = \lambda[p_{k-1}(t) - p_k(t)] \text{ for } k \in \mathbb{N}, \tag{1.49}$$

and

$$p_0'(t) = -\lambda p_0(t). \tag{1.50}$$

The boundary condition for this ODEs is $N(0) = 0$, which equivalently can be

written as

$$p_k(0) = \delta_{k0} = \begin{cases} 1 & \text{if } k = 0, \\ 0 & \text{otherwise.} \end{cases} \tag{1.51}$$

We can solve this ODEs by mathematical induction as follow. For $k = 0$ we solve equation (1.50) with boundary condition $p_k(0) = \delta_{k0}$ to obtain

$$p_0(t) = e^{-\lambda t}. \tag{1.52}$$

Substituting (1.52) in (1.49) for $k = 1$, gives us to the following ODE

$$p_1'(t) + \lambda p_1(t) = \lambda e^{-\lambda t}. \tag{1.53}$$

By solving (1.53) with the boundary condition $p_k(0) = \delta_{k0}$, we obtain

$$p_1(t) = \lambda t e^{-\lambda t}. \tag{1.54}$$

Similarly, by Substituting (1.54) in (1.49) for $k = 2$, and solve the resulting ODE with the boundary condition given in (1.51) we obtain

$$p_2(t) = \frac{1}{2}(\lambda t)^2 e^{-\lambda t}. \tag{1.55}$$

By carrying on the same process, we obtain by induction that

$$\mathbb{P}(N(t) = k) = \frac{(\lambda t)^k}{k!} e^{-\lambda t}, \text{ for all } k \in \mathbb{N}_0. \tag{1.56}$$

□

Arrival and interarrival times

Let $\{T_k\}_{k\in\mathbb{N}}$ be a sequence of arrival times of a Poisson process, which is defined by

$$T_k = \inf\{t > 0 : N(t) = k\}. \tag{1.57}$$

Here, T_k is the time of kth arrival. We define the random variables $\{X_1, X_2, ...\}$ to be are interarrival times such that

$$X_k = T_k - T_{k-1}. \tag{1.58}$$

The kth arrival time can be obtained as

$$T_k = \sum_{i=1}^{k} X_i. \tag{1.59}$$

The distribution of the interarrival times of the counting proccess $N(t)$ is given in the following theorem.

Theorem 1.3.2. *The interarrival times $\{X_k\}_{k\in\mathbb{N}}$ of a Poisson process $N(t)$ with intensity λ are independent and*

$$X_k \sim \text{Exp}(\lambda) \text{ for all } k \in \mathbb{N}, \tag{1.60}$$

where $\text{Exp}(\lambda)$ *is the exponential distribution with parameter* λ.

Proof. For the proof please see [20] page 249. Before introducing the distribution of arrival time we need to introduce the definition of Erlang distribution and some facts about Erlang distribution.

Definition 1.3.2. *A random variable X has an Erlang distribution with parameter $n \in \mathbb{N}$ and $\lambda > 0$ if its density function of the form*

$$f_X(x) = \frac{\lambda^n x^{n-1} e^{-\lambda x}}{(n-1)!} \text{ for } x \geq 0, \tag{1.61}$$

and zero otherwise. We write $X \sim \text{Erlang}(n, \lambda)$.

Lemma 1.3.1. *The moment generating function of a random variable $X \sim \text{Erlang}(n, \lambda)$*

is given by

$$M_X(s) = \mathbb{E}[e^{sX}] = \frac{\lambda^n}{(\lambda - s)^n} \text{ for } s < \lambda. \tag{1.62}$$

Proof. Let $X \sim \text{Erlang}(n, \lambda)$, then we have

$$\begin{aligned} M_X(s) =& \mathbb{E}[e^{sX}] \\ =& \int_{-\infty}^{\infty} e^{sx} f_X(x)\, dx \\ =& \int_0^{\infty} e^{sx} \frac{\lambda^n x^{n-1} e^{-\lambda x}}{(n-1)!}\, dx = \frac{\lambda^n}{(\lambda - s)^n} \text{ for } s < \lambda. \end{aligned} \tag{1.63}$$

Lemma 1.3.2. *The sum of n independent exponential random variables each with rate $\lambda > 0$ is an* Erlang(n, λ) *random variable.*

Proof. Let $X_1, X_2, ..., X_n$ be n independent and identically distributed exponential random variables with rate λ. Let $Y = \sum_{i=1}^{n} X_i$. For $i \in \{1, 2, ..., n\}$, the moment generating function (MGF) of X_i is

$$M_{X_i}(s) = \frac{\lambda}{\lambda - s} \quad \text{for } s < \lambda. \tag{1.64}$$

The moment generating function of the random variable Y is

$$\begin{aligned} M_Y(s) =& \mathbb{E}[e^{sY}] \\ =& \mathbb{E}[e^{s\sum_{i=1}^{n} X_i}] \\ =& \mathbb{E}[e^{sX_1} e^{sX_2} ... e^{sX_n}] \\ =& \mathbb{E}[e^{sX_1}]\mathbb{E}[e^{sX_2}] ... \mathbb{E}[e^{sX_n}] \\ =& M_{X_1}(s) M_{X_2}(s) .... M_{X_n}(s) \\ =& \frac{\lambda}{\lambda - s} \frac{\lambda}{\lambda - s} .... \frac{\lambda}{\lambda - s} \\ =& \frac{\lambda^n}{(\lambda - s)^n} \quad \text{for } s < \lambda, \end{aligned} \tag{1.65}$$

which is the moment generating function of an Erlang(n, λ). □

Proposition 1.3.1. *For $k \in \mathbb{N}$, let T_k be the kth arrival time of a Poisson process with intensity λ, then*

$$T_k \sim \text{Erlang}(k, \lambda).$$

The probability density function of T_k is

$$f_{T_k}(t) = \frac{\lambda^k t^{k-1} e^{-\lambda t}}{(k-1)!};\ \textit{for } \lambda, t \geq 0. \tag{1.66}$$

Proof. For the proof please see [27] page 171.

Non-homogeneous Poisson processes

A Poisson process is said to be non-homogeneous if the intensity $\lambda = \lambda(t)$ is not a constant. In this case the increments of the process are not stationary. The non-homogeneous Poisson process is defined as follows.

Definition 1.3.3. *A stochastic process $\{N(t) : t \geq 0\}$ is called a non-homogeneous Poisson process with intensity $\lambda(t) : [0, \infty) \to [0, \infty)$ if it is satisfies the following conditions*

1) $N(0) = 0$.

2) $N(t)$ has independent increments.

3) for all $t \geq 0$ and as $\delta t \to 0$, we have

$$\mathbb{P}(N(t+\delta t) = n+1 | N(t) = n) = \lambda(t)\delta t + o(\delta t)$$
$$\mathbb{P}(N(t+\delta t) = n+k | N(t) = n) = o(\delta t) \quad \textit{for } k > 1.$$

For $0 < s < t$, $N(t) - N(s)$ has a Poisson distribution with parameter $\mathbb{E}[N([s,t))] = \int_s^t \lambda(x)dx$.

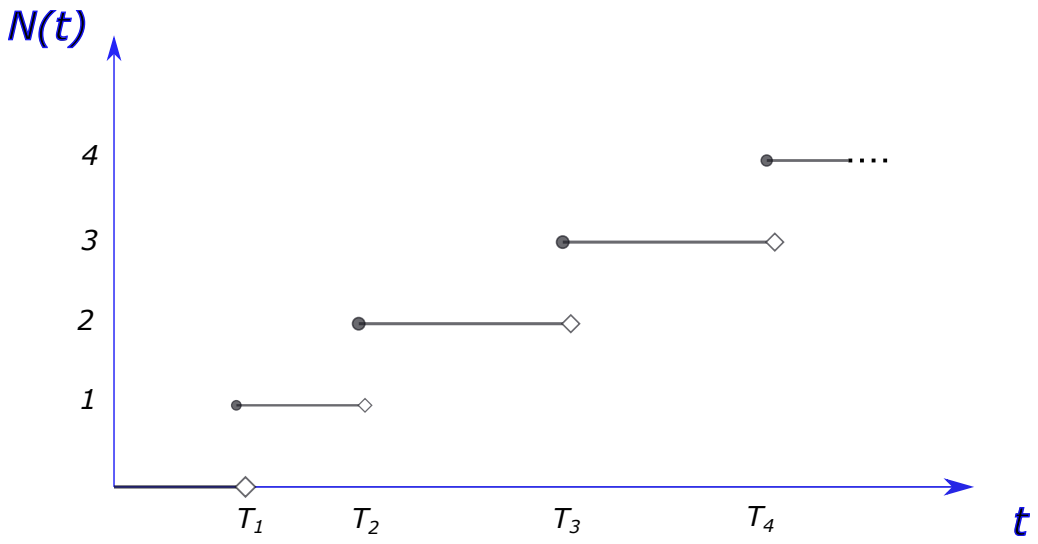

Figure 1.7: Visitation of the arrival times and the corresponding accounting process.

Arrival times of non-homogeneous Poisson process

Suppose we have a non-homogeneous Poisson process $\{N(t)\}_{t\geq 0}$ with intensity function $\lambda(t)$. Let T_k be the $k-$th arrival time for $k \in \mathbb{N}$. The inverse relation between the arrival times $T = \{T_k\}_{k\in\mathbb{N}}$ and the counting process $N = \{N(t) : t \geq 0\}$ is given by

$$T_k = \inf\{t > 0 : N(t) = k\}, \tag{1.67}$$

and

$$N(t) = \#\{n \in \mathbb{N} : T_n \leq t\}. \tag{1.68}$$

Figure 1.7 illustrate the inverse relation between the counting process N and the arrival times T. The probability density function of T_k given by

$$f_{T_k}(t) = \frac{m(t)^{k-1}}{(k-1)!}\lambda(t)e^{-m(t)}, \text{ for } t \geq 0, \tag{1.69}$$

where $m(t) = \mathbb{E}[N(t)] = \int_0^t \lambda(s)ds$.

1.3.2 Brownian motion

Brownian motion (or Wiener process) is a continuous-time stochastic process that may be constructed as a scaled limit of simple random walks. Here we briefly introduce some of the principal concepts of Brownian motion.

Definition 1.3.4. *A stochastic process* $W = \{W(t) : t \geq 0\}$ *is a standard Brownian Motion if satisfies the following properties*

1) $W(0) = 0$.

2) $W(t)$ *has independent increments, that is*

$$W(t_1), W(t_2) - W(t_1), ..., W(t_n) - W(t_{n-1}) \tag{1.70}$$

are independent for any $0 < t_1 < t_2 < ... < t_n < \infty$.

3) For all $0 \leq s < t < \infty$; $W(t) - W(s)$ *has has normal distribution with mean* $\mu = 0$ *and variance* $\sigma^2 = t - s$.

4) $W(t)$ *has stationary increments, that is,*

$$W(t) - W(s) \text{ has the same distribution as } W(t - s). \tag{1.71}$$

for any $0 \leq s < t < \infty$;

5) The paths of $W(t)$ *are continuous, that is, the function* $t \mapsto W(t)$ *is a continuous function of* t *with probability* 1.

Recall that the covariance of the two random variables X and Y is defined by

$$Cov(X, Y) = \mathbb{E}[XY] - \mathbb{E}[X]\mathbb{E}[Y]. \tag{1.72}$$

The following lemma gives some basic properties of covariance.

Lemma 1.3.3. *For any random variables* X, Y *and* Z, *and* $a, b \in \mathbb{R}$, *then*

1) $Cov(X, X) = \mathbb{V}[X]$.

2) $Cov(X, Y) = Cov(Y, X)$.

3) $Cov(aX, Y) = a\,Cov(X, Y)$.

4) If X *and* Y *are independent then* $Cov(X, Y) = 0$.

5) $Cov(X + Y, Z) = Cov(X, Z) + Cov(Y, Z)$.

where $\mathbb{V}[X]$ *is the variance of* X.

Proof. 1) and 2) are obvious.

3) By using (1.72) and the properties of expectation we have

$$\begin{aligned} Cov(aX, Y) =& \mathbb{E}[aXY] - \mathbb{E}[aX]\mathbb{E}[Y] \\ =& a\mathbb{E}[XY] - a\mathbb{E}[X]\mathbb{E}[Y] \\ =& a(\mathbb{E}[XY] - \mathbb{E}[X]\mathbb{E}[Y]) = aCov(X, Y). \end{aligned}$$

4) If $X$and Y are independent, then

$$\begin{aligned} Cov(X, Y) =& \mathbb{E}[XY] - \mathbb{E}[X]\mathbb{E}[Y] \\ =& \mathbb{E}[X]\mathbb{E}[Y] - \mathbb{E}[X]\mathbb{E}[Y] = 0. \end{aligned}$$

5)

$$\begin{aligned} Cov(X + Y, Z) =& \mathbb{E}[(X + Y)Z] - \mathbb{E}[X + Y]\mathbb{E}[Z] \\ =& \mathbb{E}[XZ + YZ] - (\mathbb{E}[X] + \mathbb{E}[Y])\,\mathbb{E}[Z] \\ =& \mathbb{E}[XZ] - \mathbb{E}[X]\mathbb{E}[Z] + \mathbb{E}[YZ] - \mathbb{E}[Y]\mathbb{E}[Z] \\ =& Cov(X, Z) + Cov(Y, Z). \end{aligned}$$

Recall that the correlation coefficient of two random variables X and Y, $\rho(X,Y)$, is given by

$$\rho(X,Y) = \frac{Cov(X,Y)}{\sqrt{\mathbb{V}[X]\mathbb{V}[Y]}}, \tag{1.73}$$

whenever $\mathbb{V}[X]\mathbb{V}[Y] \neq 0$. □

Proposition 1.3.2. *For a standard Brownian Motion W and for $0 \leq s \leq t$, we have*

$$Cov(W(s), W(t)) = s, \tag{1.74}$$

and

$$\rho(W(s), W(t)) = \sqrt{\frac{s}{t}}. \tag{1.75}$$

Proof. For the proof we refer the reader to [28] page 49.

Remark 1.3.1. *By removing the order relation between s and t in Proposition 1.3.2 we have*

$$Cov(W(s), W(t)) = \min\{s,t\}, \tag{1.76}$$

and

$$\rho(W(s), W(t)) = \sqrt{\frac{\min\{s,t\}}{\max\{s,t\}}}. \tag{1.77}$$

Before introducing the next theorem, we need to define the multivariate normal distribution and the Gaussian process.

Definition 1.3.5. *The vector $X = (X_1, X_2, ..., X_n)$ has a multivariate normal distribution, written $X \sim \mathcal{N}(\mu, V)$, if its joint density function is*

$$f(x) = \frac{1}{\sqrt{(2\pi)^n |V|}} \exp\{-\frac{1}{2}(x-\mu)V^{-1}(x-\mu)^T\}, \text{ for } x \in \mathbb{R}^n, \tag{1.78}$$

where $\mu = (\mathbb{E}[X_1], ..., \mathbb{E}[X_n])$, $|V|$ is the determinant of covariance matrix $V = [v_{ij}]$ which is defined by $v_{ij} = Cov(X_i, X_j)$ for $1 \leq i, j \leq n$ and $(x-\mu)^T$ is the transpose of the vector $(x-\mu)$.

Definition 1.3.6 (Gaussian process)**.** *A continuous-time stochastic process $\{X(t) :$*

$t \geq 0\}$ *is called Gaussian process if random variables* $X(t_1), X(t_2), ..., X(t_n)$ *have a multivariate normal distribution for all* $0 \leq t_1 < t_2 < ... < t_n$.

Brownian motion can be also viewed as a Gaussian process, this is captured in the following theorem:

Theorem 1.3.3. *A stochastic process* $W = \{W(t) : t \geq 0\}$ *is a standard Brownian Motion if and only if it satisfies the following conditions*

1) $W(0) = 0$.

2) $W(t)$ *is a Gaussian process.*

3) $\mathbb{E}[W(t)] = 0$ *for all* $t \geq 0$.

4) $Cov(W(s), W(t)) = \min\{s, t\}$ *for all* $s, t \geq 0$.

5) Paths of $W(t)$ *are continuous, that is, the function* $t \mapsto W(t)$ *is continuous.*

Proof. For the proof we refer the reader to [21] page 332.
The next proposition shows that one may reverse the time and still obtain a Brownian motion. We use this property later in Chapter 3 where we calculate the shape of spatial memory of a foraging animal.

Proposition 1.3.3 (Time-Reversal)**.** *For* $T > 0$, *let* $\{W(t) : t \in [0, T]\}$ *be a standard Brownian motion. Then the process*

$$X(t) = W(T) - W(T - t) \quad \textit{for } 0 \leq t \leq T \tag{1.79}$$

is a standard Brownian motion.

Proof. The process X is standard Brownian motion on $[0, T]$ if it satisfies properties in Theorem 1.3.3.

1) Clearly, $X(0) = W(T) - W(T) = 0$.

2) Since W is standard Brownian motion, then the process X is a Gaussian process.

3) For $0 \leq t \leq T$,

$$\begin{aligned}\mathbb{E}[X(t)] &= \mathbb{E}[W(T) - W(T-t)] \\ &\mathbb{E}[W(T)] - \mathbb{E}[W(T-t)] = 0.\end{aligned}$$

4) For $s, t \geq 0$, by applying Lemma 1.3.3 and the stationarity property in Definition 1.3.4, we have

$$\begin{aligned}Cov[X(s), X(t)] &= Cov[W(T) - W(T-s), W(T) - W(T-t)] \\ &= \mathbb{V}[W(T)] - \mathbb{V}[W(T)] + Cov[W(s), W(T)] - \mathbb{V}[W(T)] \\ &\quad + Cov[W(T), W(t)] + \mathbb{V}[W(T)] - Cov[W(s), W(T)] \\ &\quad - Cov[W(T), W(t)] + Cov[W(s), W(t)] \\ &= \min\{s, t\}.\end{aligned}$$

5) Paths of the process X are continuous on $[0, T]$ since W is standard Brownian motion. □

1.3.3 Brownian Bridge

A Brownian bridge is a continuous-time stochastic process that can be constructed from a standard Brownian motion by conditioning on the event $W(1) = 0$. The Brownian bridge process is used to model systems that expected to return to the same starting point in the future [29]. In this section we introduce the definition of Brownian bridge and some important properties that we will be using later in Chapter 4.

Definition 1.3.7 (Brownian Bridge)**.** *A stochastic process $B = \{B(t) : t \geq 0\}$ is a standard Brownian Bridge if it satisfies the following properties*

1) $B(0) = B(1) = 0$.

2) $B(t)$ is a Gaussian process.

3) $\mathbb{E}[B(t)] = 0$ *for all* $t \in [0,1]$.

4) $Cov(B(s), B(t)) = \min\{s,t\} - st$ *for all* $s, t \in [0,1]$.

5) The paths of $B(t)$ *are continuous, that is, the function* $t \mapsto B(t)$ *is continuous on* $[0,1]$.

One way to construct a Brownian bridge from a standard Brownian motion is given in the next lemma.

Lemma 1.3.4. *Suppose that* $W = \{W(t) : t \geq 0\}$ *is a standard Brownian motion, and let* $B(t) = W(t) - tW(1)$ *for all* $t \in [0,1]$*, then the process* $B = \{B(t) : t \in [0,1]\}$ *is a Brownian bridge.*

Proof. The process B is a Brownian bridge on $[0,1]$ if it satisfies Definition 1.3.7 (the definition of Brownian bridge) .

1) Since $W(t)$ is standard Brownian motion, then it clear that

$$B(0) = B(1) = 0.$$

2) Since W is a Gaussian process (By Theorem 1.3.3), then B is Gaussian process.

3) $\mathbb{E}[B(t)] = \mathbb{E}[W(t)] - t\mathbb{E}[W(1)] = 0$, for all $t \in [0,1]$.

4) For $0 \leq s, t \leq 1$, we have

$$\begin{aligned} Cov[B(s), B(t)] =& Cov[W(s) - sW(1), W(t) - tW(1)] \\ =& Cov[W(s), W(s)] - tCov[(W(s), W(1)] \\ & - sCov[W(1), W(t)] + tsCov[W(1), W(1)] \quad (\text{ by Lemma 1.3.3}) \\ =& \min\{s,t\} - t\min\{1,s\} - s\min\{t,1\} + st\mathbb{V}[W(1)] (\text{ by Theorem 1.3.3}) \\ =& \min\{t,s\} - ts. \end{aligned}$$

5) Paths of the process B are continuous on $[0,1]$ since W is standard Brownian motion.

□

Similarly, we can also construct a standard Brownian motion from a Brownian bridge, namely:

Lemma 1.3.5. *Suppose that $B = \{B(t) : t \in [0,1]\}$ is a Brownian bridge, and let Z is a standard normal random variable independent of B. If $W(t) = B(t) + tZ$ for $0 \leq t \leq 1$, then the process $W = \{W(t) : t \in [0,1]\}$ is a standard Brownian motion on $[0,1]$.*

Proof. The process W is a standard Brownian motion on $[0,1]$ if it satisfies the conditions in Theorem 1.3.3.

1) Clearly we can see that $W(0) = 0$.

2) W is a Gaussian process since B is a Gaussian process.

3) For $t \in [0,1]$, we have

$$\begin{aligned}\mathbb{E}[W(t)] =& \mathbb{E}[B(t) + tZ] \\ =& \mathbb{E}[B(t)] + t\mathbb{E}[Z] = 0.\end{aligned} \tag{1.80}$$

4) For $0 \leq s, t \leq 1$, we have

$$\begin{aligned}Cov[W(s), W(t)] =& Cov[B(s) + sZ, B(t) + tZ] \\ =& Cov[B(s), B(t)] + tCov[B(s), Z] \\ & + sCov[Z, B(t)] + stCov[Z, Z] \quad (\text{ by Lemma 1.3.3})\end{aligned} \tag{1.81}$$

By knowing that Z and B are independent, and by using Lemma 1.3.3, we have $Cov[B(s), Z] = Cov[Z, B(t)] = 0$ and $Cov[Z, Z] = \mathbb{V}[Z] = 1$, then

$$\begin{aligned}Cov[W(s), W(t)] =& Cov[B(s), B(t)] + st\mathbb{V}[Z] \\ =& \min\{s,t\} - st + st \qquad (1.82) \\ =& \min\{s,t\}. \qquad (1.83)\end{aligned}$$

5) Paths of the process W are continuous on $[0,1]$ since B is Brownian bridge.

□

1.3.4 Itô's calculus

In this section we discuss the rudiments of stochastic integration. We focus on the Itô integral; it was introduced by Kiyosi Itô in 1944 [30, 31]. Here we are interested in Itô integral with respect to a Brownian motion. For an elaborate exposition of the theory of Itô calculus we refer the reader to [28].

Motivation

The Riemann integral $\int_a^b F(x)\,dx$ gives us the work done by the force F from $x = a$ to $x = b$. The term $F(x)dx$ gives the work that has been done by force F during the spatial displacement dx. Likewise, $F(t)dW(t)$ is the work that has been done by the force F during an infinitesimal Brownian motion jump $dW(t)$. The integration $\int_a^b F(t)\,dW(t)$, which of interest in this section, gives the cumulative effect done by the force F along the path of a particle modelled by a Brownian motion between times $t = a$ and $t = b$.

The Itô integral

The Itô integral is defined in similar way as in the Riemann integral, we will point out the differences further in this section. The Itô integral is integrated with respect to infinitesimal increments of a Brownian motion $dW(t)$. For a stochastic process $\{X(t) : t \geq 0\}$, for example the integral $\int_0^T X(t)W(t)$ is defined as

$$\int_0^T X(t)\,dW(t) = \lim_{n\to\infty} \sum_{k=0}^{n-1} X(t_k)\left(W(t_{k+1}) - W(t_k)\right), \tag{1.84}$$

for $0 = t_0 < t_1 < ... < t_n = T$. We emphasize that in the approximation of the Itô integral, given in equation (1.84), unlike in Riemann integral, the function X

is always evaluated at left endpoint of each subinterval $[t_k, t_{k+1}]$. The Itô integral $\int_0^T X(t)\,dW(t)$ exists if the following conditions are satisfied

1) $\int_0^T \mathbb{E}[X^2(t)]dt < \infty$.

2) The process $X(t)$ is nonanticipating to a given Brownian motion, that is, $X(t)$ depend only on $\{W(s) : s \leq t\}$.

3) The limit in (1.84), $S_n(X) = \sum_{k=0}^{n-1} X(t_k)\,(W(t_{k+1}) - W(t_k))$, converges in the mean-square sense, that is, there is a random variable $S(X,T)$ such that

$$\lim_{n\to\infty} \mathbb{E}[|S_n(X) - S(X,T)|^2] = 0. \tag{1.85}$$

We call $S(X,T)$ an Itô integral of X over the interval $[0,T]$ and denoted by $\int_0^T X(t)\,dW(t)$.

The nonanticipating process is defined as follow

Definition 1.3.8 (nonanticipating processes)**.** *For the Brownian motion W. A process X is called nonanticipating if $X(t)$ is independent of any future increment $W(s) - W(t)$ for any $t < s$.*

Properties of Itô integral

The following proposition introduces some of the basic properties of the Itô integral.

Proposition 1.3.4. *Given two nonanticipating processes $\{X(t) : t \geq 0\}$ and $\{Y(t) : t \geq 0\}$, and $0 \leq S < T < \infty$, we have*

1) For constants a, b, we have

$$\int_S^T (aX(t) + bY(t))\,dW(t) = a\int_S^T X(t)dW(t) + b\int_S^T Y(t)dW(t). \tag{1.86}$$

2) For any $S < R < T$, we have

$$\int_S^T X(t)dW(t) = \int_S^R X(t)dW(t) + \int_R^T X(t)dW(t). \tag{1.87}$$

3) The Itô integral $\int_S^T X(t)dW(t)$ *is a random variable with zero mean, that is,*

$$\mathbb{E}\left[\int_S^T X(t)dW(t)\right] = 0. \tag{1.88}$$

4) Itô Isometry:

$$\mathbb{E}\left[\int_S^T X(t)dW(t)\int_S^T Y(t)dW(t)\right] = \mathbb{E}\left[\int_S^T X(t)Y(t)dt\right]. \tag{1.89}$$

Proof. For the proof please see [28] page 122.

The following table summarizes some important properties of standard Brownian motion that used extensively with Itô calculus.

$\times$	dt	$dW(t)$
dt	0	0
$dW(t)$	0	dt

Table 1.1: Itô product rules

In order to provide simple heuristic proof for the Itô multiplication properties in Table 1.1, consider partitioning $[0, T]$ to n subintervals of length $\delta t > 0$. The first property $(dt)^p = 0$ for $p > 1$ can be proved by considering

$$\sum_{k=0}^{n-1}(\delta t)^p = n\left(\frac{T}{n}\right)^p = 0 \text{ as } n \to \infty \text{ for } p > 1. \tag{1.90}$$

Since δt is a discrete analogue of dt, hence $(dt)^p = 0$ for $p > 1$. The remaining properties $dtdW(t) = 0$ and $(dW(t))^2 = dt$ can be proved as follows. We first show that the expectation of the left hand side equal to the expectation of the right hand side (RHS), then we show that the variance of the left hand side (LHS) is zero, which mean the LHS is not random and the two sides are equal. For the second property $dtdW(t) = 0$, we have that $\mathbb{E}[dtdW(t)] = dt\,\mathbb{E}[dW(t)] = dt \times 0 = 0$. Now

the variance of $dtdW(t)$ is obtained by

$$\begin{aligned}\mathbb{V}[dtdW(t)] =& \mathbb{E}[(dtdW(t))^2] - \mathbb{E}[dtdW(t)] \\ =& (dt)^2\mathbb{E}[dW(t)^2] - 0 \\ =& 0 \times \mathbb{E}[dW(t)^2] = 0. \end{aligned} \tag{1.91}$$

For the third property $(dW(t))^2 = dt$, the expectation of LHS is $\mathbb{E}[dW(t))^2] = dt$ and the variance of LHS is given by

$$\begin{aligned}\mathbb{V}[dW(t))^2] =& \mathbb{E}[dW(t))^4] - \left(\mathbb{E}[dW(t))^2]\right)^2 \\ =& 3(dt)^2 - (dt)^2 = 0 \quad \text{(by using Table 1.1).} \end{aligned} \tag{1.92}$$

Itô's lemma is a key tool in stochastic calculus and stochastic differential equations as it provides the chain rule in a stochastic calculus. Itô's lemma can be applied to wide class of stochastic processes, which are solutions to stochastic integral equations of the form

$$X(T) - X(0) = \int_0^T \mu(t, X(t))dt + \int_0^T \sigma(t, X(t))dW(t), \tag{1.93}$$

which are often written in a shorthand differential form as follows:

$$dX(t) = \mu(t, X(t))dt + \sigma(t, X(t))dW(t), \tag{1.94}$$

where μ and σ are continuous functions of t and X. The term $\mu(t, X(t))dt$ is called the drift, and $\sigma(t, X(t))dW(t)$ is called the diffusion. The process that satisfies (1.94) is called as Itô process.

Lemma 1.3.6 (Itô's lemma)**.** *Suppose that $f : [0, \infty) \times \mathbb{R} \to \mathbb{R}$ is twice differentiable, and let $\{X(t) : t \geq 0\}$ be an Itô process, which is satisfying (1.94), then*

$$df(t, X(t)) = \frac{\partial f}{\partial t}(t, X(t))dt + \frac{\partial f}{\partial x}(t, X(t))dX(t) + \frac{1}{2}\frac{\partial^2 f}{\partial x^2}(t, X(t))(dX(t))^2. \tag{1.95}$$

In particular,

$$\begin{aligned} df(t,X(t)) =&[\frac{\partial f}{\partial t}(t,X(t)) + \mu(t,X(t))\frac{\partial f}{\partial x}(t,X(t)) \\ &+ \frac{1}{2}\sigma^2(t,X(t))\frac{\partial^2 f}{\partial x^2}(t,X(t))]dt \\ &+ \sigma(t,X(t))\frac{\partial f}{\partial x}(t,X(t))dW(t). \end{aligned} \tag{1.96}$$

Proof. By applying Taylor's expansion to the function f we have

$$\begin{aligned} df(t,X(t)) =&\frac{\partial f}{\partial t}(t,X(t))dt + \frac{\partial f}{\partial x}(t,X(t))dX(t) \\ &+\frac{1}{2}[\frac{\partial^2 f}{\partial x^2}(t,X(t))(dX(t))^2 + \frac{\partial^2 f}{\partial t^2}(t,X(t))(dt)^2 \\ &+2\frac{\partial^2}{\partial t\partial x}(t,X(t))dX(t)dt] + ... \end{aligned} \tag{1.97}$$

By using Table 1.1, all terms containing $(dt)^p$ for $p > 1$ in equation (1.97) are zeros and then we obtain formula (1.95). By substituting (1.94) to the equation (1.95) and using Table 1.1 we obtain (1.96). □

Chapter 2

Survival probability and optimal arrangement of holes

The work in this chapter concerns chase-capture problems in lattices with hiding places. Chase-capture problems have been studied extensively in the past. Many scenarios have been considered such as chase and capture for one chaser and one escaper [32], multiple-pursuer with one evader [2], one pursuer against multiple-evaders [33, 34] and multiple-pursuers with multiple-evaders [35, 36, 37]. The rising impacts of several predators on prey are addressed in [38]. In the last few decades there have been many studies of the optimal strategies for the pursuers or evaders [39, 40, 41, 42, 43, 44]. In [39] the authors investigate for two agents (pursuer and evader) deterministic motion strategies that optimize the opportunities of pursuit or evasion. Weihs and Webb [40] conducted a kinematic analysis to find out whether there is an optimal avoidance and evasion strategy for the prey. Nair et al. [41] argue that escaping in the optimal direction [40], or by varying its direction randomly [45, 46] does not necessarily enhance the prey survival. This study believe that prey survival is increased when the prey identify the threat and scape from a greater distance. When predation risk is uniformly distributed across the foraging environment, the prey animals concentrate their efforts over smaller numbers of foraging patches [47].

The prey survival has been studied extensively in the past few decades [2, 22,

23, 48]. Most studies on the survival of the evaders have been conducted in the absence of the hiding places. It has recently been noted [3] that, at least in some cases, the pattern of hiding places (e.g. burrows) created by prey species is regular at large spatial scales. It is speculated that this arrangement increases fitness by reducing predation risk. The work in this chapter is motivated in part by the desire to understand the survival advantage conferred by optimizing hiding place arrangements. Before we introduce our model we briefly review other work that study the prey survival using statistical physics. Oshanin et al. [2] studied the survival probability of a prey hunted by multiple predators performing random walks on a square lattice. They studied the prey survival probability of the stay still strategy against least-effort escape strategy in which the prey attempts to evade the predators by moving one step away from the predator whenever any of the predators appears within its sighting range, otherwise the prey stays still. The study showed that the least-effort escape strategy leads to a significant rise of the prey survival probability in comparison with the stay still strategy. In the case of the least-effort strategy when the sighting range of both the prey and the predators equal to one step, then at least three predators are required to catch the prey. Krapivsky and Redner [22] studied the survival probability of a prey $S_N(t)$ hunted by N independent predators preforming random walks in one dimension. The prey survival probability for the previous model calculated exactly using probabilistic techniques in [23] for very small number of predators. The prey survival probability in the presence of a hiding place (the probability that the prey reaches the hiding place before being eaten by the predator) studied in [48] for one prey hunted by N predators diffusing in one dimension. For given initial positions x and $L > x$ for the prey and predator respectively, the study found that for large and finite N the prey survival probability S_N behave asymptotically as $S_N(z) \sim N^{-z^2}$ where $z = x/L$.

To our knowledge, the prey survival problems when one prey is hunted by one predator in the presence of hiding places have not been studied using statistical physics approaches, and lattice models. In this chapter, we investigate the prey

survival probability in a two dimensional system in the presence of hiding places, and we study the effect of the shape of the system on the prey survival probability. Moreover, we investigate the optimal arrangement of hiding places that maximize the prey survival probability in different shape of systems. We find exact expressions for the prey survival probability for one hole, and we approximately compute the optimal survival probability for n holes. This is compared to the survival probability in a null model where holes are arranged randomly in space.

2.1 Walk on a lattice with holes

In this chapter we model a chase-capture problem of one prey hunted by a predator in the presence of holes for the prey to hide in. Our work is inspired by the work done in [2]. Oshanin et al. [2] analyse the prey survival probability on a lattice when there are no holes for the prey to hide in. Here we explore chase-capture problem in similar way using lattice model but our contribution is to study how the presence of holes effects prey survival. In this model the prey and predator perform a simple random walk on a rectangular $L_1 \times L_2$ lattice with n holes. The prey and predator are moving in discrete time. For the sake of the mathematical tractability we try to keep the rules of the walks as simple as possible. We assume the prey has a perfect memory for where the holes are. In the next chapter we consider the case when the prey memory decline with time and we will examine the shape of the region the prey remembers. The predator has no knowledge of the location of the prey hiding places and how the prey move. The distance between the prey and the predator is measured by Manhattan distance d which is defined between any two points (x_1, y_1) and (x_2, y_2) as

$$d = |x_1 - x_2| + |y_1 - y_2|. \tag{2.1}$$

A precise definition of the walk rules are:

1) The predator always moves to the prey. For visual illustration of how the predator moves see figure 2.1.

2) When the distance between the prey and predator is more than two steps ($d > 2$), then the prey performs random walk.

3) When $d = 2$ the prey stays still.

4) When $d = 1$ then the prey moves according to the following rules:

   (a) If the prey, predator and the hole are in a horizontal line and the predator is between the prey and the hole, then the prey moves up or down with equal probability.

   (b) If the prey, predator and the hole are in a vertical line and the predator is between the prey and the hole, then the prey moves left or right with equal probability.

   (c) Otherwise, the prey moves to the closest hole if it is safe to do so, or else the prey moves away from the predator.

5) At each time step when the distance between the prey and the predator is equal to one step, the predator catches the prey with probability ϵ.

6) During the chase, the prey and predator are permitted to exceed the boundary of the system. Figure 2.2 gives a visual illustration of how the prey moves when $d = 1$.

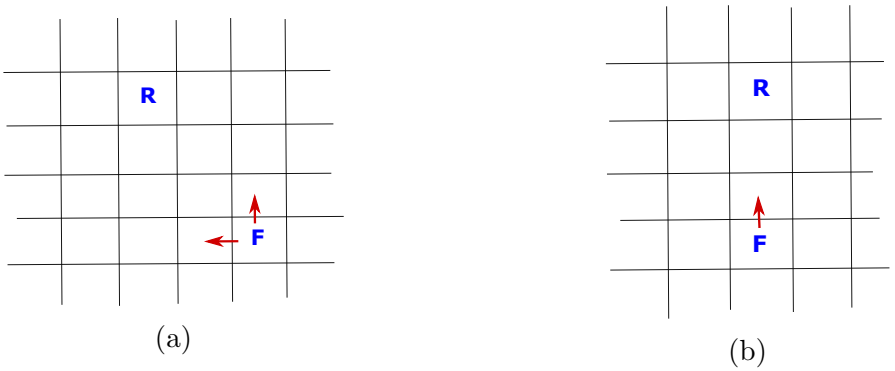

Figure 2.1: The walk rules for the predator. The letters F and R represent the predator (Fox) and the prey (Rabbit) respectively. The red arrows show the possible directions of the next step for the predator.

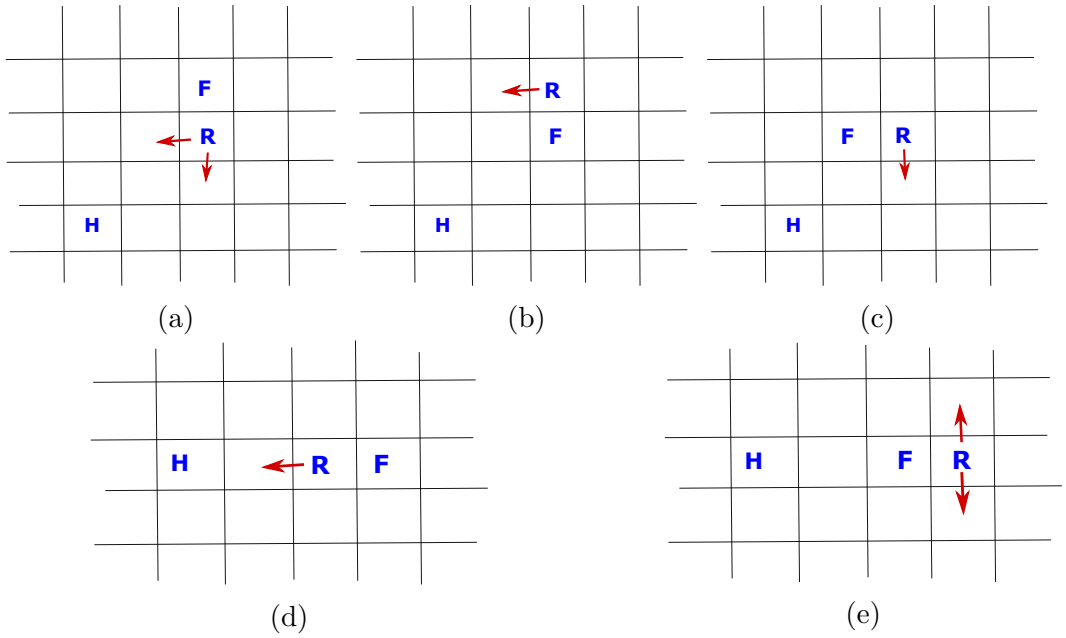

Figure 2.2: How the prey moves when the distance between the prey and the predator is one step. The three letters R, F and H represent the prey, predator and the closest hole respectively. The red arrows show the possible directions of the next step for the prey.

In this chapter we aim to calculate exactly the prey survival probability, and investigate the effect of the shape of the home range by varying L_1 and L_2 without changing the system size $L_1 \times L_2 = 10000$. We explore the optimal arrangement of holes that maximizes the prey survival probability inside different system shapes. In the following two sections we calculate the prey survival probability exactly for a few scenarios that may occur nearby a hole. We then compute the survival probability starting from any location.

2.1.1 Exact result when prey is near a hole

In this section we aim to calculate exactly the prey survival probability for a few scenarios that may occur when the chase started near a hole. We represent the prey, the predator and the hole by three letters R, F and H respectively. The notation $\overline{R}$ and $\overline{F}$ indicates the next move is for the prey and the predator respectively. Let P_k for $k \in \mathbb{N}_0$ be the prey survival probability when the chase started from the k-th scenario and t_i be the prey survival probability in one situation i for $i \in \mathbb{N}$. When

the distance between the prey and the predator $d = 1$ we have $t_i = 1 - \epsilon$, otherwise $t_i = 1$.

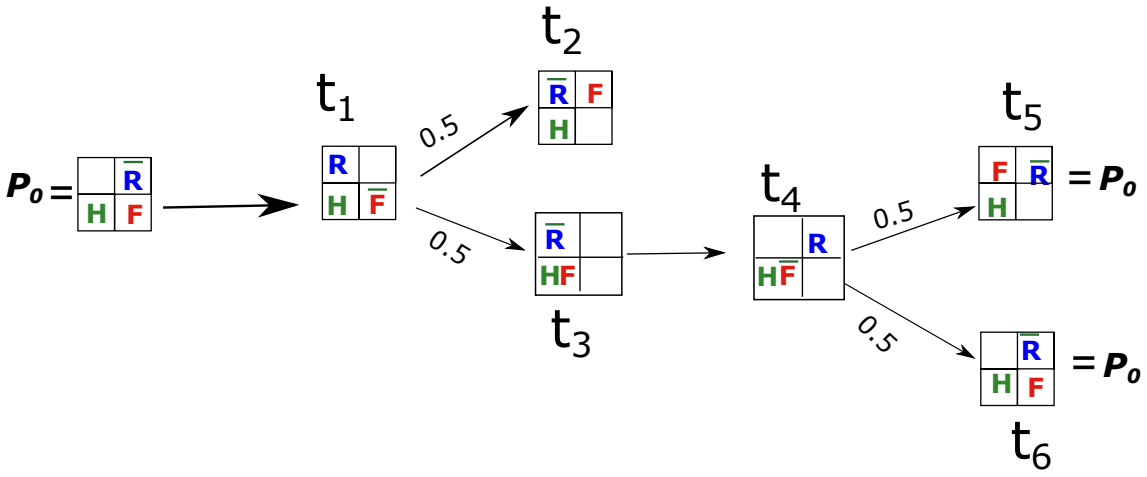

Figure 2.3: Tree digram of a scenario when the chase started near a hole. The three letter R, F and H are representing the prey, the predator and the hole respectively.

Example 2.1.1. *The prey survival probability of the scenario shown in figure 2.3. In this tree calculation we considered all possible states that we can go from where we are now. Some roots take us back again to where we started and close the equation to allow us solve the equation.*

$$\begin{aligned} P_0 &= \frac{1}{2}t_1t_2 + \frac{1}{4}t_1t_3t_4t_5P_0 + \frac{1}{4}t_1t_3t_4t_6P_0 \\ &= \frac{1}{2}(1-\epsilon) + \frac{1}{2}(1-\epsilon)^2P_0. \end{aligned} \tag{2.2}$$

Solving the equation for P_0 yield

$$P_0 = \frac{1-\epsilon}{2-(1-\epsilon)^2}. \tag{2.3}$$

For $\epsilon = 0.01$, the prey survival probability for the given scenario is $P_0 = 0.970683$. Figure 2.4 shows that the simulation is consistent with exact calculation.

Example 2.1.2. *The prey survival probability of the scenario shown in figure 2.5*

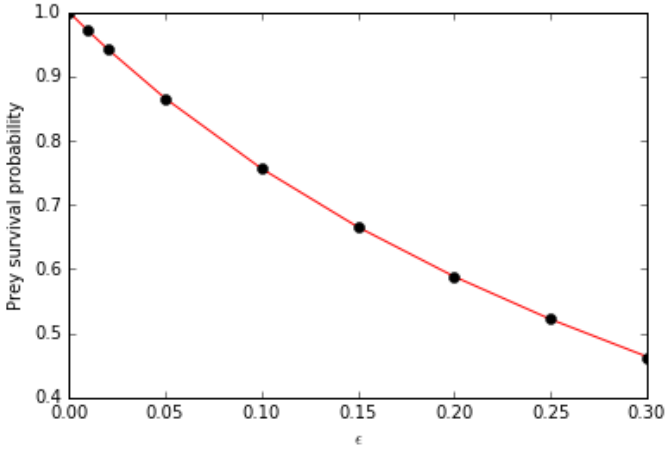

Figure 2.4: Prey survival probability calculated by simulation for various values of ϵ assuming the starting position shown in figure 2.3 and done as sanity check of the formula (2.3) . The red line represent the exact prey survival probability using the formula (2.3) and the dots are obtained from simulation.

can be calculated in similar way and we have

$$\begin{aligned} P_1 &= \frac{1}{4}t_1t_3t_4t_6 + \frac{1}{8}t_1t_3t_5t_7 + \frac{1}{8}t_1t_3t_5t_8 + \frac{1}{8}t_2t_9t_{11}t_{12} + \frac{1}{8}t_2t_9t_{11}t_{13} + \frac{1}{4}t_2t_{10}t_{14}t_{15} \\ &= \frac{1}{4}(1-\epsilon)^2 + \frac{1}{8}(1-\epsilon)^2 + \frac{1}{8}(1-\epsilon)^2 + \frac{1}{8}(1-\epsilon)^2 + \frac{1}{4}(1-\epsilon)^2 \\ &= (1-\epsilon)^2. \end{aligned} \tag{2.4}$$

For $\epsilon = 0.01$ the prey survival probability is $P_1 = 0.98$ which is consistent with simulation result.

Example 2.1.3. *The survival probability when the chase start from the scenario shown in figure 2.6 can be calculated in similar way as the previous scenarios and we have*

$$P_2 = \frac{3 - 5\epsilon - 5\epsilon^2 + 15\epsilon^3 - 10\epsilon^4 + 2\epsilon^5}{(-3 - 2\epsilon + \epsilon^2)(-1 - 2\epsilon + \epsilon^2)}. \tag{2.5}$$

For $\epsilon = 0.01$ we have $P_2 = 0.958$ which is consistent with simulation.

Example 2.1.4. *The survival probability starting from the scenario shown in figure*

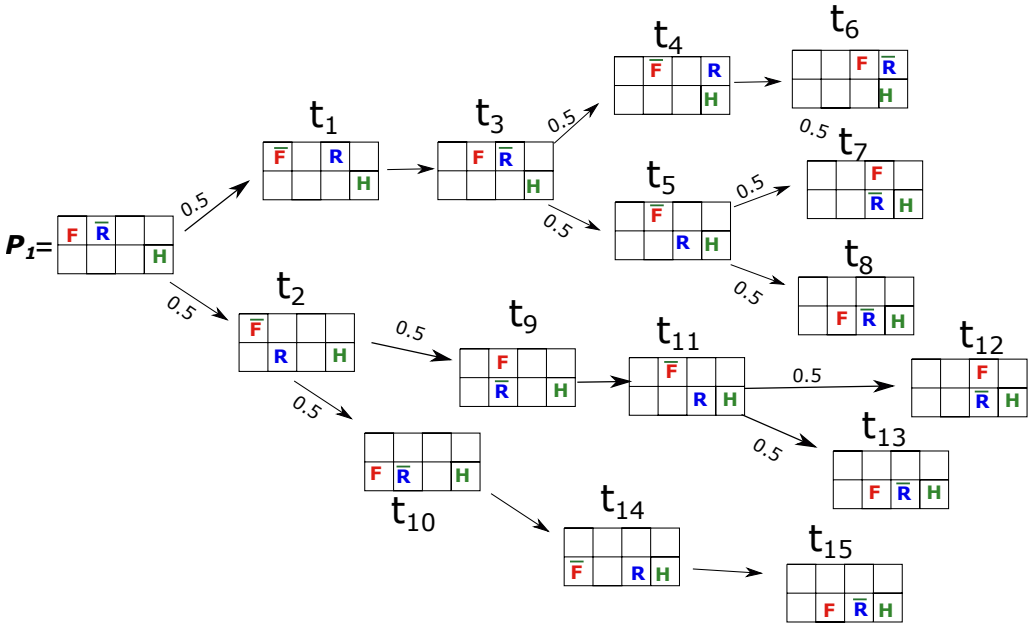

Figure 2.5: Tree digram of a scenario when the chase started near a hole and the predator is not between the prey and the closest hole.

Figure 2.6: A scenario when the prey, predator and hole are on a line.

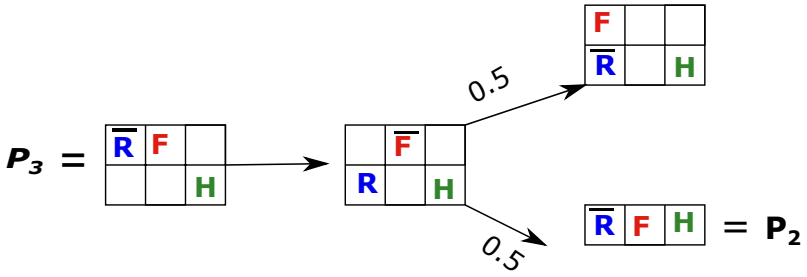

Figure 2.7: Another scenario when the chase started near a hole

2.7 is

$$P_3 = \frac{1}{2}(1-\epsilon)P_2 + \frac{1}{2}(1-\epsilon)^2. \tag{2.6}$$

By substituting the value of P_2 *from (2.5) we obtain*

$$P_3 = \frac{(2\epsilon^5 - 10\epsilon^4 + 15\epsilon^3 - 5\epsilon^2 - 5\epsilon + 3)(1-\epsilon)}{2(\epsilon^2 - 2\epsilon - 3)(\epsilon^2 - 2\epsilon - 1)} + \frac{1}{2}(1-\epsilon)^2 \tag{2.7}$$

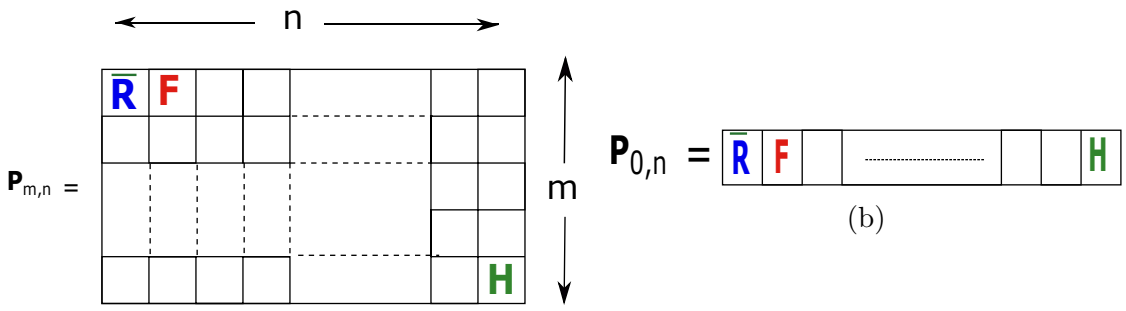

(a) (b)

Figure 2.8: Two scenarios when the chase started far from the closest hole . Left: a scenario when the chase started while the prey m vertical steps and n horizontal steps from the closest hole. Right: a scenario when the chase started while the prey $m = 0$ vertical steps and n horizontal steps from the closest hole .The three letter R, F and H are representing the prey, the predator and the hole respectively.

2.1.2 Survival probability for general starting point

Let $P_{m,n}$ for $m, n \in \mathbb{N}$ be the prey survival probability when the predator is between the prey and the closest hole and the prey is m vertical steps and n horizontal steps from the closest hole in the system. For the scenario shown in figure 2.8, for $m = 1$ and $n \in \mathbb{N}$ the prey survival probability is

$$P_{1,n} = \frac{1}{2}(1-\epsilon)P_{0,n} + \frac{1}{2}(1-\epsilon)^n, \tag{2.8}$$

where the first term in the right hand side corresponding to the case where the prey moves down and the predator moves down as well (shown in figure 2.8b) and the second term corresponding to the case where the prey moves down and the predator moves left. For $m = 2$ and $n \in \mathbb{N}$ we have

$$P_{2,n} = \frac{1}{2}(1-\epsilon)P_{1,n} + \frac{1}{2}(1-\epsilon)^{n+1}, \tag{2.9}$$

by substituting (2.8) and rearranging we obtain

$$P_{2,n} = \frac{1}{2^2}(1-\epsilon)^2 P_{0,n} + \big(\frac{1}{2} + \frac{1}{2^2}\big)(1-\epsilon)^{n+1}. \tag{2.10}$$

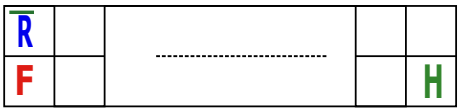

Figure 2.9: A situation result from the situation shown in figure 2.8b where the prey moves up and the predator moves left.

Similarly for $m = 3$ and $n \in \mathbb{N}$ we have

$$P_{3,n} = \frac{1}{2^3}(1-\epsilon)^3 P_{0,n} + \big(\frac{1}{2} + \frac{1}{2^2} + \frac{1}{2^3}\big)(1-\epsilon)^{n+2}. \tag{2.11}$$

Now we can deduce the prey survival probability for any $m, n \in \mathbb{N}$ to have

$$\begin{aligned} P_{m,n} &= \frac{1}{2^m}(1-\epsilon)^m P_{0,n} + (1-\epsilon)^{n+m-1} \sum_{k=1}^{m} \frac{1}{2^k} \\ &= \frac{1}{2^m}(1-\epsilon)^m P_{0,n} + (1-\epsilon)^{n+m-1}(1 - \frac{1}{2^m}). \end{aligned} \tag{2.12}$$

The survival probability $P_{0,n}$, this scenario shown in figure 2.8(b), is given by

$$P_{0,n} = \frac{1}{2}(1-\epsilon)P_{1,n} + \frac{1}{2}(1-\epsilon)P_{n,1}, \tag{2.13}$$

where the first term in the right hand side corresponding to the case where the prey moves up and the predator moves up as well and the second term corresponding to an equivalent situation (shown in figure 2.10) of the case where the prey moves up and the predator moves left (shown in figure 2.9). Note that the order of indices on P in the second term has been reversed. This is because the situation in figure 2.9 cannot be captured using our notation, but is equivalent to the situation obtained by rotating the system 90° about the hole and then reflecting about the vertical line between the hole and the predator. By substituting (2.8) and rearranging we obtain

$$P_{0,n} = \frac{\frac{1}{4}(1-\epsilon)^{n+1} + \frac{1}{2}(1-\epsilon)P_{n,1}}{1 - \frac{1}{4}(1-\epsilon)^2} \tag{2.14}$$

Now we need to derive a formula to calculate the prey survival probability $P_{n,1}$ when the chase start from the situation shown in figure 2.10

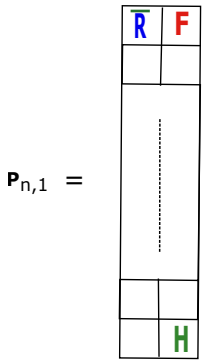

Figure 2.10: The equivalent situation of the scenario shown in figure 2.9

For $n = 2$ we have

$$P_{2,1} = \frac{1}{2}(1-\epsilon)^2 + \frac{1}{2}\frac{(1-\epsilon)^2}{2-(1-\epsilon)^2} \tag{2.15}$$

For $n = 3$ we have

$$\begin{aligned} P_{3,1} &= \frac{1}{2}(1-\epsilon)^3 + \frac{1}{2^2}(1-\epsilon)^3 + \frac{1}{2^2}\frac{(1-\epsilon)^3}{2-(1-\epsilon)^2} \\ &= \left(\frac{1}{2} + \frac{1}{2^2}\right)(1-\epsilon)^3 + \frac{1}{2^2}\frac{(1-\epsilon)^3}{2-(1-\epsilon)^2} \end{aligned} \tag{2.16}$$

For $n = 4$ we have

$$\begin{aligned} P_{4,1} &= \frac{1}{2}(1-\epsilon)^4 + \frac{1}{2^2}(1-\epsilon)^4 + \frac{1}{2^3}(1-\epsilon)^4 + \frac{1}{2^3}\frac{(1-\epsilon)^4}{2-(1-\epsilon)^2} \\ &= \left(\frac{1}{2} + \frac{1}{2^2} + \frac{1}{2^3}\right)(1-\epsilon)^4 + \frac{1}{2^3}\frac{(1-\epsilon)^4}{2-(1-\epsilon)^2} \end{aligned} \tag{2.17}$$

It can be proved by induction that

$$\begin{aligned} P_{n,1} &= (1-\epsilon)^n \sum_{k=1}^{n-1} \frac{1}{2^k} + \frac{1}{2^{n-1}}\frac{(1-\epsilon)^n}{2-(1-\epsilon)^2} \\ &= (1-\epsilon)^n(1-2^{1-n}) + \frac{1}{2^{n-1}}\frac{(1-\epsilon)^n}{2-(1-\epsilon)^2} \end{aligned} \tag{2.18}$$

Substituting (2.18) in (2.14) gives

$$P_{0,n} = \frac{(1-\epsilon)^{n+1}\left[\frac{1}{4} + \frac{1}{2}(1-2^{1-n}) + \frac{1}{2^n}\frac{1}{2-(1-\epsilon)^2}\right]}{1-\frac{1}{4}(1-\epsilon)^2} \tag{2.19}$$

Substituting (2.19) in (2.12) yields

$$P_{m,n} = \left(1-2^{-m}\right)(1-\epsilon)^{m+n-1} + \frac{2^{-m}(1-\epsilon)^{m+n+1}}{1-\frac{1}{4}(1-\epsilon)^2}\left(\frac{2^{-n}}{2-(1-\epsilon)^2} + \frac{1}{2}\left(1-2^{1-n}\right) + \frac{1}{4}\right). \tag{2.20}$$

Now we aim to verify our generalised formula in (2.20) for special cases and compare it with our previous results when the chase start near a hole. By substituting $m = n = 1$ in our general formula and simplify we obtain

$$P_{1,1} = \frac{1-\epsilon}{1+2\epsilon-\epsilon^2}. \tag{2.21}$$

From figure 2.11 we can note that our generalised formula matches the result obtained in Example 2.1.1. For $m = 1$ and $n = 2$ our general formula may be reduced

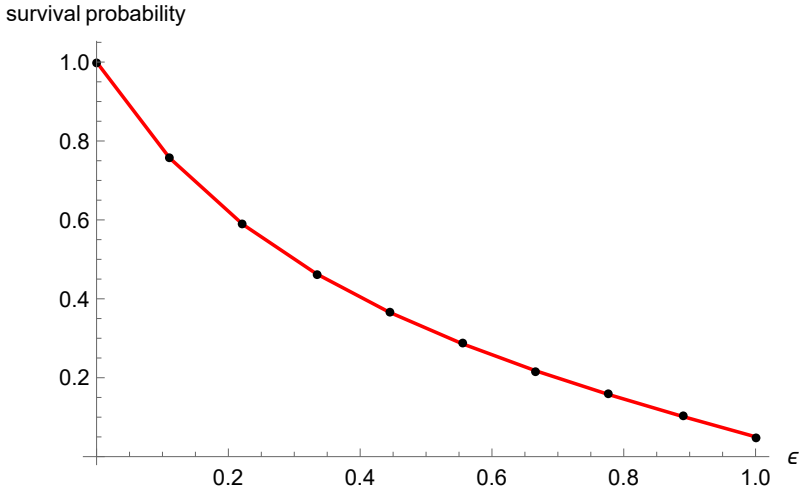

Figure 2.11: The prey survival probability for the scenario shown in figure 2.8a when $m = n = 1$ for various values of $0 \leq \epsilon \leq 1$. The dots represent the survival probability obtained by (2.21) and red line for (2.2).

to

$$P_{1,2} = -\frac{(\epsilon-1)^2\left(\epsilon^4-4\epsilon^3+7\epsilon^2-6\epsilon-6\right)}{2\left(\epsilon^4-4\epsilon^3+8\epsilon+3\right)} \tag{2.22}$$

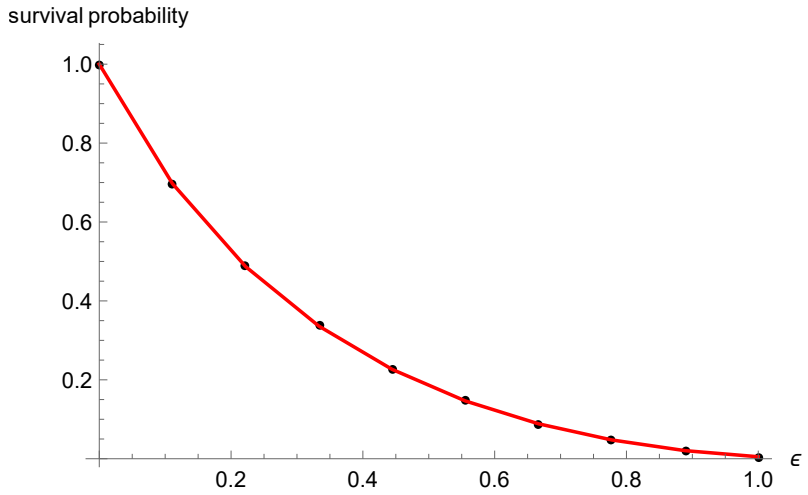

Figure 2.12: The prey survival probability when $m = 1$ and $n = 2$ for various values of $0 \leq \epsilon \leq 1$.The red line indicate the survival probability obtained by (2.22) and the dots represent the survival probability from (2.7) for $0 \leq \epsilon \leq 1$.

Figure 2.12 shows that (2.22) is consistence with the result in Example 2.1.4. Note that our formula in (2.20) is not symmetric, that is,

$$P_{m,n} \neq P_{n,m} \quad \text{for } m \neq n. \tag{2.23}$$

A reason for this is when the start form a situation where the prey and predator on a horizontal line, the prey will continue moving vertically towards the closest hole until reach the situation shown in figure 2.8(b)(the prey, predator and hole are in a horizontal line) or until the predator make a mistake and move to the site directly above the prey and be behind the prey. Our formula calculates the prey survival probability exactly for $m, n \in \mathbb{N}$ for scenarios when the chase start from a situation where the prey and predator on a horizontal line and the predator between the prey and the closest hole. A general formula to calculate the survival probability when the chase start from a scenario where the prey and predator are on a vertical line and the predator is between the prey and the closest hole can be obtained by

$$Q_{m,n} = \left(1 - 2^{-n}\right)(1-\epsilon)^{m+n-1} + \frac{2^{-n}\left(\frac{2^{-m}}{2-(1-\epsilon)^2} + \frac{1}{2}\left(1 - 2^{1-m}\right) + \frac{1}{4}\right)(1-\epsilon)^{m+n+1}}{1 - \frac{1}{4}(1-\epsilon)^2}. \tag{2.24}$$

Our formula in (2.20) can be written as

$$P_{m,n} = (1-\epsilon)^{m+n-1}\left(\frac{2^{2-m}\left(\frac{2^{-n}}{-\epsilon^2+2\epsilon+1} - 2^{1-n} + \frac{5}{4}\right)}{-\epsilon^2+2\epsilon+3} - 2^{-m} + 1\right) \tag{2.25}$$

$$\sim (1-\epsilon)^{m+n-1}\left[\left(\frac{5}{3+2\epsilon-\epsilon^2} - 1\right)2^{-m} + 1\right] \quad \text{as } n \to \infty, \tag{2.26}$$

the term $(1-\epsilon)^{m+n-1}$ gives us the survival probability after the early part of interaction (dance steps) between the prey and the predator (when the predator is behind the prey) and the remaining terms in (2.25) are the survival probability during the early part of interaction (dance steps) when the prey is trying to get a direct escape path to the hole. After number of steps, the predator will be within one step from the prey and a complicated interaction between the prey and predator begins followed by a chase where the predator following the prey. Once the chase begins the probability that the prey survival at each step is $(1-\epsilon)$. We later presume that the number of steps throughout the interaction (dance steps) is negligible in comparison with the number of steps separating the prey and the nearest hole. In this case we need only consider the asymptotic behaviour as $m, n \to \infty$, where

$$P_{m,n} \sim (1-\epsilon)^{m+n-1}.$$

Also, Consider the case when there is no interaction the survival probability $\sim (1-\epsilon)^{m+n-1}$. Table 2.1 shows the prey survival probability calculated for the scenario shown in figure 2.8(a) using different methods. From the table we observe that the prey survival probability can be approximated by $(1-\epsilon)^{d-1}$, where d is the Manhattan distance between the prey and the closest hole when the chase started.

2.1.3 Optimal arrangement of holes

A recent ecological study [3] found that prey animals dig their hiding places in a regular pattern at a large spatial scale. The study speculates that this arrangement increases fitness by reducing predation risk. In this section, we are going to consider

m	n	$(1-\epsilon)^{m+n-1}$	$P_{m,n}$	Simulation	Standard error
1	1	0.990	0.970683	0.970586	0.000055
2	1	0.9801	0.970538	0.970491	0.000048
10	5	0.868746	0.868723	0.868581	0.000088
10	10	0.826169	0.826147	0.825730	0.000096
20	10	0.747172	0.747172	0.747295	0.000160
20	20	0.675729	0.675729	0.675806	0.000089
20	30	0.611117	0.611117	0.611134	0.000141
40	40	0.452044	0.452044	0.452476	0.000108
50	50	0.369730	0.369730	0.369825	0.000170

Table 2.1: The prey survival probability for $\epsilon = 0.01$ in the case the chase start while the prey is m vertical steps and n horizontal steps from the closest hole calculated using different methods. The simulation computed for 10^6 trials as a sanity test.

a problem with multiple holes rather than one hole as previously discussed. In figure 2.13, we see a comparison of the survival probability with random arrangement of holes and with the optimal arrangement of holes. The optimal arrangement of holes has a notable impact on survival probability. Here we investigate the optimal arrangement of holes inside a $L_1 \times L_2$ lattice that maximizes the survival probability of the prey. In addition, we are interested in studying whether the shape of the home range affects the prey survival probability. The average prey survival probability for fixed set of holes can be calculated by

$$\mathbb{E}[P_{X,Y}] \simeq \frac{1}{L_1 \times L_2} \int_0^{L_2} \int_0^{L_1} p_{X,Y}(x,y)\, dxdy, \tag{2.27}$$

where $p_{X,Y}(x,y) = (1-\epsilon)^{-1+\min(d_1,..,d_k)}$ is the prey survival probability in one chase, and $d_k = d_k(x,y)$ for $k \in \mathbb{N}$ is the Manhattan distance defined in (2.1) from the position (x,y) of the prey when the chase started to the k-th hole in the system. In (2.27) we integrate the approximation of the prey survival probability (we neglect the dance term) instead of (2.25) for the sake of the mathematical tractability. To calculate the average prey survival probability for fixed set of holes we run a python code on the computer to compute (2.27) for all possible starting chase points on $L_1 \times L_2$ lattice. We then use numerical optimization (BFGS algorithm [49]) to find the optimal location of the set of holes that gives the highest survival probability.

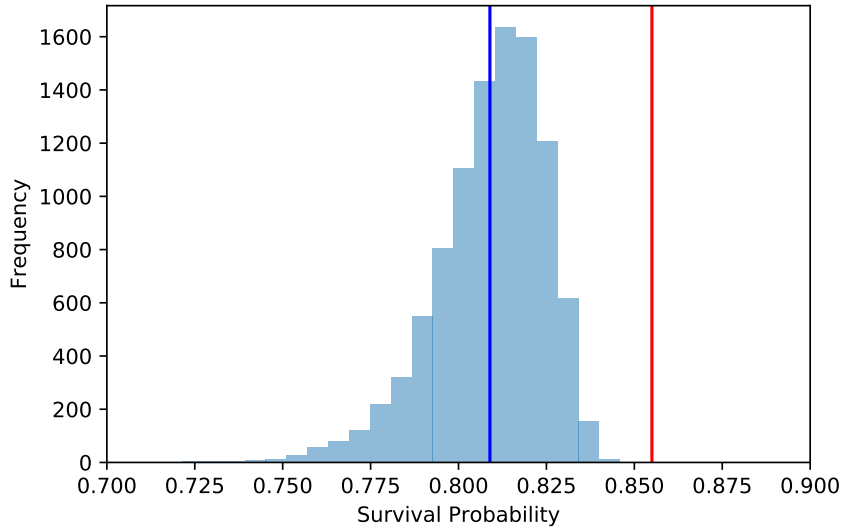

Figure 2.13: A comparison between the survival probability of random arrangement and optimal arrangements of 10 of holes. The blue line indicate the average survival probability with random arrangements and the red line for the optimal arrangement inside a symmetric system ($L_1 = L_2 = 100$) when $\epsilon = 0.01$.

Tables 2.2, 2.3 and 2.4 illustrate the approximate optimal arrangement of three, four and five holes inside different system shape with keeping the same system size. For visual illustration of the optimal arrangements of holes see figures 2.14-2.16. The effects of the shape of home range on survival probability are illustrate in figures 2.17-2.19. We observe that the survival probability drop when the home range stretched to the limit where the ratio $L_2/L_1 \lesssim 0.1$. We investigate the behaviour of survival probability for small ratios L_2/L_1 with optimal arrangement of n holes using exact method and compare it to our optimization. For small ratios the optimal arrangements of holes are arranged in a straight line. In this case we can think of our system as n small systems with one hole in the middle. The survival probability in this case can be calculate by

$$\begin{aligned}
\mathbb{E}[P_{X,Y}] &= \frac{4n}{L_1 \times L_2} \int_0^{\frac{L_2}{2}} \int_0^{\frac{L_1}{2n}} (1-\epsilon)^{x+y-1} dxdy \\
&= \frac{4n}{A} \int_0^{\frac{A}{2L_1}} \int_0^{\frac{L_1}{2n}} (1-\epsilon)^{x+y-1} dxdy \\
&= -\frac{4n\left(-1+(1-\epsilon)^{\frac{A}{2L_1}}\right)\left(-1+(1-\epsilon)^{\frac{L_1}{2n}}\right)}{A(\epsilon-1)\log(1-\epsilon)^2},
\end{aligned} \tag{2.28}$$

where $A = L_1 \times L_2$. Figure 2.20 shows a comparison between the results obtained by (2.28) against our optimization for different values of n. The difference shown for larger ratio L_2/L_1 between the two methods result from the fact that our exact formula designed for the cases when the n hole's optimal arrangement are in straight line. Figure 2.21 illustrate the survival probability with optimal arrangements of $3 \leq n \leq 10$ holes. We observe that the critical value of the ratio L_2/L_1 (the value of the ratio L_2/L_1 at which the survival probability starts dropping dramatically) are dependent on the number of holes n. We calculated numerically the critical values and we found that it is $\frac{1}{n}$ for n holes. When the ratio L_2/L_1 is equal or more than the critical value the shape of the system does not effect the survival probability and the survival probability decrease for ratios less than the critical value. The ϵ value is chosen to be $\frac{1}{\sqrt{L_1 \times L_2}}$, since the problem becomes more interesting about this value. For large or very small ϵ values the model is not realistic (either the prey always dies, or always survives) and the arrangements of holes become less relevant.

L_1	L_2	hole 1	hole 2	hole 3	p	standard error
100	100	$(22, 31)$	$(77, 30)$	$(50, 81)$	0.7457	0.0000125
125	80	$(26, 42)$	$(83, 18)$	$(94, 61)$	0.7446	0.000415
200	50	$(33, 25)$	$(101, 26)$	$(167, 24)$	0.7490	8×10^{-6}
250	40	$(40, 20)$	$(123, 20)$	$(207, 20)$	0.7377	0.0000143
500	20	$(252, 10)$	$(82, 9)$	$(418, 10)$	0.6422	0.0000221
1000	10	$(172, 6)$	$(502, 5)$	$(834, 5)$	0.4716	0.000108

Table 2.2: Survival probability p calculated with approximations of the optimal arrangements of three holes inside different system shapes with $L_1 \times L_2 = 10000$ when $\epsilon = 0.01$.

L_1	L_2	hole 1	hole 2	hole 3	hole 4	p	standard error
100	100	$(24, 74)$	$(77, 25)$	$(25, 23)$	$(74, 76)$	0.7801	0.0000133667
125	80	$(103, 57)$	$(22, 22)$	$(40, 62)$	$(83, 18)$	0.7765	0.000247784
200	50	$(125, 26)$	$(175, 24)$	$(75, 24)$	$(25, 25)$	0.7795	0.0000102773
250	40	$(31, 20)$	$(93, 20)$	$(157, 20)$	$(220, 20)$	0.7750	6.33122×10^{-6}
500	20	$(64, 10)$	$(193, 11)$	$(317, 10)$	$(439, 10)$	0.7042	0.0000106005
1000	10	$(127, 5)$	$(380, 4)$	$(629, 5)$	$(877, 6)$	0.5535	0.000033033

Table 2.3: Survival probability p calculated with approximations of the optimal arrangements of four holes inside different system shapes with $L_1 \times L_2 = 10000$ when $\epsilon = 0.01$.

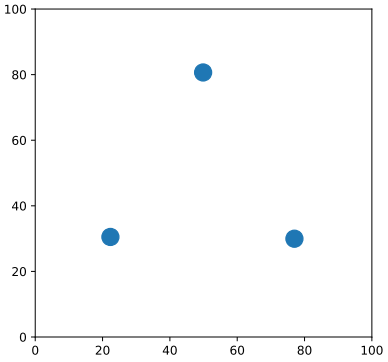

(a) The optimal arrangement of 3 holes when $L_1 = L_2 = 100$ approximately at $(22, 31), (77, 30)$ and $(50, 81)$ with $p = 0.75$

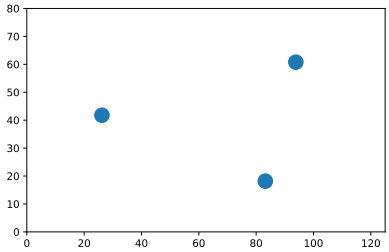

(b) The optimal arrangement of the tree holes when $L_1 = 120$ and $L_2 = 80$ approximately at $(26, 42), (83, 18)$ and $(94, 61)$ with $p = 0.75$

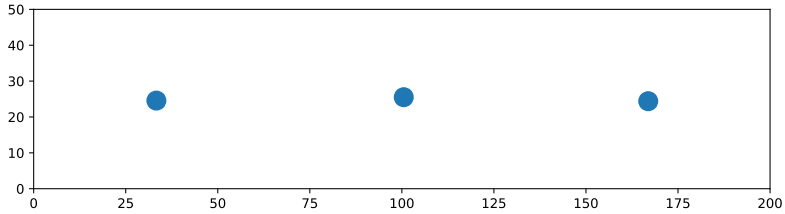

(c) The optimal arrangement of 3 holes when $L_1 = 200$ and $L_2 = 50$ approximately at $(33, 25), (101, 26)$ and $(167, 24)$ with $p = 0.75$

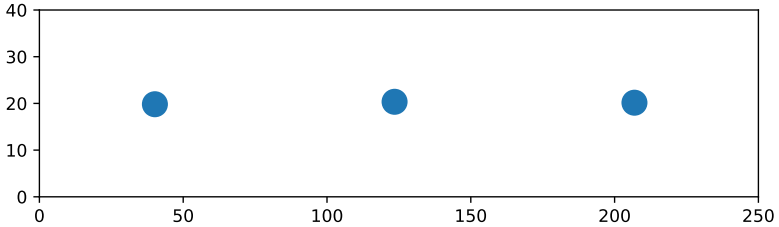

(d) The optimal arrangement of 3 hole approximately at $(40, 20), (123, 20)$ and $(207, 20)$ when $L_1 = 250$ and $L_2 = 40$.

(e) The optimal arrangement of 3 holes when $L_1 = 500$ and $L_2 = 20$.

Figure 2.14: Optimal arrangements of 3 holes when $\epsilon = 0.01$ inside different shapes of system. Blue dots represent holes.

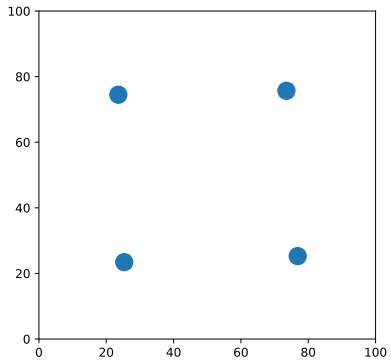

(a) Blue dots represent an approximation of the positions of the optimal arrangement of 4 holes when $L_1 = L_2$ and $\epsilon = 0.01$.

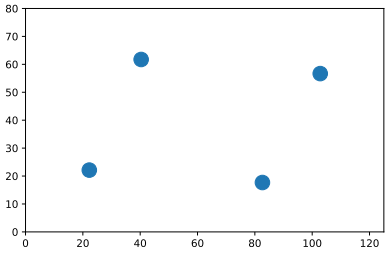

(b) Blue dots represent an approximation of the positions of the optimal arrangement of 4 holes when $L_1 = 125, L_2 = 80$ and $\epsilon = 0.01$.

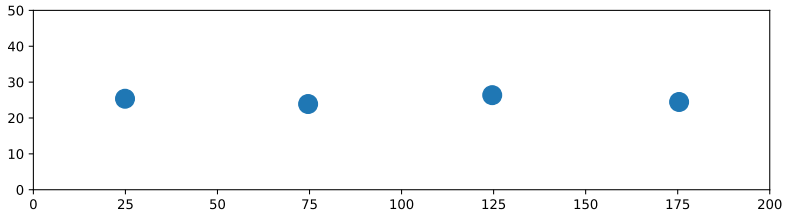

(c) Blue dots represent an approximation of the positions of the optimal arrangement of 4 holes when $L_1 = 200, L_2 = 50$ and $\epsilon = 0.01$.

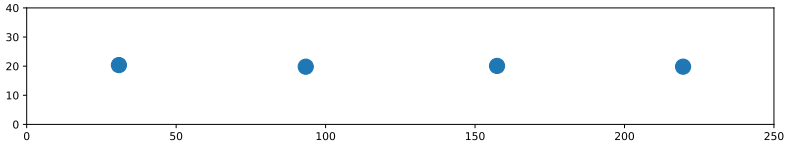

(d) Blue dots represent an approximation of the positions of the optimal arrangement of 4 holes when $L_1 = 250, L_2 = 40$ and $\epsilon = 0.01$.

(e) Blue dots represent an approximation of the positions of the optimal arrangement of 4 holess when $L_1 = 500, L_2 = 20$ and $\epsilon = 0.01$.

Figure 2.15: An approximation of the positions of the optimal arrangements of four holes for different system shapes.

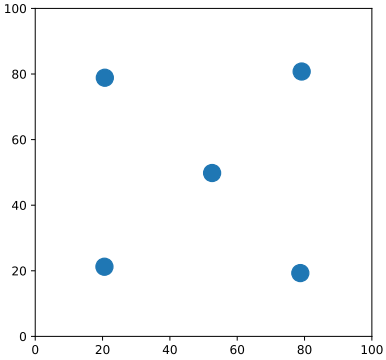

(a) Blue dots represent an approximation of the positions of the optimal arrangement of five holes when $L_1 = L_2 = 100$ and $\epsilon = 0.01$.

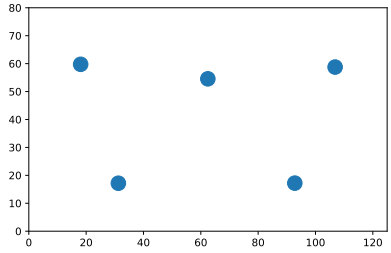

(b) Blue dots represent an approximation of the positions of the optimal arrangement of five holes when $L_1 = 125, L_2 = 80$ and $\epsilon = 0.01$.

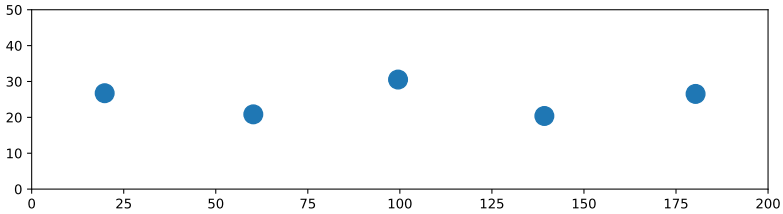

(c) Blue dots represent an approximation of the positions of the positions of the optimal arrangement of five holes when $L_1 = 200, L_2 = 50$ and $\epsilon = 0.01$.

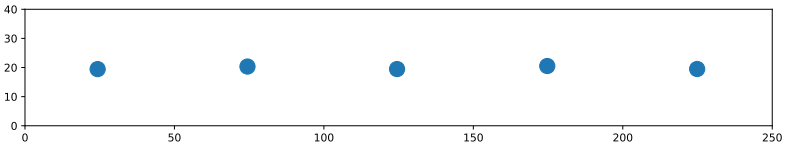

(d) Blue dots represent an approximation of the positions of the optimal arrangement of five holes when $L_1 = 250, L_2 = 40$ and $\epsilon = 0.01$.

Figure 2.16: An approximation of the positions of the optimal arrangements of five holes for different system shapes.

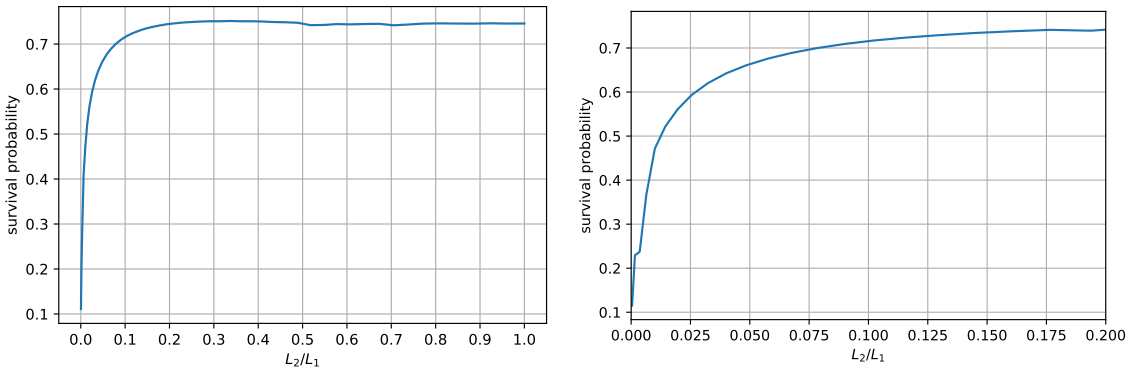

(a) (b)

Figure 2.17: (a) Survival probability with the optimal arrangement of 3 holes when $\epsilon = 0.01$ for various values of the ratio L_2/L_1. (b) a close look about the critical value of the ratio L_2/L_1.

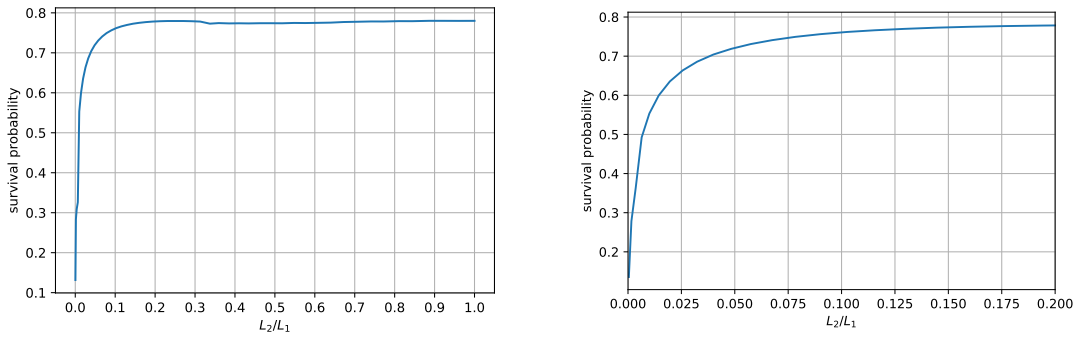

(a) (b)

Figure 2.18: (a) Survival probability with optimal arrangement of 4 holes when $\epsilon = 0.01$ against different values of the ratio L_2/L_1. (b) a close look at the curve when the ratio L_2/L_1 less than the critical value.

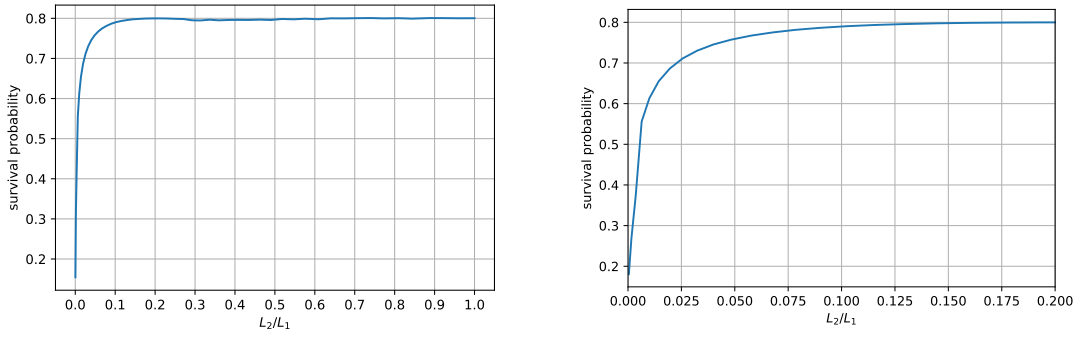

(a) (b)

Figure 2.19: (a) Survival probability with optimal arrangement of 5 holes when $\epsilon = 0.01$ against different values of the ratio L_2/L_1. (b) a close look at the curve beyond the critical value of the ratio L_2/L_1.

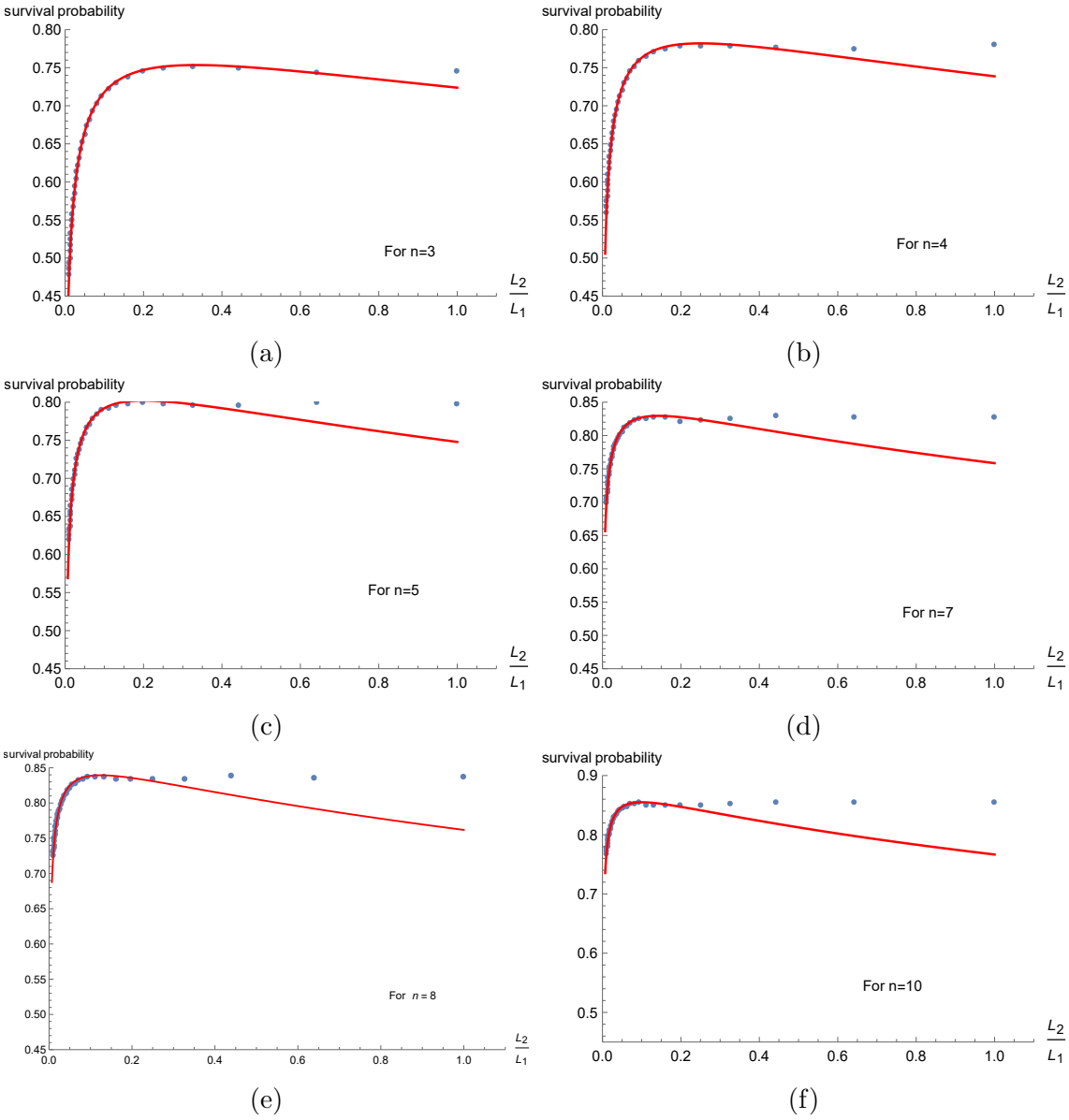

Figure 2.20: Survival probability with n holes when $\epsilon = 0.01$. Red line represent exact results using (2.28) and dots from numerical optimization.

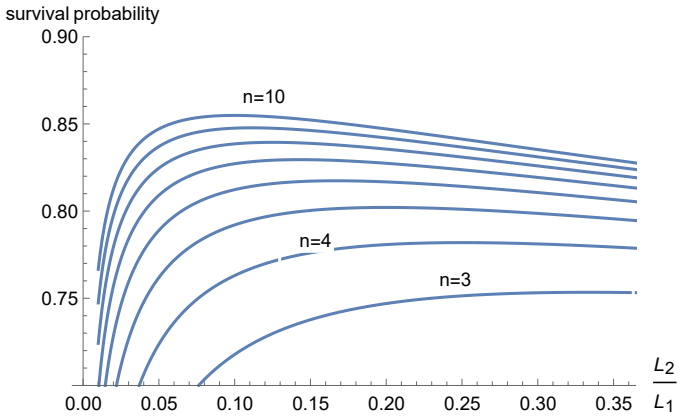

Figure 2.21: Survival probability with optimal arrangement of $3 \leq n \leq 10$ holes obtained by (2.28) when $\epsilon = 0.01$.

L_1	L_2	hole 1	hole 2	hole 3	hole 4	hole 5	p	standard error
100	100	$(79, 81)$	$(53, 50)$	$(21, 79)$	$(21, 21)$	$(79, 19)$	0.8003	0.000331919
125	80	$(93, 17)$	$(18, 60)$	$(107, 59)$	$(62, 55)$	$(31, 17)$	0.8000	0.00039964
200	50	$(20, 27)$	$(139, 20)$	$(60, 21)$	$(100, 31)$	$(180, 27)$	0.7988	0.000630782
250	40	$(24, 19)$	$(124, 19)$	$(74, 20)$	$(225, 19)$	$(175, 21)$	0.7987	9×10^{-6}
500	20	$(50, 10)$	$(451, 10)$	$(150, 11)$	$(351, 10)$	$(250, 10)$	0.7455	6×10^{-6}
1000	10	$(100, 5)$	$(300, 5)$	$(499, 5)$	$(699, 5)$	$(900, 5)$	0.6132	0.0000303139

Table 2.4: Survival probability p calculated with approximations of the optimal arrangements of five holes inside different system shapes with $L_1 \times L_2 = 10000$ when $\epsilon = 0.01$.

2.1.4 Conclusion

In this chapter we have studied a discrete chase and capture model on $L_1 \times L_2$ lattice with n holes for the prey to hide in. We derived a formula to calculate the prey survival probability exactly. Inside different shape of the home range (the shape of $L_1 \times L_2$ lattice) we succeed in attaining approximate optimal arrangements of holes that minimize the average distance between the prey and the closest hole in the system and maximize the prey survival probability. We then investigated the impact of the shape of home range on the prey survival probability and then explore the optimal arrangement of holes that maximize the prey survival probability. We observe that survival probability with optimal arrangement of n holes is independent of the shape of the home range when the ratio $L_2/L_1 \geq \frac{1}{n}$. For $L_2/L_1 \geq \frac{1}{n}$ it always there is an optimal arrangement of holes that ensure the maximum survival probability. From figure 2.13 we see than the optimal hole arrangement can substantially impact survival probability. The best arrangements are regular, reflecting field observations [3], and suggesting that digging burrows in a non-random spatial pattern may confer survival advantage. However, the benefits obtained by doing this must be balanced against the physiological cost of the larger brain [50] required to perform such a task. It has been noted that the optimal arrangement has other applications such as optimal facility location in operation research. The objective in optimal facility location is to identify the best location that that maximise the

spatial coverage [51, 52], convenience of facility users [53] or time efficiency [54]. In this chapter we considered the case where the prey has perfect memory of all hiding palaces and in the next chapter we consider the case when the memory of the prey declines with time and investigate the average shape of the region memorised.

Chapter 3

The shape of a memorised random walk

There is considerable interest among biologists in studying animal movement patterns and the evolutionary forces that influence them [55, 56, 57]. The foraging paths of many animals are reminiscent of random walks [58, 59], providing a connection to statistical physics. For generations the two fields are working together: the patterns of insect movement were first analysed in 1983 by modelling the movement as a correlated random walk [55]. This study provided analytic formulae to calculate the mean net displacement, giving an overview of the consequences of various searching behaviours. The growing availability of creature trajectory data in the last few decades [60] has prompted the modelling done by ecologists and physicists. Various random walks (discrete and continuous time) have been used for modelling animal foraging paths, for instance, Lévy walks [61, 62, 63, 64] are an optimal search strategy for locating targets when their densities are low [65], whereas Brownian movement is the most efficient searching strategy for the case of high density targets. Modelling animal trajectories using Markovian (memoryless) processes [19] is mathematically tractable. However, when trajectories are influenced by memory then more complicated processes are needed. Some organisms, such as hummingbirds [66] and bumblebees [67] follow regular foraging paths within their area, known as traplines

[68]. Some other foraging creatures such as monkeys and humans follow repeated long-distance relocations to sites visited in the past [69, 70], such behaviour leads to slow diffusion (logarithmic in time) and occupation patterns tend to a Gaussian distribution as a result of the balance between relocation to previously visited places and the effect of long range memory steps. From an evolutionary point of view, one must consider the prices and gains of spatial memory when considering its influence on animal movement [56]. The ability to remember cached food or hiding places, or to precisely navigate long distances, must be balanced against the physiological and metabolic expenditure of a larger brain [50], and the necessity of sleep [71]. Larger brains require additional tissue, which rises body mass and energetic expense [50]. Higher primates such as wild chimpanzees possess detailed Euclidean maps of their surroundings which enables them to select the most efficient route when returning to food sources, instead of following landmarks or repeated routes [11]. Maintenance of such maps demands a spatial memory which must be reinforced and sustained. The decline of this memory may highly affect movement patterns [72].

The relation between the shape of spatial memory and the memory (its rate of decline) is the centre of this chapter. By utilizing a method used to describe the shape of random walks [73], we link the asphericity (elongation) of the region memorised by a forager preforming a random walk to the rate of memory decay [14]. If the forager's trajectory is seen as a search path, then the shape of the mental map gives a description of the effective search region of the foraging animal. In literature we note another method for measuring the shape of random walks called convex hulls [74, 75]. This method is simple and effective for describing the shape of any type of random walks. In [74] given the distributions of the perimeter and the area of convex hulls of random walks in two dimensions. Shape measurement is a common way used for describing objects. In general the shape measurement techniques can be grouped in two classes [76]: boundary-based methods and region-based methods. In boundary-based method the shape is extracted from the object boundary only such as circularity (perimeter^2/area) [77], whereas in the region-based methods the

shape are obtain from the whole shape region such as convex hull [74] (convex hull of an object is the smallest convex shape that contains all the points of that object). For more information about the shape measuring techniques we refer the reader to [76]. The method used in this chapter is region-based.

3.1 Shapes of random walks

It has been known for several decades that the overall shape of random walks is not spherical [78, 79]. In the literature, there are several mathematical methods for the description of the shape of an object [79]. In [73] a well studied method is applied to describe the shape of random walks by utilising the radius of gyration tensor. If $\mathbf{r}^{(k)} = (r_1^{(k)}, r_2^{(k)}, .., r_d^{(k)})$ is the position vector of k-th step (for $1 \leq k \leq N$) of d-dimensional random walk, the gyration tensor $T = [T_{mn}]$ about the mass centre of the whole walk is defined as

$$T_{mn} = \frac{1}{N} \sum_{k=1}^{N} (r_m^{(k)} - r_m^{cm})(r_n^{(k)} - r_n^{cm}), \tag{3.1}$$

where $r_m^{(k)}$ is the m-th Cartesian coordinate of the position vector of the k-th step, and r_m^{cm} is the centre of mass of the m-th Cartesian coordinate of the position vector, and it is given by

$$r_m^{cm} = \frac{1}{N} \sum_{k=1}^{N} r_m^{(k)}. \tag{3.2}$$

The matrix T given in (3.1) is symmetric and positive definite [80], therefore it has d positive eigenvalues λ_i, and d orthogonal eigenvectors $\mathbf{v}_i$ (for $1 \leq i \leq d$). The eigenvalues, and the corresponding eigenvectors of the tensor T provide useful information about the shape of the random walk. The eigenvalue λ_i gives the mean square deviation of the walk locations from the centre of mass of the walk in the direction of the corresponding eigenvector $\mathbf{v}_i$. In case of two dimension walk the

gyration tensor can be written as

$$T = \begin{bmatrix} \frac{1}{N}\sum_{k=1}^{N}(x^{(k)} - x^{cm})^2 & \frac{1}{N}\sum_{k=1}^{N}(x^{(k)} - x^{cm})(y^{(k)} - y^{cm}) \\ \frac{1}{N}\sum_{k=1}^{N}(x^{(k)} - x^{cm})(y^{(k)} - y^{cm}) & \frac{1}{N}\sum_{k=1}^{N}(y^{(k)} - y^{cm})^2 \end{bmatrix}. \quad (3.3)$$

The shape of random walk in two dimensions may be approximated by an ellipse centred at (x^{cm}, y^{cm}) and given by

$$\mathbf{v}^T T^{-1} \mathbf{v} = \kappa^2, \quad (3.4)$$

where $\kappa > 0$ and $\mathbf{v} = \begin{bmatrix} x - x^{cm} \\ y - y^{cm} \end{bmatrix}$. If $\lambda_1 > \lambda_2$ are the eigenvalues of (3.3), then the semi-major axis and semi-minor axis (the eigenvectors of T) of the ellipse have lengths equal to $\kappa\sqrt{\lambda_1}$ and $\kappa\sqrt{\lambda_2}$ respectively. The choice of the parameter κ does not influence the asphericity, and this parameter will only be selected so that path of a random walk fits inside the ellipse.

3.1.1 Average shape of random walks

Averaging over the tensor T in order to find the average shape of the random walks will obscure information regarding anisotropy of the random walk. A better way is by averaging functions of the of eigenvalues of T obtained from the gyration tensor. The average asphericity, A_d^c, of d-dimension random walks is defined as [73]

$$A_d^c = \frac{\sum_{i>j}^{d} \mathbb{E}[(\lambda_i - \lambda_j)^2]}{(d-1)\mathbb{E}[(\sum_{i=1}^{d} \lambda_i)^2]}, \quad (3.5)$$

where the expectation are taken over all walks. The average asphericity, A_d^c, is a measure from 0 to 1 which gives the average deviation of the overall shape of the random walk from a spherical shape. The overall shape of the random walk is spherical if $A_2^c = 0$, and extremely elongated if $A_2^c = 1$. For unrestricted random

walk in d-dimensions the asphericity as in [73] is given by

$$A_d^c = \frac{2(d+2)}{(5d+4)}. \tag{3.6}$$

For example, the asphericity of a three dimensional unrestricted random walk is $A_3^c = \frac{10}{19} = 0.526316$. Rudnick [73] concludes that the asphericity of unrestricted random walk tend to the limit $\frac{2}{5}$ as $d \to \infty$, and the differentiation between unrestricted and restricted (self-avoiding) random walk becomes irrelevant [73] for $d > 4$. In the case of two dimension random walk, equation (3.5) can be reduced to

$$A_2^c = \frac{\mathbb{E}[(\lambda_1 - \lambda_2)^2]}{\mathbb{E}[(\lambda_1 + \lambda_2)^2]}. \tag{3.7}$$

It is worthwhile to remark that the concept of the average asphericity does not necessarily mean that there is a particular shape of the random walk. The random walks have wide ranges of shapes, and the average asphericity provides a general overview of the elongation of walks. To give some intuition about the behaviour of asphericity we define the "single walk" asphericity as

$$\widetilde{A_2^c} = \frac{(\lambda_1 - \lambda_2)^2}{(\lambda_1 + \lambda_2)^2}. \tag{3.8}$$

In example 3.1.1 we calculate the single walk asphericity $\widetilde{A_2^c}$ for a given set of points.

Example 3.1.1. *Consider the following set of points*

$$P = \{(0,0), (1,1), (2,2), (3,2), (3,4), (4,3)\}.$$

The centre of mass of P is

$$x^{cm} = \frac{1}{N}\sum_{k=1}^{N} x^{(k)} = \frac{13}{6}, \qquad y^{cm} = \frac{1}{N}\sum_{k=1}^{N} y^{(k)} = \frac{12}{6} = 2.$$

The gyration matrix T of the set P is given by (3.3), and the elements of T are

calculated as follows

$$\begin{aligned} T_{11} &= \frac{1}{N}\sum_{k=1}^{N}\left(x^{(k)} - x^{cm}\right)^2 \\ &= \frac{65}{36}, \\ T_{22} &= \frac{1}{N}\sum_{k=1}^{N}(y^{(k)} - y^{cm})^2 \\ &= \frac{5}{3}, \\ T_{12} &= \frac{1}{N}\sum_{k=1}^{N}\left(x^{(k)} - x^{cm}\right)\left(y^{(k)} - y^{cm}\right) \\ &= \frac{3}{2}. \end{aligned}$$

Then

$$T = \begin{bmatrix} T_{11} & T_{12} \\ T_{12} & T_{22} \end{bmatrix} = \begin{bmatrix} \frac{65}{36} & \frac{3}{2} \\ \frac{3}{2} & \frac{5}{3} \end{bmatrix}. \tag{3.9}$$

The eigenvalues of T *are* $\lambda_1 = 3.23772$*, and* $\lambda_2 = 0.234504$*. The asphericity of the set* P *is*

$$\widetilde{A_2^c} = \frac{(\lambda_1 - \lambda_2)^2}{(\lambda_1 + \lambda_2)^2} = 0.748096.$$

The shape of the set P *is described by (3.4) as shown in figure 3.1 .*

3.2 Memorised random walks

While a foraging animal is exploring its landscape, perhaps searching for food or evading predation, a mental map of its surrounding is being formed [11]. Such mental map formation requires the forager to memorise the sites it previously visited. In order to model the mental map (the set of points/locations at certain times that stays in the memory may be viewed as a map) of the forger we exploit a non-homogenous Poisson point process on $[0, \infty)$ with intensity function $\lambda(t) = c\mu(t)$ where c is a positive constant and $\mu(t)$ is a non-increasing probability density

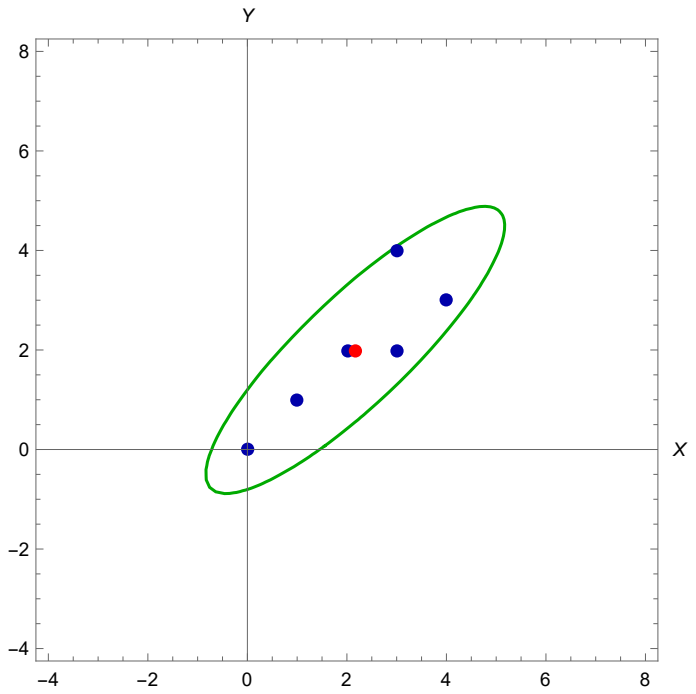

Figure 3.1: The shape of the set P (blue dots) is approximated by an ellipse centred at the centre of mass of P and given by equation (3.4) when $\kappa = 5$. The red dot represent the centre of mass of the set P.

function of a continuous probability distribution supported on $[0, \infty)$ with finite mean so that its arrival times are viewed as the set of times so that the corresponding locations (observed at these times) of the forager are stored in the memory. We refer to the function $\mu(t)$ as the memory kernel of the walk. The constant $c > 0$ might be viewed as controlling the overall rate of memory formation. Indeed the constant c gives us the mean number of observations, since $\mathbb{E}[|S|] = \int_0^\infty \lambda(t)dt = c$. The one-dimensional memorised random walk is defined as $\{W(t) : t \in S \cup \{0\}\}$ where $\{W(t)\}_{t\geq 0}$ is a standard Brownian motion introduced previously in Definition 1.3.4. For technical reason, we have appended the time $t = 0$ in the memory. If $t_k \in S$ is $k-$th arrival time, the memorised walk is generated by

$$W(t_{k+1}) - W(t_k) \sim \mathcal{N}(0, t_{k+1} - t_k), \tag{3.10}$$

where $\mathcal{N}(\mu, \sigma)$ is the normal distribution with expected value μ and variance σ^2. Figure 3.2 shows an example of a one dimensional Brownian motion and the corresponding memorised Brownian motion.

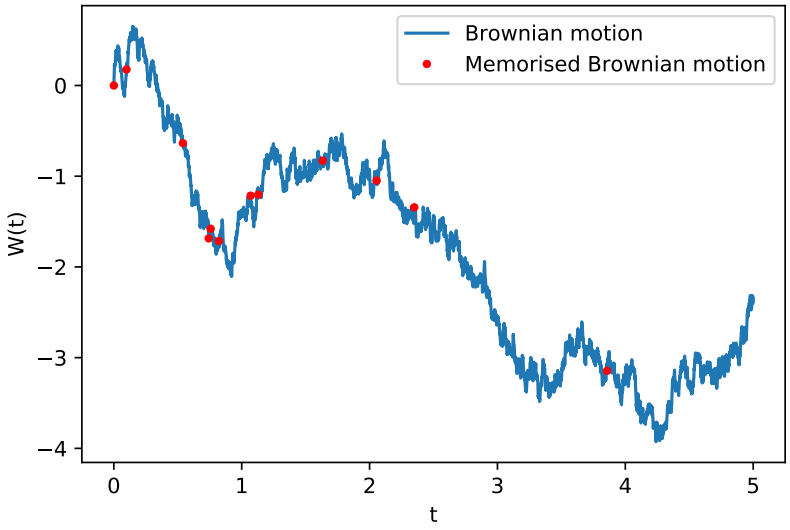

Figure 3.2: One dimensional memorised Brownian motion for the memory kernel $\mu(t) = e^{-t}$ when $c = 50$.

In similar way as in one dimension memorised Brownian motion, the two dimension memorised Brownian motion is defined as

$$\{(W_1(t), W_2(t)) : t \in S \cup \{0\}\}, \tag{3.11}$$

where $W_1(t)$ and $W_2(t)$ are independent standard Brownian motions. Figure 3.3 illustrates an example of Two-dimension Brownian motion and the corresponding memorised walk to give an idea of what is hearby meant by a memorised walk.

3.3 The shape of memorised random walks

The trajectory of a particle (e.g. a foraging animal) is modelled as two dimensional standard Brownian motion $\{(X(t), Y(t))\}_{t\geq 0}$. Since Brownian motion is time reversal invariant (see Proposition 1.3.3), we reversed the conventional direction of time so that $t = 0$ represent the current time and by increasing t we go further into the past. From the definition, we know that $X(0) = Y(0) = 0$ and therefore the current location of the foraging animal is the origin. The time was reversed so that we could model the end of the walk as the origin of coordinates and hence consider standard

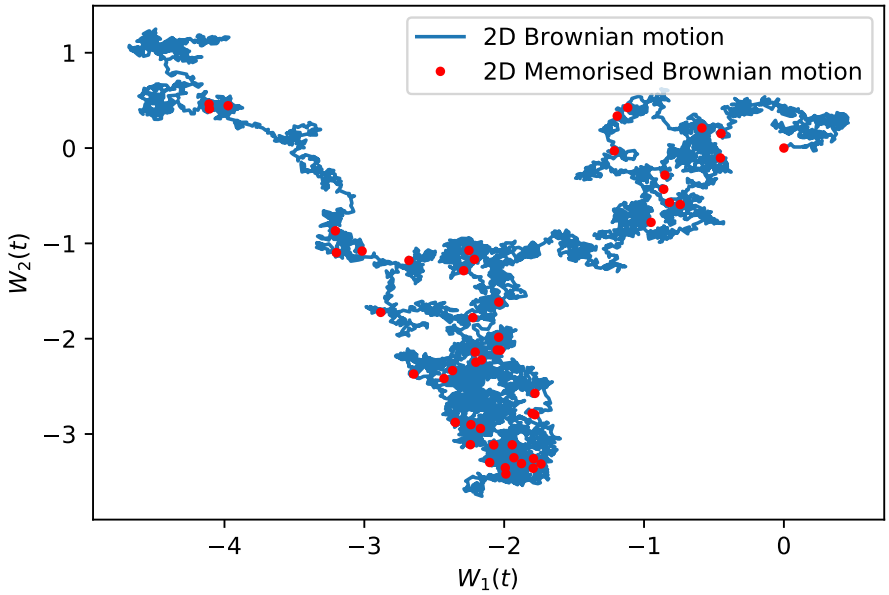

Figure 3.3: Two dimension memorised walk for the uniform memory kernel $\mu(t) = \frac{1}{\tau}$ when walk duration $\tau = 5$ and $c = 200$.

Brownian motion. The memorised random walk is defined by equation (3.11), that is,

$$L = \{(X(t), Y(t)) : t \in S \cup \{0\}\}, \tag{3.12}$$

where X and Y are two independent one-dimension standard Brownian motions. The egocentric gyration tensor (by using equation (3.3)) of the locations in memory, the set L, is

$$T = \begin{bmatrix} T_{11} & T_{12} \\ T_{12} & T_{22} \end{bmatrix} = \begin{bmatrix} \frac{1}{1+|S|}\sum_{t\in S} X^2(t) & \frac{1}{1+|S|}\sum_{t\in S} X(t)Y(t) \\ \frac{1}{1+|S|}\sum_{t\in S} X(t)Y(t) & \frac{1}{1+|S|}\sum_{t\in S} Y^2(t) \end{bmatrix}. \tag{3.13}$$

The egocentric asphericity in two-dimensions defined in similar way as in (3.7) and it is

$$\text{ego-}A_2 = \frac{\mathbb{E}[(\lambda_1 - \lambda_2)^2]}{\mathbb{E}[(\lambda_1 + \lambda_2)^2]}, \tag{3.14}$$

where λ_1 and λ_2 are the eigenvalues of the egocentric gyration tensor defined in (3.13). The term egocentric refers to the fact that the entries of the egocentric gyration tensor are moments calculated about the current location of the forager

instead of the centre of mass of all memorised locations. For $\mathbf{v} = \begin{bmatrix} x \\ y \end{bmatrix}$, the shape of memorised walk can be approximated by

$$\mathbf{v}^T T^{-1} \mathbf{v} = \kappa^2, \tag{3.15}$$

which is an ellipse centred on the origin whose semi-major axis and semi-minor axis have lengths equal to $\kappa\sqrt{\lambda_1}$ and $\kappa\sqrt{\lambda_2}$ respectively. Figure 3.4 illustrates two examples of such ellipses used to approximate the memorised walks (the sets L) for different memory kernels.

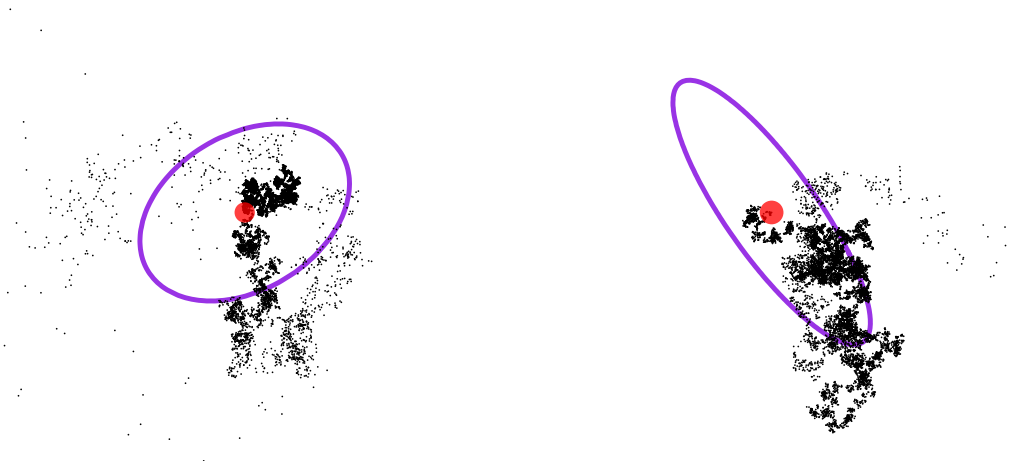

Figure 3.4: Left: memorised Brownian path (the set L) correspond to the Lomax memory kernel (taken to be the density function of the Lomax distribution [1]) with $a = 1.05$ and $\lambda = 1$ as $c = 10000$. Right: The memorised Brownian path for the stretched exponential memory kernel for $a = 2$ as $c = 10000$. The red dots represent current position of the walker (the origin). The purple ellipses are obtained by equation (3.15) with $\kappa = 2$.

Example 3.3.1. *Consider the set of points P given in Example 3.1.1. The egocentric gyration tensor T for the set P is given by (3.3), where the elements of T are calculate as follows*

$$T_{11} = \frac{1}{N}\sum_{k=1}^{N}(x^{(k)})^2 = \frac{13}{2}, \quad T_{22} = \frac{1}{N}\sum_{k=1}^{N}(y^{(k)})^2 = \frac{17}{3}, \text{ and } T_{12} = \frac{1}{N}\sum_{k=1}^{N} x^{(k)}y^{(k)} = \frac{35}{6}.$$

Then

$$T = \begin{bmatrix} \frac{13}{2} & \frac{35}{6} \\ \frac{35}{6} & \frac{17}{3} \end{bmatrix}. \tag{3.16}$$

The eigenvalues of T *are* $\lambda_1 = 11.9315$, *and* $\lambda_2 = 0.235138$. *The egocentric single walk asphericity of the set* P *is*

$$ego\text{-}\widetilde{A_2} = \frac{(\lambda_1 - \lambda_2)^2}{(\lambda_1 + \lambda_2)^2} = 0.924188.$$

The shape of the set P *is approximated by (3.15) as shown in figure 3.5. By comparing the egocentric single walk asphericity ego-*$\widetilde{A_2}$ *calculate in example 3.3.1 with the standard single walk asphericity* $\widetilde{A_2^c}$ *in Example 3.1.1, we note that the shape described by the egocentric single walk asphericity ego-*$\widetilde{A_2}$ *is more elongated. For more examples please see figure 3.6 that illustrates the difference between the egocentric and the standard asphericity.*

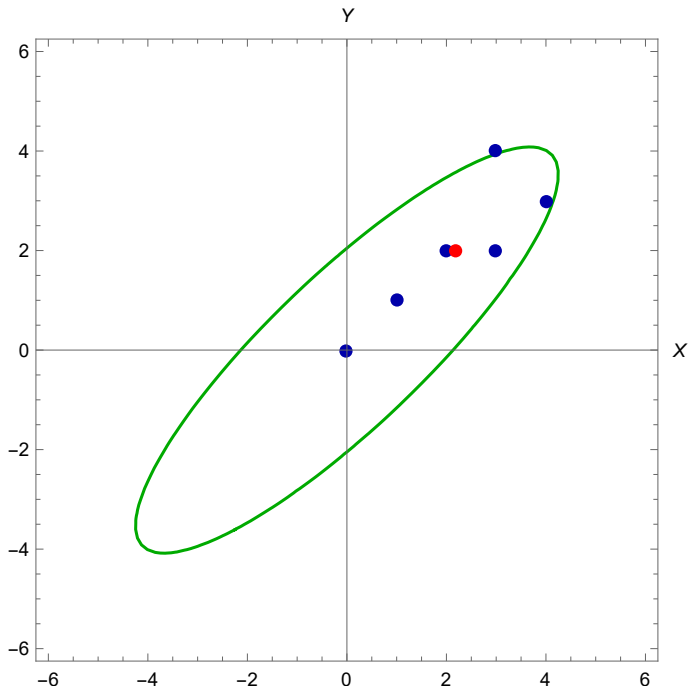

Figure 3.5: The shape of the set P is described by equation (3.15) when $\kappa = 10$. The red dot indicate the centre of mass of the set P.

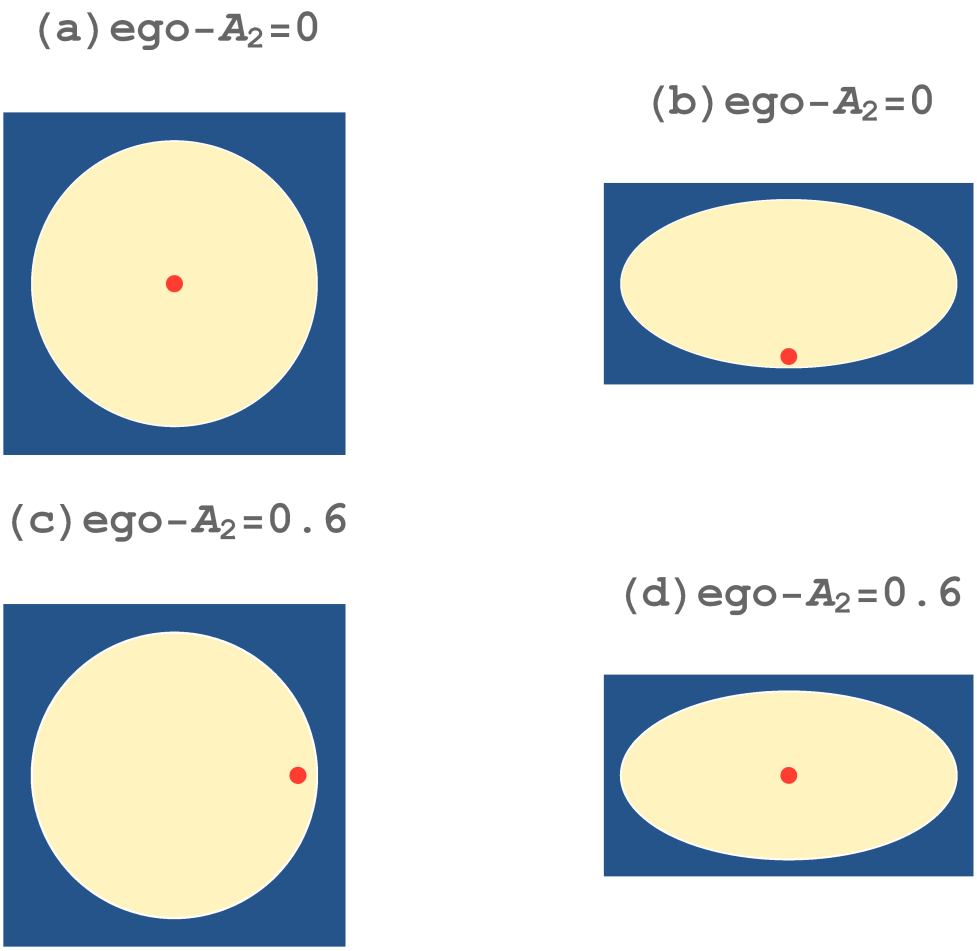

Figure 3.6: Selected examples to illustrate the behaviour of egocentric single walk asphericity. Red dots indicate the current position of walkers (the origin) and yellow areas give the spatial memories. The same memorised shapes may have different asphericity depending on current position of the walker. When the current location of the walker near the edge of the spatial memory our egocentric single walk asphericity may overestimate or underestimates the actual egocentric asphericity. This downside does not affect our formula (3.14) since we calculate the average.

3.3.1 Analytic asphericity

For high rate of memory formation (as $c \to \infty$), the elements of matrix (3.13) can be approximated by integrals with stochastic integrands. By applying Corollary A.1.4, from the appendix, the matrix (3.13) can be replaced with

$$T = \begin{bmatrix} T_{11} & T_{12} \\ T_{12} & T_{22} \end{bmatrix} = \begin{bmatrix} \int_0^\infty X^2(s)\mu(s)ds & \int_0^\infty X(s)Y(s)\mu(s)ds \\ \int_0^\infty X(s)Y(s)\mu(s)ds & \int_0^\infty Y^2(s)\mu(s)ds \end{bmatrix}. \tag{3.17}$$

The following theorem allows us to calculate analytically the average asphericity of two dimension memorised Brownian motion according to given memory kernel $\mu(t)$.

Theorem 3.3.1 (Egocentric asphericity)**.** *Let $M(t) = \int_0^t \mu(s)ds$. The egocentric asphericity of two dimension memorised Brownian motion defined by (3.12) as $c \to \infty$ is given by*

$$\textit{ego-}A_2 = 1 - 4 \lim_{\tau\to\infty} \frac{\alpha(\tau)}{\beta(\tau)}, \tag{3.18}$$

where

$$\begin{aligned}\alpha(\tau) =& \frac{1}{2}\left[\left(\int_0^\tau s\mu(s)ds\right)^2 + \left(\int_0^\tau M(s)ds\right)^2 - \tau^2 M^2(\tau)\right] \\ &+ \int_0^\tau [(4s-\tau)M(\tau) - 2sM(s)]M(s)ds,\end{aligned} \tag{3.19}$$

and

$$\begin{aligned}\beta(\tau) =& 2\left[\left(\int_0^\tau s\mu(s)ds\right)^2 + \left(\int_0^\tau M(s)ds\right)^2 + 3\tau^2 M^2(\tau)\right] \\ &- 4\int_0^\tau [(4s+\tau)M(\tau) - 2sM(s)]M(s)ds.\end{aligned} \tag{3.20}$$

In order to prove Theorem 3.3.1, we need to state and prove the following five lemmas. For $t \geq 0$, let $M(t) = \int_0^t \mu(s)ds$, where $\mu(t)$ is the memory kernel.

Lemma 3.3.1. *If W is a one-dimension standard Brownian motion, then*

$$W^2(t) = 2\int_0^t W(s)dW(s) + t, \quad \textit{for } t \geq 0. \tag{3.21}$$

Proof. By applying Ito's lemma with $f(t, W(t)) = W^2(t)$. □

Lemma 3.3.2. *If W is a one-dimension standard Brownian motion, then*

$$\begin{aligned}\int_0^t W^2(s)\mu(s)ds =& M(t)W^2(t) - 2\int_0^t M(s)W(s)dW(s) \\ &- \int_0^t M(s)ds \quad \textit{for } t \geq 0.\end{aligned} \tag{3.22}$$

Proof. Let $f(t,s) = M(t)s^2$, where $M(t) = \int_0^t \mu(s)ds$. By applying Lemma 1.3.6, we have

$$df(t,W(t)) = \mu(t)W^2(t)dt + 2M(t)W(t)dW(t) + M(t)\left(dW(t)\right)^2. \tag{3.23}$$

From table 1.1, we substitute $\left(dW(t)\right)^2 = dt$, to obtain

$$d(M(t)W^2(t)) = \mu(t)W^2(t)dt + 2M(t)W(t)dW(t) + M(t)dt. \tag{3.24}$$

Integrating both side and rearranging gives (3.22). □

Lemma 3.3.3. *If W is a standard Brownian motion, then*

1)

$$\mathbb{E}\left[\int_0^t W^2(s)\mu(s)ds\right] = \int_0^t s\mu(s)ds. \tag{3.25}$$

2)

$$\begin{aligned}\mathbb{E}\left[\left(\int_0^t W^2(s)\mu(s)ds\right)^2\right] =& 3t^2M^2(t) + 4\int_0^t sM^2(s)ds + \left(\int_0^t M(s)ds\right)^2 \\ &- 8M(t)\int_0^t sM(s)ds - 2tM(t)\int_0^t M(s)ds.\end{aligned} \tag{3.26}$$

Proof. 1) By using Fubini Theorem and the fact that $\mathbb{E}[W^2(t)] = t$, we have

$$\begin{aligned}\mathbb{E}\left[\int_0^t W^2(s)\mu(s)ds\right] &= \int_0^t \mathbb{E}[W^2(s)]\mu(s)ds \\ &= \int_0^t s\mu(s)ds.\end{aligned}$$

□

2) By using Lemma 3.3.2, we have

$$\begin{aligned}\mathbb{E}\left[\left(\int_0^t W^2(s)\mu(s)ds\right)^2\right] =& M^2(t)\mathbb{E}[W^4(t)] + 4\mathbb{E}\left[\left(\int_0^t M(s)W(s)dW(s)\right)^2\right] \\ &+ \left(\int_0^t M(s)ds\right)^2 - 4M(t)\mathbb{E}\left[W^2(t)\int_0^t M(s)W(s)dW(s)\right] \\ &- 2M(t)\mathbb{E}[W^2(t)]\int_0^t M(s)ds \\ &+ 4\mathbb{E}\left[\int_0^t M(s)W(s)dW(s)\right]\int_0^t M(s)ds. \quad (3.27)\end{aligned}$$

By using Itô properties the last expectation in (3.27) is zero, and by using the fact that $W^2(t) = t + 2\int_0^t W(s)dW(s)$ and Itô's isometry, we have

$$\begin{aligned}\mathbb{E}\left[\left(\int_0^t W^2(s)\mu(s)ds\right)^2\right] =& 3t^2M^2(t) + 4\int_0^t sM^2(s)ds + \left(\int_0^t M(s)ds\right)^2 \\ &- 8M(t)\int_0^t sM(s)ds - 2tM(t)\int_0^t M(s)ds. \quad \square\end{aligned}$$

Lemma 3.3.4. *Let W_1 and W_2 be two independent standard Brownian motion, then*

$$\int_0^t W_1(s)W_2(s)\mu(s)ds = \int_0^t W_3^2(s)\mu(s)ds - \frac{1}{2}\int_0^t W_1^2(s)\mu(s)ds - \frac{1}{2}\int_0^t W_2^2(s)\mu(s)ds, \quad (3.28)$$

where $W_3(t) = \dfrac{W_1(t) + W_2(t)}{\sqrt{2}}$ is standard Brownian motion. Particularly, the correlation coefficient of W_3 with W_1 and W_2 is $\rho(W_3(t), W_1(t)) = \rho(W_3(t), W_2(t)) = \dfrac{1}{\sqrt{2}}$.

Proof. By substituting $W_3(t) = \dfrac{W_1(t) + W_2(t)}{\sqrt{2}}$ in $\int_0^t W_3^2(s)\mu(s)ds$ and rearrangement, Lemma 3.3.4 holds.

Lemma 3.3.5. *Let W_1 and W_2 be two correlated Brownian motions with correlation*

coefficients $\rho \in [-1, 1]$, *then*

$$\mathbb{E}\left[\int_0^t W_2^2(s)\mu(s)ds \int_0^t W_1^2(s)\mu(s)ds\right] = \left(\int_0^t M(s)ds\right)^2 - 2tM(t)\int_0^t M(s)ds + (1+2\rho^2)t^2M^2(t) - 8\rho^2 M(t)\int_0^t sM(s)ds + 4\rho^2\int_0^t sM^2(s)ds. \tag{3.29}$$

Proof. By applying Lemma 3.3.2, we have

$$\begin{aligned}
&\mathbb{E}\left[\int_0^t W_2^2(s)\mu(s)ds \int_0^t W_1^2(s)\mu(s)ds\right] \\
&= \mathbb{E}\left[\left(M(t)W_2^2(t) - 2\int_0^t M(s)W_2(s)dW_2(s)\right)\left(M(t)W_1^2(t) - 2\int_0^t M(s)W_1(s)dW_1(s)\right)\right] \\
&= M^2(t)\mathbb{E}[W_2^2(t)W_1^2(t)] - 2M(t)\mathbb{E}\left[W_2^2(t)\int_0^t M(s)W_1(s)dW_1(s)\right] \\
&- M(t)\mathbb{E}[W_2^2(t)]\int_0^t M(s)ds - 2M(t)\mathbb{E}\left[W_1^2\int_0^t M(s)W_2(s)dW_2(s)\right] \\
&+ 4\mathbb{E}\left[\int_0^t M(s)W_2(s)dW_2(s)\int_0^t M(s)W_1(s)dW_1(s)\right] + 2\int_0^t M(s)ds\,\mathbb{E}\left[\int_0^t M(s)W_2(s)dW_2(s)\right] \\
&- M(t)\mathbb{E}[W_1^2(t)]\int_0^t M(s)ds + 2\mathbb{E}\left[\int_0^t M(s)W_1(s)dW_1(s)\right]\int_0^t M(s)ds + \left(\int_0^t M(s)ds\right)^2
\end{aligned}$$

By using Itô properties, we have

$$\mathbb{E}\left[\int_0^t M(s)W_1(s)dW_1(s)\right] = \mathbb{E}\left[\int_0^t M(s)W_2(s)dW_2(s)\right] = 0. \tag{3.30}$$

By using the fact that $\mathbb{E}[W^2(t)] = t$, and by (3.30) we obtain

$$\begin{aligned}
&\mathbb{E}\left[\int_0^t W_2^2(s)\mu(s)ds \int_0^t W_1^2(s)\mu(s)ds\right] \\
&= \left(\int_0^t M(s)ds\right)^2 - 2tM(t)\int_0^t M(s)ds + M^2(t)\mathbb{E}[W_2^2(t)W_1^2(t)] \\
&- 2M(t)\mathbb{E}\left[W_2^2(t)\int_0^t M(s)W_1(s)dW_1(s)\right] \\
&- 2M(t)\mathbb{E}\left[W_1^2(t)\int_0^t M(s)W_2(s)dW_2(s)\right] \\
&+ 4\mathbb{E}\left[\int_0^t M(s)W_2(s)dW_2(s)\int_0^t M(s)W_1(s)dW_1(s)\right].
\end{aligned} \tag{3.31}$$

The first expectation term in the right hand side of (3.31) is calculated as follow

$$\begin{aligned}\mathbb{E}[W_2^2(t)W_1^2(t)] =&\mathbb{E}\left[\left(t+2\int_0^t W_2(s)dW_2(s)\right)\left(t+2\int_0^t W_1(s)dW_1(s)\right)\right]\\ &= t^2+2t\mathbb{E}\left[\int_0^t W_1(s)dW_1(s)\right]+2t\mathbb{E}\left[\int_0^t W_2(s)dW_2(s)\right]\\ &+4\mathbb{E}\left[\int_0^t W_2(s)dW_2(s)\int_0^t W_1(s)dW_1(s)\right] \qquad (3.32)\end{aligned}$$

The first two expectation terms here are zero by applying Itô properties, then

$$\begin{aligned}\mathbb{E}[W_2^2(t)W_1^2(t)] &= t^2+4\mathbb{E}\left[\int_0^t W_2(s)dW_2(s)\int_0^t W_1(s)dW_1(s)\right]\\ &= t^2+4\mathbb{E}\left[\int_0^t W_2(s)W_1(s)\rho d(s)\right] \quad \text{(by using Table 1.1)}\\ &= t^2+4\rho\int_0^t \mathbb{E}[W_2(s)W_1(s)]ds \quad \text{(by using Fubini's theorem)}\\ &= t^2+4\rho\int_0^t \rho s ds = (1+2\rho^2)t^2. \qquad (3.33)\end{aligned}$$

The second expectation terms in the right hand side of (3.31) calculated by using the fact that $W_2^2(t) = t + 2\int_0^t W_2(s)dW_2(s)$

$$\begin{aligned}\mathbb{E}\left[W_2^2(t)\int_0^t M(s)W_1(s)dW_1(s)\right] =&\mathbb{E}\left[\left(t+2\int_0^t W_2(s)dW_2(s)\right)\int_0^t M(s)W_1(s)dW_1(s)\right]\\ =&t\mathbb{E}\left[\int_0^t M(s)W_1(s)dW_1(s)\right]\\ &+2\mathbb{E}\left[\int_0^t W_2(s)dW_2(s)\int_0^t M(s)W_1(s)dW_1(s)\right]\\ =&2\mathbb{E}\left[\int_0^t M(s)W_2(s)W_1(s)\rho ds\right]\\ =&2\rho\int_0^t M(s)\mathbb{E}[W_2(s)W_1(s)]ds \quad \text{(by using Fubini's theorem)}\\ =&2\rho\int_0^t M(s)\rho s ds = 2\rho^2\int_0^t sM(s)ds. \qquad (3.34)\end{aligned}$$

Similarly,

$$\mathbb{E}\left[W_1^2(t)\int_0^t M(s)W_2(s)dW_2(s)\right] = 2\rho^2\int_0^t sM(s)ds \qquad (3.35)$$

The last expectation term in the right hand side of (3.31) is calculated as follow

$$\begin{aligned}
&\mathbb{E}\left[\int_0^t M(s)W_2(s)dW_2(s)\int_0^t M(s)W_1(s)dW_1(s)\right]\\
&=\mathbb{E}\left[\int_0^t M^2(s)W_2(s)W_1(s)\rho d(s)\right] \quad \text{(by using Itô product rule)}\\
&=\rho\int_0^t M^2(s)\mathbb{E}[W_2(s)W_1(s)]ds \quad \text{(by using Fubini's theorem)}\\
&=\rho^2\int_0^t sM^2(s)ds. \qquad (3.36)
\end{aligned}$$

By substituting (3.32)-(3.35) in (3.31), Lemma 3.3.5 holds. □

Lemma 3.3.6. *Let W_1 and W_2 be independent standard Brownian motions, then the second moment of $\int_0^t W_1(s)W_2(s)\mu(s)ds$ is*

$$\begin{aligned}
\mathbb{E}\left[\left(\int_0^t W_1(s)W_2(s)\mu(s)ds\right)^2\right] =&\frac{1}{2}\left(\int_0^t s\mu(s)ds\right)^2+\frac{1}{2}t^2M^2(t)+2\int_0^t sM^2(s)ds\\
&-\frac{1}{2}\left(\int_0^t M(s)ds\right)^2-4M(t)\int_0^t sM(s)ds\\
&+tM(t)\int_0^t M(s)ds. \qquad (3.37)
\end{aligned}$$

Proof. Let $W_3(t)=\dfrac{W_1(t)+W_2(t)}{\sqrt{2}}$, clearly $W_3(t)$ is a standard Brownian motion such that the correlation coefficient of W_3 with W_1 and W_2 is $\rho(W_3(t),W_1(t)) = \rho(W_3(t),W_2(t))=\dfrac{1}{\sqrt{2}}$. Employing Lemma 3.3.4 yields that

$$\begin{aligned}
&\mathbb{E}\left[\left(\int_0^t W_1(s)W_2(s)\mu(s)ds\right)^2\right]\\
&=\mathbb{E}\left[\left(\int_0^t W_3^2(s)\mu(s)ds-\frac{1}{2}\int_0^t W_1^2(s)\mu(s)ds-\frac{1}{2}\int_0^t W_2^2(s)\mu(s)ds\right)^2\right]\\
&=\mathbb{E}\left[\left(\int_0^t W_3^2(s)\mu(s)ds\right)^2\right]+\frac{1}{4}\mathbb{E}\left[\left(\int_0^t W_1^2(s)\mu(s)ds\right)^2\right]+\frac{1}{4}\mathbb{E}\left[\left(\int_0^t W_2^2(s)\mu(s)ds\right)^2\right]\\
&-\mathbb{E}\left[\int_0^t W_3^2(s)\mu(s)ds\int_0^t W_2^2(s)\mu(s)ds\right]-\mathbb{E}\left[\int_0^t W_3^2(s)\mu(s)ds\int_0^t W_1^2(s)\mu(s)ds\right]\\
&+\frac{1}{2}\mathbb{E}\left[\int_0^t W_1^2(s)\mu(s)ds\right]\mathbb{E}\left[\int_0^t W_2^2(s)\mu(s)ds\right]. \qquad (3.38)
\end{aligned}$$

The first three expectation terms in the right hand side(RHS) of (3.38) obtained by applying Lemma 3.3.3, we have

$$\mathbb{E}\left[\left(\int_0^t W_3^2(s)\mu(s)ds\right)^2\right] = \mathbb{E}\left[\left(\int_0^t W_1^2(s)\mu(s)ds\right)^2\right] = \mathbb{E}\left[\left(\int_0^t W_2^2(s)\mu(s)ds\right)^2\right]$$
$$= 3t^2M^2(t) + 4\int_0^t sM^2(s)ds + \left(\int_0^t M(s)ds\right)^2$$
$$- 8M(t)\int_0^t sM(s)ds - 2tM(t)\int_0^t M(s)ds. \tag{3.39}$$

The fourth and fifth expectation terms in (RHS) of (3.38) are calculated by applying Lemma 3.3.5 as follow

$$\mathbb{E}\left[\int_0^t W_3^2(s)\mu(s)ds\int_0^t W_2^2(s)\mu(s)ds\right] = \mathbb{E}\left[\int_0^t W_3^2(s)\mu(s)ds\int_0^t W_1^2(s)\mu(s)ds\right]$$
$$= \left(\int_0^t M(s)ds\right)^2 - 2tM(t)\int_0^t M(s)ds$$
$$+ (1+2\rho^2)t^2M^2(t) - 8\rho^2M(t)\int_0^t sM(s)ds$$
$$+ 4\rho^2\int_0^t sM^2(s)ds. \tag{3.40}$$

The last two expectation terms in (RHS) of (3.38) are calculated by applying Fubini's theorem as follow

$$\mathbb{E}\left[\int_0^t W_1^2(s)\mu(s)ds\right] = \mathbb{E}\left[\int_0^t W_2^2(s)\mu(s)ds\right] = \int_0^t \mathbb{E}[W_2^2(s)]\mu(s)ds$$
$$= \int_0^t s\mu(s)ds \tag{3.41}$$

Substituting (3.39)-(3.41) in (3.38) yields

$$\mathbb{E}\left[\left(\int_0^t W_1(s)W_2(s)\mu(s)ds\right)^2\right] = \frac{1}{2}\left(\int_0^t s\mu(s)ds\right)^2 + \frac{1}{2}t^2M^2(t) + 2\int_0^t sM^2(s)ds$$
$$- \frac{1}{2}\left(\int_0^t M(s)ds\right)^2 - 4M(t)\int_0^t sM(s)ds$$
$$+ tM(t)\int_0^t M(s)ds. \tag{3.42}$$

□

Proof of Theorem 3.3.1. Consider matrix T as in (3.17) and note that

$$\lambda_1 + \lambda_2 = Tr(T) = T_{11} + T_{22}, \tag{3.43}$$

and

$$\lambda_1 \lambda_2 = \det(T) = T_{11}T_{22} - T_{12}^2. \tag{3.44}$$

We can write

$$(\lambda_1 - \lambda_2)^2 = (\lambda_1 + \lambda_2)^2 - 4\lambda_1\lambda_2. \tag{3.45}$$

Substituting (3.43) and (3.44) in (3.45) gives

$$(\lambda_1 - \lambda_2)^2 = (T_{11} + T_{22})^2 - 4(T_{11}T_{22} - T_{12}^2). \tag{3.46}$$

Substituting (3.43) and (3.46) in (3.7) lead to

$$\text{ego-}A_2 = \frac{\mathbb{E}[(T_{11} + T_{22})^2] - 4\mathbb{E}[T_{11}T_{22} - T_{12}^2]}{\mathbb{E}[(T_{11} + T_{22})^2]} = 1 - 4\frac{\mathbb{E}[T_{11}T_{22}] - \mathbb{E}[T_{12}^2]}{\mathbb{E}[T_{11}^2] + 2\mathbb{E}[T_{11}T_{22}] + \mathbb{E}[T_{22}^2]}. \tag{3.47}$$

Let $\tau > 0$ and define

$$T_{11}(\tau) = \int_0^\tau X^2(s)\mu(s)ds, T_{12}(\tau) = \int_0^\tau X(s)Y(s)\mu(s)ds, \text{ and } T_{22}(\tau) = \int_0^\tau Y^2(s)\mu(s)ds, \tag{3.48}$$

where

$$T_{ij} = \lim_{\tau \to \infty} T_{ij}(\tau) \text{ for all } i \leq j \in \{1, 2\}. \tag{3.49}$$

By monotone and dominated convergence theorems [20], we have

$$\mathbb{E}[T_{ij}] = \lim_{\tau \to \infty} \mathbb{E}[T_{ij}(\tau)] \text{ for all } i \leq j \in \{1, 2\}. \tag{3.50}$$

The independence of X and Y and Lemma 3.3.3 gives us

$$\mathbb{E}[T_{11}(\tau)T_{22}(\tau)] = \mathbb{E}[T_{11}(\tau)]\mathbb{E}[T_{22}(\tau)] = \left(\int_0^\tau s\mu(s)ds\right)^2. \tag{3.51}$$

By using Lemma 3.3.6, we have

$$\begin{aligned}\mathbb{E}[T_{12}^2(\tau)] =& \mathbb{E}\left[\left(\int_0^\tau X(s)Y(s)\mu(s)ds\right)^2\right] \\ &= \frac{1}{2}\left(\int_0^\tau s\mu(s)ds\right)^2 + \frac{1}{2}\tau^2M^2(\tau) + 2\int_0^\tau sM^2(s)ds \\ &- \frac{1}{2}\left(\int_0^\tau M(s)ds\right)^2 - 4M(\tau)\int_0^\tau sM(s)ds \\ &+ \tau M(\tau)\int_0^\tau M(s)ds. \end{aligned} \tag{3.52}$$

Clearly, $\mathbb{E}[T_{11}^2(\tau)] = \mathbb{E}[T_{22}^2(\tau)]$. By applying Lemma 3.3.3, we obtain

$$\begin{aligned}\mathbb{E}[T_{11}^2(\tau)] &= \mathbb{E}[T_{22}^2(\tau)] \\ &= 3\tau^2M^2(\tau) + 4\int_0^\tau sM^2(s)ds + \left(\int_0^\tau M(s)ds\right)^2 \\ &- 8M(\tau)\int_0^\tau sM(s)ds - 2\tau M(\tau)\int_0^\tau M(s)ds. \end{aligned} \tag{3.53}$$

Substituting (3.51)-(3.53) in (3.47) result in (3.18). □

3.3.2 Examples

In this section we calculate the egocentric asphericity of selected memory kernel by applying Theorem 3.3.1. Table 3.1 shows the exact asphericity for various memory kernels.

Uniform memory kernel:

The memory kernel here taken to be the probability density function of a continuous uniform distribution supported on $[0, r]$ where $r > 0$, that is, $\mu(t) = \frac{1}{r}\mathbf{1}_{\{t<r\}}$ and

Name of the distribution	$\mu(t)$	ego-A_2
Uniform supported on $[0,r], r>0$	$\frac{1}{r}\mathbf{1}_{\{t<\tau\}}$	$\frac{4}{5}=0.8$
Half normal with scale equal to 1	$\frac{\sqrt{2}}{\sqrt{\pi}}\exp(\frac{-t^2}{2})$	$2-\frac{4}{\pi}=0.727$
Exponential with rate $\lambda=1$	$\exp(-t)$	$\frac{2}{3}\approx 0.667$
Stretched exponential with exponent $\frac{1}{2}$	$\frac{1}{2}\exp(-t^{\frac{1}{2}})$	$\frac{10}{17}\approx 0.588$
Stretched exponential with exponent $\frac{1}{4}$	$\frac{1}{24}\exp(-t^{\frac{1}{4}})$	$\frac{594}{1193}\approx 0.498$
Lomax with scale $\lambda=1$ and shape $a=1.5$	$1.5(1+t)^{-2.5}$	$\frac{2}{5}=0.4$
Lomax with scale $\lambda=1$ and shape $a=1.25$	$1.25(1+t)^{-2.25}$	$\frac{2}{7}\approx 0.286$
Lomax with scale $\lambda=1$ and shape $a=1.05$	$1.05(1+t)^{-2.05}$	$\frac{2}{23}\approx 0.0870$

Table 3.1: Asphericity of memorised random walk calculated analytically by Theorem 3.3.1 for different memory kernels.

then

$$M(t)=\begin{cases}\dfrac{t}{r} & \text{if } t<r\\ 1 & \text{if } t\geq r\end{cases}.$$

For $\tau>r$ and $r>0$, by Theorem 3.3.1, we have

$$\alpha(\tau)=\frac{r^2}{12} \text{ and } \beta(\tau)=\frac{5r^2}{3}, \tag{3.54}$$

and the corresponding Asphericity is

$$\text{ego-}A_2=1-4\lim_{\tau\to\infty}\frac{\alpha(\tau)}{\beta(\tau)}=\frac{4}{5}. \tag{3.55}$$

Exponential memory kernel:

Consider the exponential memory kernel $\mu(t)=\lambda\exp(-\lambda t)$ for $\lambda>0$ and the corresponding CDF is $M(t)=1-e^{-\lambda t}$. For $\lambda,\tau>0$, we have

$$\alpha(\tau)=\frac{e^{-2\lambda\tau}\left(\lambda^2\tau^2-e^{\lambda\tau}\left(\lambda^2\tau^2+4\lambda\tau-4\right)-2\lambda\tau+e^{2\lambda\tau}-5\right)}{2\lambda^2}, \tag{3.56}$$

$$\beta(\tau)=\frac{e^{-2\lambda\tau}\left(8\lambda^2\tau^2+20\lambda\tau+6e^{2\lambda\tau}-8e^{\lambda\tau}(\lambda\tau+3)+18\right)}{\lambda^2}. \tag{3.57}$$

Since λ has no influence on the asphericity so for simplicity we choose $\lambda = 1$, we have

$$\lim_{\tau\to\infty} \frac{\alpha(\tau)}{\beta(\tau)} = \frac{1}{12}. \tag{3.58}$$

Therefore, the asphericity of the memorised random walk with exponential memory kernel is

$$\text{ego-}A_2 = 1 - 4 \lim_{\tau\to\infty} \frac{\alpha(\tau)}{\beta(\tau)} = \frac{2}{3}. \tag{3.59}$$

Stretched exponential memory kernel:

We take the memory kernel to be the Stretched exponential probability density function

$$\mu(t) = \frac{ae^{-t^a}}{\Gamma\left(\frac{1}{a}\right)}, \tag{3.60}$$

where Γ is the Gamma function which is defined as $\Gamma(a) = \int_0^\infty t^{a-1}e^{-t}dt$. The corresponding CDF is

$$M(t) = \frac{\gamma(a^{-1}, t^a)}{\Gamma\left(\frac{1}{a}\right)}, \tag{3.61}$$

where γ is the lower incomplete gamma function

$$\gamma(a, x) = \int_0^x t^{a-1}e^{-t}dt. \tag{3.62}$$

As an example we calculate the asphericity of the memorised random walk with stretch exponential memory kernel with $a = \frac{1}{2}$. In order to calculate the limits of $\alpha(\tau)$ and $\beta(\tau)$ we note that

$$\int_0^\tau s\mu(s)ds = \gamma(4,\sqrt{\tau}),$$
$$\int_0^\tau M(s)ds = \tau - 2\gamma(2,\sqrt{\tau}) - 2\gamma(3,\sqrt{\tau}),$$
$$\int_0^\tau sM(s)ds = \frac{1}{2}\tau^2 M(\tau) - \frac{1}{2}\gamma(6,\sqrt{\tau}),$$
$$\int_0^\tau sM^2(s)ds = \frac{1}{2}\tau^2 M^2(\tau) - \gamma(6,\sqrt{\tau}) + \frac{1}{2^6}\left(\gamma(6,2\sqrt{\tau}) + \frac{1}{2}\gamma(7,2\sqrt{\tau}\right).$$

Thus, we have

$$\lim_{\tau\to\infty}\alpha(\tau) = \lim_{\tau\to\infty}\left[2\left(\gamma(2,\sqrt{t}) + \gamma(3,\sqrt{t})\right)^2 + \frac{\gamma^2(4,\sqrt{t})}{2} - \frac{1}{32}\left(\gamma(6,2\sqrt{t}) + \frac{\gamma(7,2\sqrt{t})}{2}\right)\right] = 21,$$
$$\lim_{\tau\to\infty}\beta(\tau) = \lim_{\tau\to\infty}\left[8\left(\gamma(2,\sqrt{t}) + \gamma(3,\sqrt{t})\right)^2 + 2\gamma^2(4,\sqrt{t}) + \frac{1}{8}\left(\gamma(6,2\sqrt{t}) + \frac{\gamma(7,2\sqrt{t})}{2}\right)\right] = 204.$$

Hence,

$$\text{ego-}A_2 = 1 - 4\frac{21}{204} = \frac{10}{17}.$$

Lomax memory kernel:

The memory kernel here taken to be the density function of the Lomax distribution (also called the Pareto Type II distribution), then

$$\mu(t) = \frac{a}{\lambda}\left(1 + \frac{t}{\lambda}\right)^{-(a+1)},$$

where $a > 0$ is a shape parameter and $\lambda > 0$ is a scale parameter. The mean of the Lomax distribution defined and equal $\dfrac{\lambda}{a-1}$ for $a > 1$. The corresponding CDF is $M(t) = 1 - (1 + \frac{t}{\lambda})^{-a}$. Since λ has no effect on asphericity, we fix $\lambda = 1$ for simplicity. For $a > 1$ and $\lambda = 1$ we note the following

$$\int_0^\tau s\mu(s)ds = \frac{(\tau+1)^a - a\tau - 1}{(\tau+1)^a(a-1)},$$
$$\int_0^\tau M(s)ds = \tau + \frac{1+\tau-(\tau+1)^a}{(\tau+1)^a(a-1)},$$
$$\int_0^\tau sM(s)ds = \frac{\tau^2}{2} - \frac{(\tau+1)^a - a\tau(\tau+1) + \tau^2 - 1}{(a-1)(a-2)(\tau+1)^a},$$
$$\int_0^\tau sM^2(s)ds = \frac{\tau^2}{2} + \frac{(\tau+1)^{2a} - 2a\tau(\tau+1) + \tau^2 - 1}{2(a-1)(2a-1)(\tau+1)^{2a}} - \frac{4(\tau+1)^a - a\tau(\tau+1) + \tau^2 - 1}{2(a-1)(a-2)(\tau+1)^a}.$$

By using Theorem 3.3.1, we have

$$\lim_{\tau\to\infty} \alpha(\tau) = \frac{a}{(a-1)^2(2a-1)}, \text{ and}$$
$$\lim_{\tau\to\infty} \beta(\tau) = \frac{4(3a-2)}{(a-1)^2(2a-1)}.$$

Hence,

$$\text{ego-}A_2 = \frac{2(a-1)}{3a-2}.$$

We observe that

$$\lim_{a\to 1} \frac{2(a-1)}{3a-2} = 0,$$

which mean that the memorised random walk becomes more spherical as a approaches 1.

3.3.3 Simulated asphericity

The set of memory times here (the set S) is viewed as the arrival times of an non-homogeneous Poisson process with intensity function $\lambda(t) = c\mu(t)$. At time $\tau \geq 0$, the cumulative distribution function (CDF) of the next arrival time Z is

$$\mathbb{P}[Z \leq t | Z > \tau] = F_\tau(t) = \begin{cases} 1 - \exp(-c\int_\tau^t \mu(s)ds) & \text{if } t \geq \tau \\ 0 & \text{otherwise .} \end{cases} \tag{3.63}$$

Let $M(t) = \int_0^t \mu(s)\, ds$ and $p(\tau) = \lim_{t\to\infty} F_\tau(t)$. The notation $p(\tau)$ represents the probability of having at least one sample (arrival time) in the interval $[\tau, \infty)$. If $u \in [0, p(\tau))$, then the inverse cumulative function exists and can be written as

$$F_\tau^{-1}(u) = M^{-1}\left(M(\tau) - \frac{\ln(1-u)}{c}\right). \tag{3.64}$$

If Z_k is the kth sample (arrival) time, then the next sample time in memory may be simulated by $Z_{k+1} \overset{d}{=} F_{Z_k}^{-1}(U)$ where the notation $\overset{d}{=}$ indicate equality in distribution and U is a standard uniform random variable. The case $U > p(Z_k)$ indicates that Z_k is the last sample time. The set L (locations in memory) may be generated by knowing that

$$X(Z_{k+1}) - X(Z_k) \sim \mathcal{N}(0, Z_{k+1} - Z_k) \tag{3.65}$$

$$Y(Z_{k+1}) - Y(Z_k) \sim \mathcal{N}(0, Z_{k+1} - Z_k) \tag{3.66}$$

where $\mathcal{N}(\mu, \sigma^2)$ is the normal (Gaussian) distribution with expectation μ and variance σ^2.

Visualising the shape of a memorised walk

We provide two ways for visualising the shape of a memorised walk to give clear intuition about egocentric asphericity.

1) **Averaging over many paths of a given memory kernel**: In order to visualise the shape of memorised walk for given memory kernel, we generate large number of memory locations sets $\{L_1, L_2, ...\}$. By constructing a smooth spatial density function of these sets we obtain a spherical and symmetric distribution that fails to show the aspherical shape of individual memorised walk. In order to obtain the asphericity in our average, before averaging we need to rotate each individual set so that the major axis of its gyration tensor is horizontally aligned. We also ensure that the horizontal coordinate of its centre of mass is positive. The last condition results in the walker being displaced from the mass centre of its memory. In figure 3.9 we have two examples of the memory distribution obtained by using kernel density

estimation tools in Mathematica. We can see that the fat-tailed (slower decaying) memory kernel is less elongated which confirms our asphericity result. The shape of memory distribution look like tear-drop shape as a result of the centre of mass condition and without that condition the memory distribution would look like ellipse rather than tear-drops. It is worth to highlight that our asphericity calculations investigate only the expected elongation of an ellipse and not the tear-drop.

2) **Examining individual paths**: Here we investigate how the egocentric gyration tensor and the corresponding ellipse are related to the shape of the memorised walk. In figures 3.7 and 3.8, the memorised walk is described by an ellipse (given by equation (3.15) with $\kappa = 2$) and the ellipse is defined in a way to enclose the majority of the memorised locations to provide a simple description of the shape of the mental map. The major and minor axes of the ellipse aligned with the principle axes (eigenvectors) of the asphericity tensor T and have lengths equal to the double the expected squared displacements of the set L. We emphasise that the memorised walks generated form given memory kernel have wide range of shapes and the egocentric asphericity used to provide a general overview of the average elongation.

Comparison between simulated and analytical asphericities

In order to verify Theorem 3.3.1 by simulation we generate large number of sets L for given memory kernel $\mu(t)$ and rate $c > 0$, and we extract the eigenvalues from the ecocentric gyration tensor for each set L, and then we estimate the egocentric asphericity ego-A_2 by averaging over the difference and sum of its eigenvalues over all sets. In figure 3.10 we illustrate the asphericity calculated using our theorem and by simulation for the stretched exponential memory kernel for various values of the parameter a. Figure 3.11 show the asphericity of memorised walk for the Lomax memory kernel obtained using our theorem and by simulation. For the two memory kernels the simulation consistence with the analytic results. Moreover, we note that slower decaying (also called fat-tailed) memory kernel result in more spherical

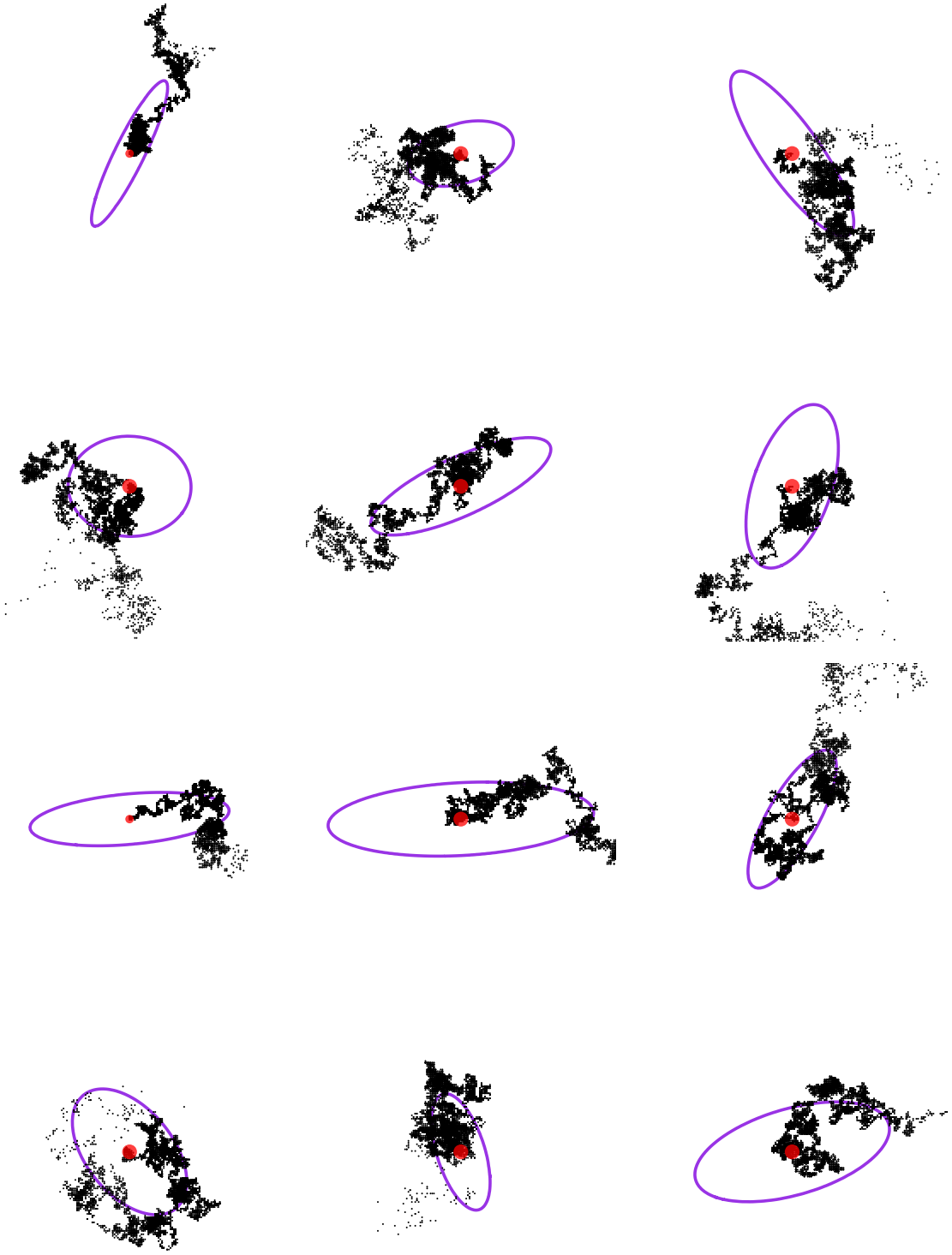

Figure 3.7: Memorised walks with stretched exponential memory kernel $\mu(t) = \frac{ae^{-t^a}}{\Gamma(a^{-1})}$ with parameter $a = 2$ when memory formation rate $c = 10^4$. The shape approximated using an ellipse (equation (3.15) with $\kappa = 2$). Red dots represent walker's current location.

shape. An intuitive interpretation of this result is that in slowly decaying kernel the time intervals between sample times increase rapidly, therefore the distances

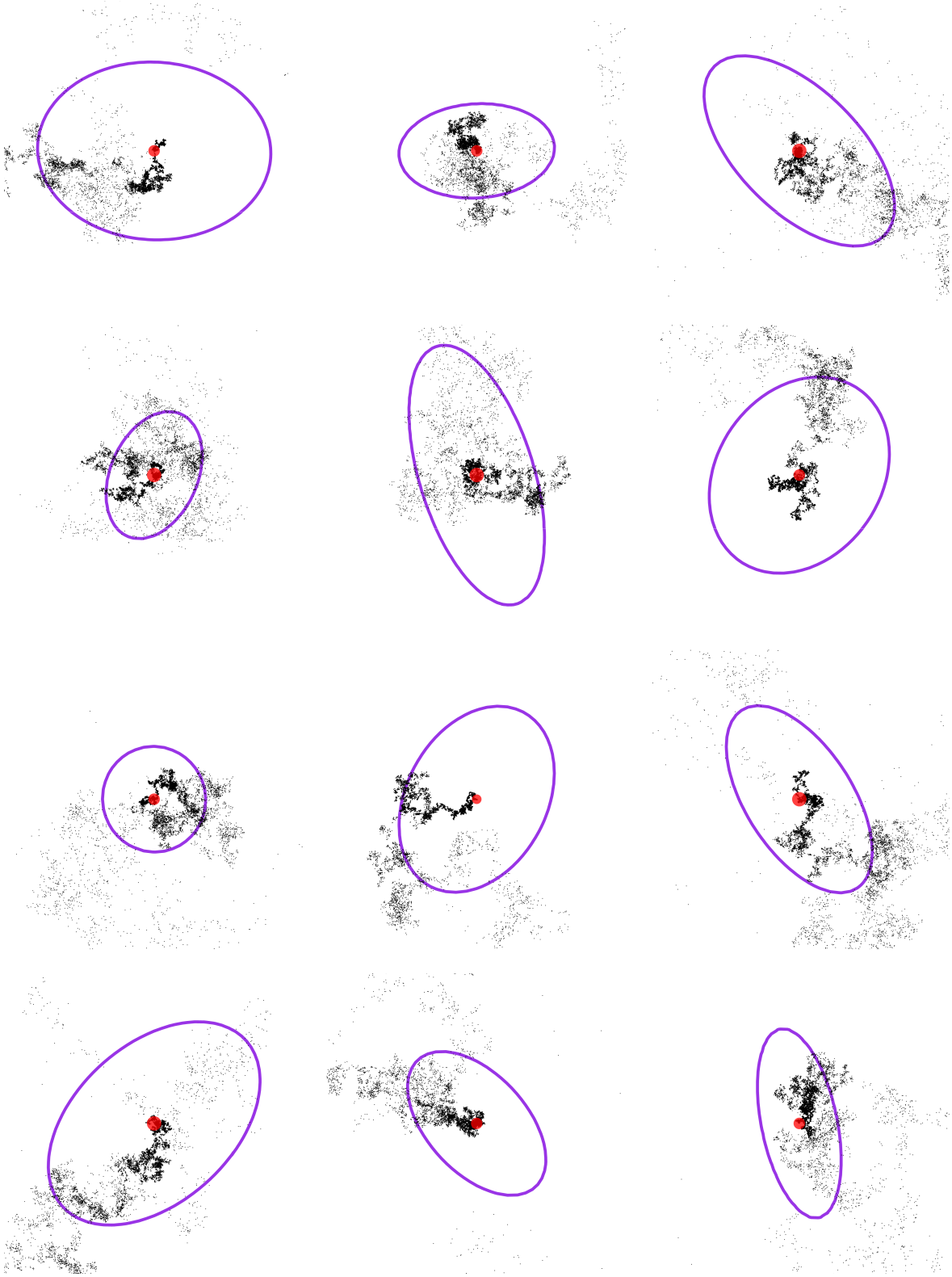

Figure 3.8: Memorised walks with stretched exponential memory kernel $\mu(t) = \frac{ae^{-t^a}}{\Gamma(a^{-1})}$ with parameter $a = 0.2$ when memory formation rate $c = 10^4$. The shape approximated using an ellipse (equation (3.15) with $\kappa = 2$). Red dots represent walker's current location.

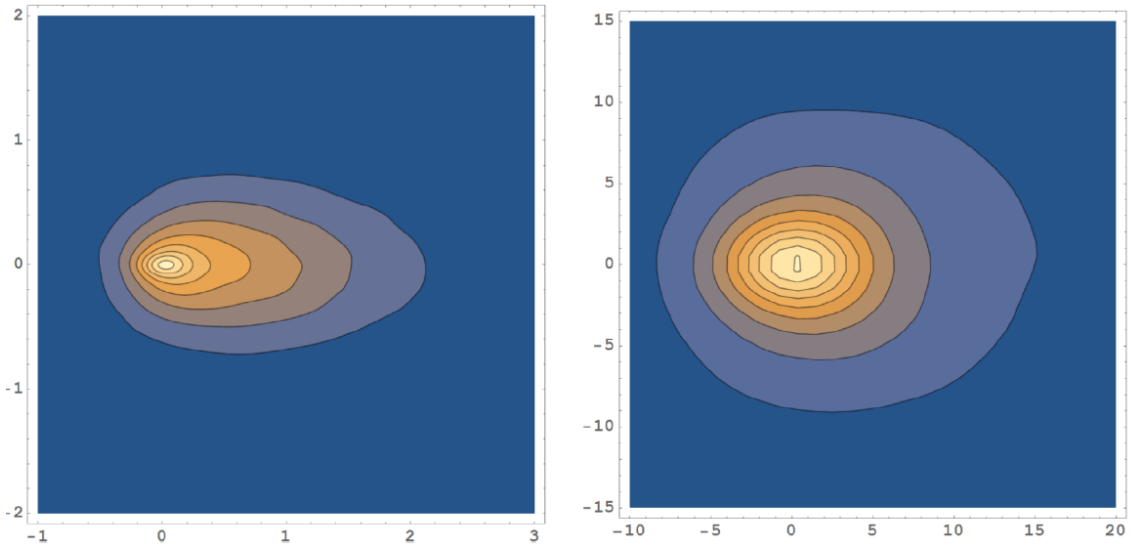

Figure 3.9: Memorised walk distribution for the stretched exponential memory kernel $\mu(t) = \frac{ae^{-t^a}}{\Gamma(a^{-1})}$ when $c = 1000$. Left: when the parameter $a = 1$ with cosponsoring asphericity ego-$A_2 = \frac{2}{3}$. Right: when the parameter $a = \frac{1}{2}$ with corresponding asphericity ego-$A_2 = \frac{10}{17}$.

between successive memorised locations become large and the space is covered more evenly with memorised locations. Figure 3.11 shows that as $a \to 1$ the simulated asphericity deviate slightly from the asphericity calculated analytically using our theorem. This deviation result from the fact that for finite rate c, the set S is finite and as a consequence the simulation cannot fully capture behaviour of $\mu(t)$ for large t. The effect becomes more obvious for smaller parameter c and for slower decaying memory kernels. The effect of the parameter c on simulated Asphericity A_2 can be seen in figure 3.12. We can see that by increasing c the simulated asphericity A_2 converges to the analytic asphericity. The rate of convergence is slower in the case of fat-tailed memory kernels.

3.3.4 Discussion

When the memory of the forager declines with time and the hiding places are regularly arranged within the home range (see chapter 2) it is worth to study the average shape of the memorised region around the current location of the foraging animal and how this shape affect the prey survival probability. In this model we studied the average shape of spatial memory of a forging animal for different memory kernel.

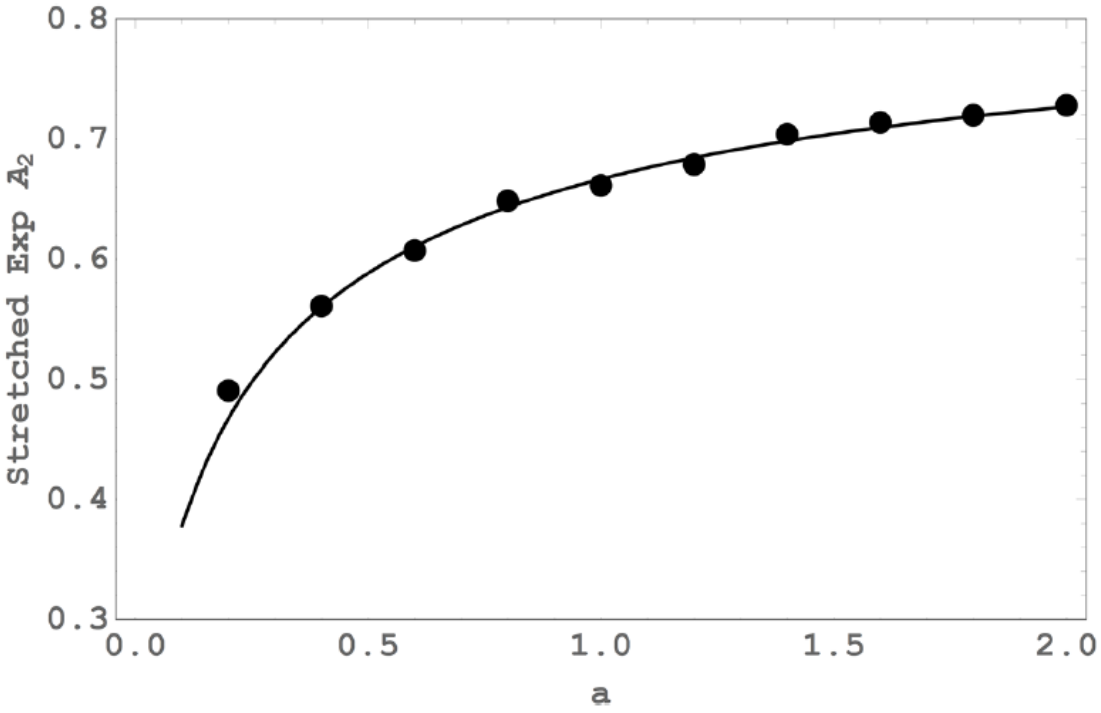

Figure 3.10: Egocentric asphericity of memorised walk with streched exponential memory kernel $\mu(t) = \frac{ae^{-t^a}}{\Gamma(a^{-1})}$ for different values of parameter a. Dots represent asphericity obtain by simulation when $c = 2000$.

The study shows that the memory kernel has a significant impact on the the shape of the spatial memory of the forager. We derived an analytic expression for calculating the egocentric version of the asphericity [73] ego-A_2 of a memorised walk (the set L) recalled according to the memory kernel μ. We confirmed our analytic result by simulation, and showed how the egocentric asphericity ego-A_2 describes the shape of the set L and how the shape of memorised walk is linked to the tail behaviour of the memory kernel μ. The fatter tailed (slower decaying) memory kernels result in more spherical shape of memorised walk.

Field studies recommend that later research in animal movement should investigate the impacts of memory [81, 82]. Many animals use memory in order to exploit efficiently their surroundings [50, 71, 11, 72], and it is known that memory affect the characteristic of foraging or search trajectories [56, 57, 68]. Field researches affirm that memory and learning play a critical role in foraging patterns of primates [8]. the movement pattern of bearded saki monkeys is more consistent with Brownian walk than Lévy walk [83]. In this chapter we modelled the walk using Brownian

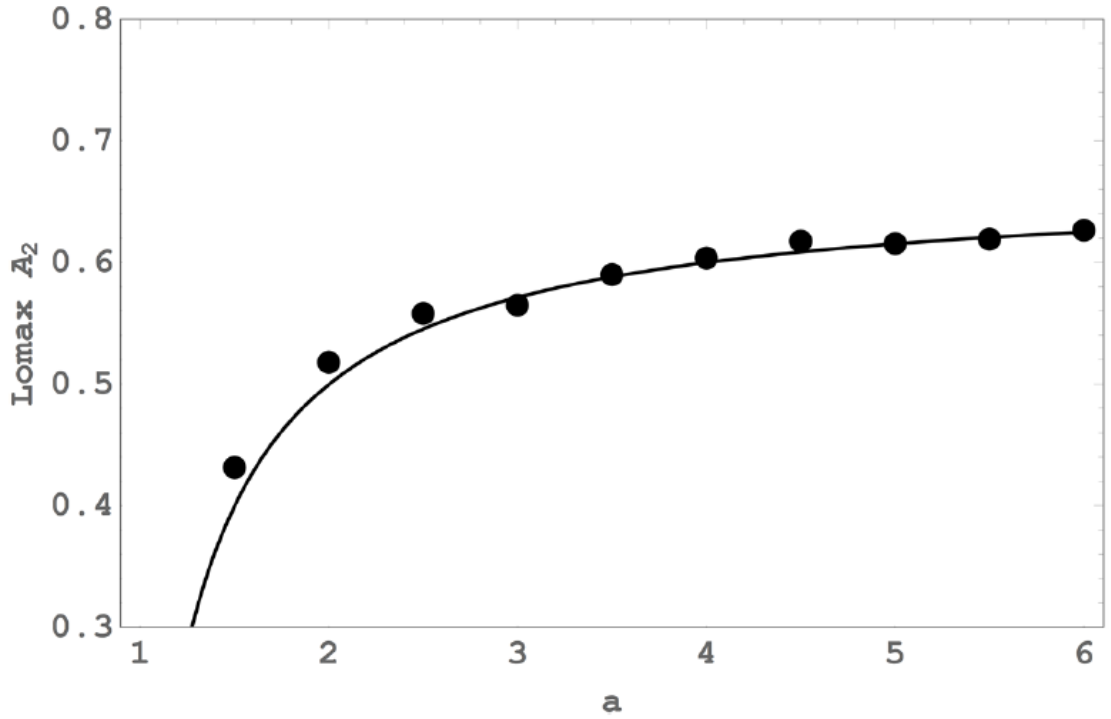

Figure 3.11: Asphericity of memorised walk for Lomax memory kernel $\mu(t) = \frac{a}{\lambda}\left(1+\frac{t}{\lambda}\right)^{-(a+1)}$ when $\lambda = 1$ for various values of parameter a. Dots represent result obained for simulation when $c = 10^4$ and computed from 10^4 simulation.

motion in combination with memory to construct the spatial map of the animal's surroundings. The possession of memory has its physiological expenses [56, 50], as does seeking for food sources, therefore in order to optimise foraging, one should optimise the use of memory and foraging trajectories simultaneously.

In this chapter we have approximated the shape of memory locations using ellipses. Since the ellipse is the simplest deformation of a circle, then a possible extension to our approximation is to consider higher-order deformations of the circle which more accurately describe the shape of memory locations.

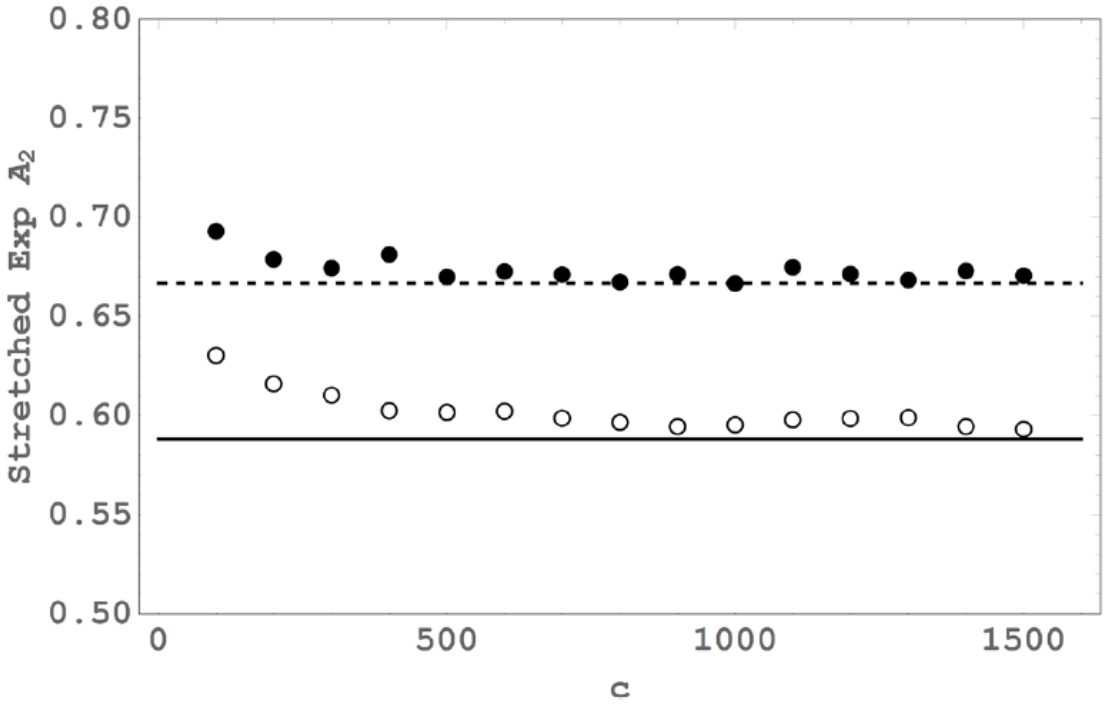

Figure 3.12: The effect of the parameter c on simulated Asphericity. Lines represent the analytic asphericities (as $c \to \infty$) for the stretched exponential kernel when $a = 1$(dashed) and $a = \frac{1}{2}$ (solid). Circles and dots represent simulated asphericities computed from 10^4 simulations.

Chapter 4

The shape and size of a tracked Brownian bridge

4.1 Introduction

The study of humans and animal movements is a rapidly evolving subject [84]. Understanding animals movement patterns have been of interests of biologist and ecologist for decades [84, 59]. The recent increase in data availability has enhanced research in animals movements to understand for examples population distributions [85], foraging behaviour [84, 65, 86, 87] competition for food resources [66, 68, 88], interaction among animals [89] and animal territories formation [90, 91]. Studying human locomotion patterns [92, 93] can enhance our comprehension of important processes, for instance, the spread of infectious diseases [94] and evolution of languages [95, 96, 97]. Recent technological advances in location-acquisition have produced automated collection of a myriad of trajectories representing the movement of various mobile objects such as animals and human [98, 60], which opened the opportunity to study the real mobility pattern and compare it with idealised mathematical models. Nevertheless, caution is required while interpreting data of incomplete trajectory because random processes sampling can bias the recoded paths' statistical properties [99]. For instance, in the case of periodic data sampling, non-Levy move-

ment can be incorrectly interpreted as Levy flight if sampling time intervals are too large [100, 101]. Human movement location data mostly collected at certain random events such as mobile phone location is collected at the time of a communication events [99, 102, 103]. Due to availableness of movement data, it is beneficial to study and understand how different tracking processes affect the statistical properties of mobility patterns.

In this chapter we are interested in calculating the average spatial pattern for the case where the walker repeatedly returns to a certain location. We use the same method used in the previous chapter where we studied the average shape of mental maps of animals, however we have used Brownian bridge rather than Brownian motion [104]. Brownian bridge is a widely used continuous-time process for modelling animals trajectories [105], for instance, investigating home ranges of snakes [106], and birds [107]. In this chapter, random walks is seen as the movement path which are tracked [99] in the sense that locations are collected at a time varying rate.

4.2 The model

In this chapter we introduce a simple model in order to study the average shapes and sizes of the recorded observations of a continuous two dimension random walks. The observations (tracking) time S is modelled as arrival times of a non-homogeneous Poisson process supported on the interval $[0, 1]$ with intensity function $\lambda(t) = c\mu(t)$, where c is a positive constant and the function μ is a probability density function of a continuous probability distribution supported on the interval $[0, 1]$ with finite mean. We refer to the constant c as the intensity rate and the function μ as the tracking strategy kernel of the walker. Given B is a Brownian bridge (for the definition of Brownian bridge we refer the reader to section 1.3.3), then the one dimension tracked Brownian bridge is defined as $\{B(t) : t \in S \cup \{0, 1\}\}$. Figure 4.1 illustrates an example of a one dimension Brownian bridge and the corresponding tracked Brownian bridge.

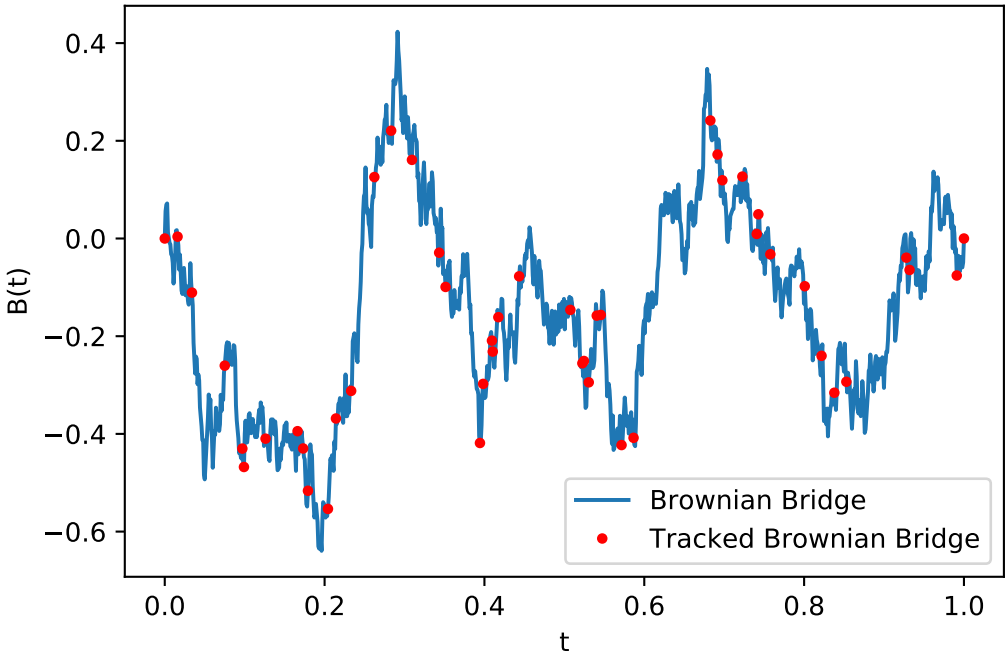

Figure 4.1: An example of one dimension Brownian bridge and the corresponding tracked Brownian bridge for tracking strategy kernel $\mu(t) = 1$ and $c = 50$.

The tracked path in two dimensions is defined similarly as in one dimension case, that is,

$$L = \{\big(X(t), Y(t)\big) : t \in S \cup \{0, 1\}\} \tag{4.1}$$

where X and Y are two independent one dimension Brownian bridges. Figure 4.2 shows an example of two dimension Brownian bridge and the corresponding tracked Brownian bridge.

In order to study the average shape of the tracked Brownian bridge in two dimensions (the set L) we use the same method used in the previous chapter which is originally applied by Rudnick and Gaspari [73] to calculate the asphericity of random walks. In this chapter and the previous chapter we calculate the egocentric asphericity which is different from the standard asphericity. In the egocentric asphericity the entries of the gyration tensor are moments calculated about the current location of the walker (the origin) instead of the centre of mass of the walk as in the standard asphericity. The egocentric gyration tensor for the tracked Brownian

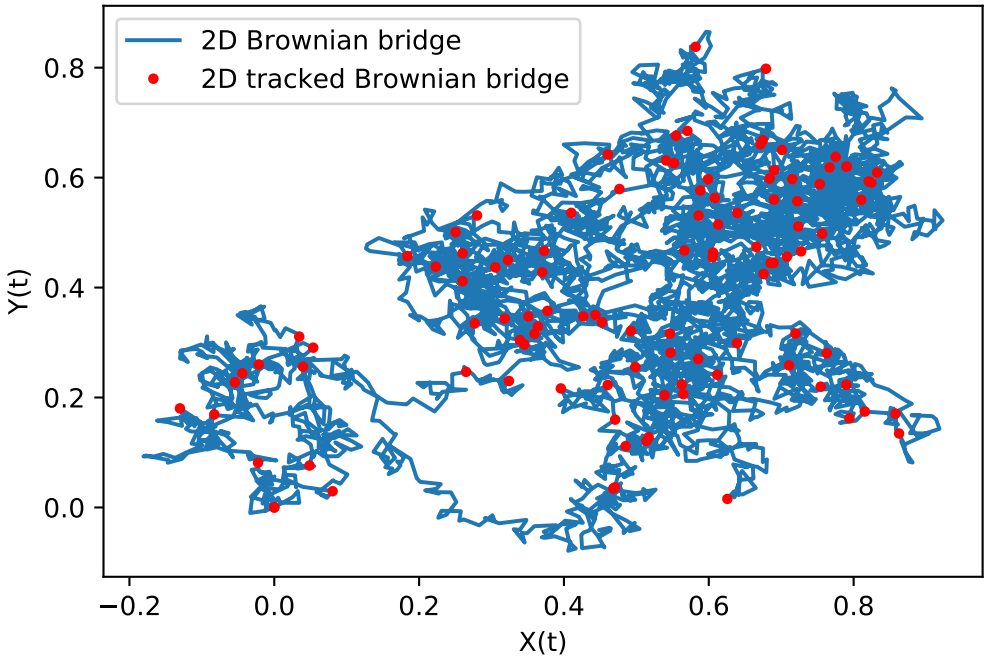

Figure 4.2: An example of two dimension Brownian bridge and the corresponding tracked Brownian bridge for tracking strategy kernel $\mu(t) = 1$ and $c = 100$.

bridge (the set L) is given by

$$T = \begin{bmatrix} T_{11} & T_{12} \\ T_{12} & T_{22} \end{bmatrix} = \begin{bmatrix} \frac{1}{2+|S|}\sum_{t\in S} X^2(t) & \frac{1}{2+|S|}\sum_{t\in S} X(t)Y(t) \\ \frac{1}{2+|S|}\sum_{t\in S} X(t)Y(t) & \frac{1}{2+|S|}\sum_{t\in S} Y^2(t) \end{bmatrix} \tag{4.2}$$

where we note a minor difference from the definition for a memorized walk: we recall *both* the start and end of the walk, not just the start. As previously noted, since the egocentric gyration tensor T is a symmetric positive definite [80], then T has two positive eigenvalues λ_1 and λ_2 and two orthogonal eigenvectors v_1 and v_2. The eigenvalues give the mean-square displacement of the tracked random walk's shape from the origin in the direction of the corresponding eigenvector. As with the memorized walk, the shape of tracked random walk may be approximated by an ellipse centred at the origin and given by the equation

$$\mathbf{v}^T T^{-1} \mathbf{v} = \kappa^2, \tag{4.3}$$

where $\kappa > 0$ and $\mathbf{v} \in \mathbb{R}^2$. Different choice of the parameter κ does not influence the asphericity, and this parameter will only be selected so that a random walk path fits inside the ellipse that given by (4.2). We are interested in calculating the average egocentric asphericity of the ellipse for different tracking strategy kernels. Figure 4.3 and figure 4.4 show an examples of the tracked Brownian bridge and the ellipse given by their gyration tensors. In the remaining of this chapter, for simplicity reason, we sometimes call the egocentric asphericity as asphericity.

4.3 Analytic Asphericity

As the intensity rate $c \to \infty$, and by applying A.1.4, the elements of the matrix T in (4.2) can be approximated as

$$T = \begin{bmatrix} T_{11} & T_{12} \\ T_{12} & T_{22} \end{bmatrix} = \begin{bmatrix} \int_0^1 X^2(s)\mu(s)ds & \int_0^1 X(s)Y(s)\mu(s)ds \\ \int_0^1 X(s)Y(s)\mu(s)ds & \int_0^1 Y^2(s)\mu(s)ds \end{bmatrix}. \tag{4.4}$$

The following theorem allows us to compute exactly the average egocentric asphericity of two dimensions tracked Brownian bridge (the set L) according to tracking strategy kernel $\mu(t)$.

Theorem 4.3.1 (Main Theorem)**.** *Letting μ is the tracking strategy kernel and*

$$M_0(t) = \int_0^t \mu(s)ds,\ M_1(t) = \int_0^t M_0(s)ds \text{ and } M_2(t) = \int_0^t M_1(s)ds \tag{4.5}$$

The egocentric asphericity of two dimension tracked Brownian bridge defined in (4.1) as $c \to \infty$ is given by

$$\textit{ego-}A_2 = 1 - 4\frac{\alpha}{\beta}, \tag{4.6}$$

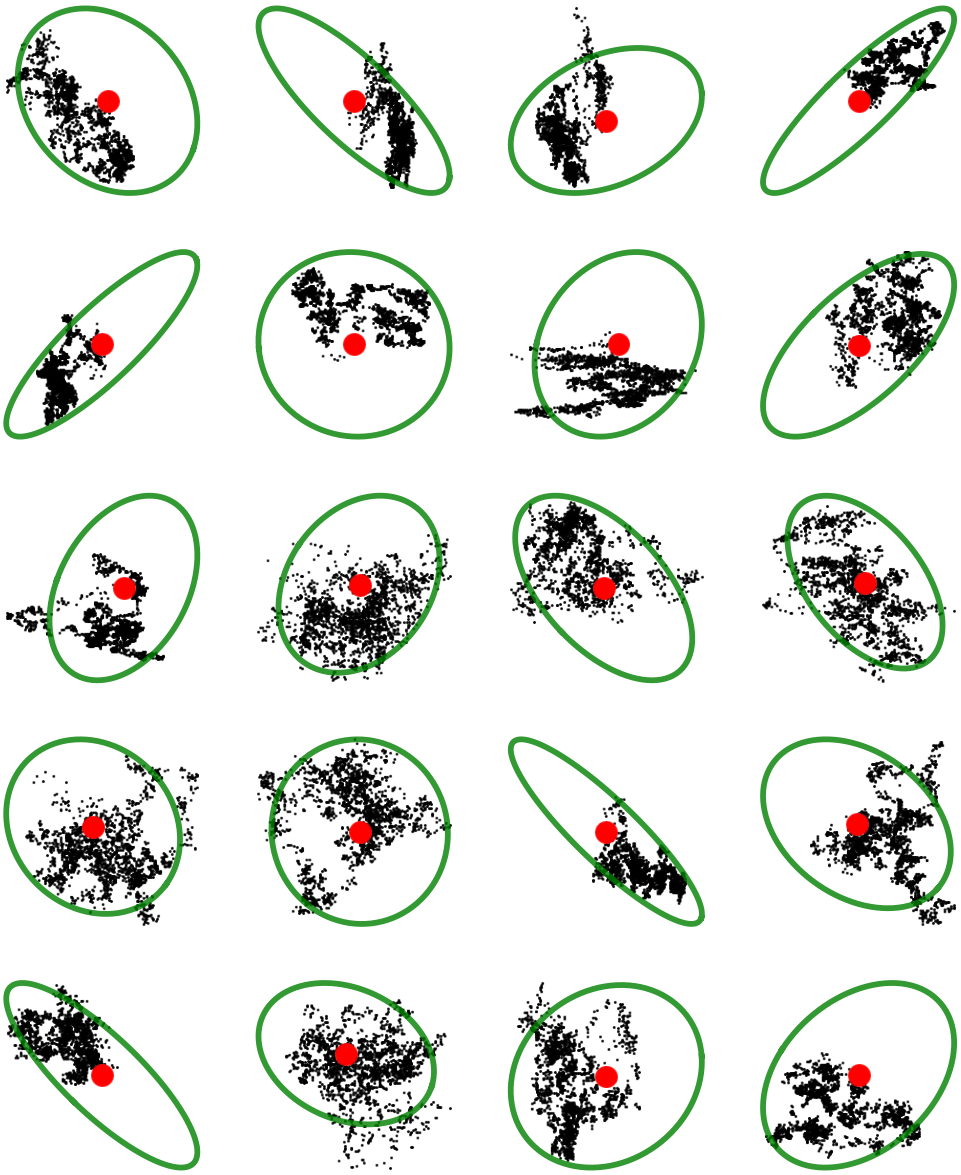

Figure 4.3: Tracked Brownian bridge for triangular kernel with $a = 0.5$ and $c = 2000$. Red dot represent the point $(0, 0)$ and green ellipse given by equation (4.3) when $\kappa = 1$

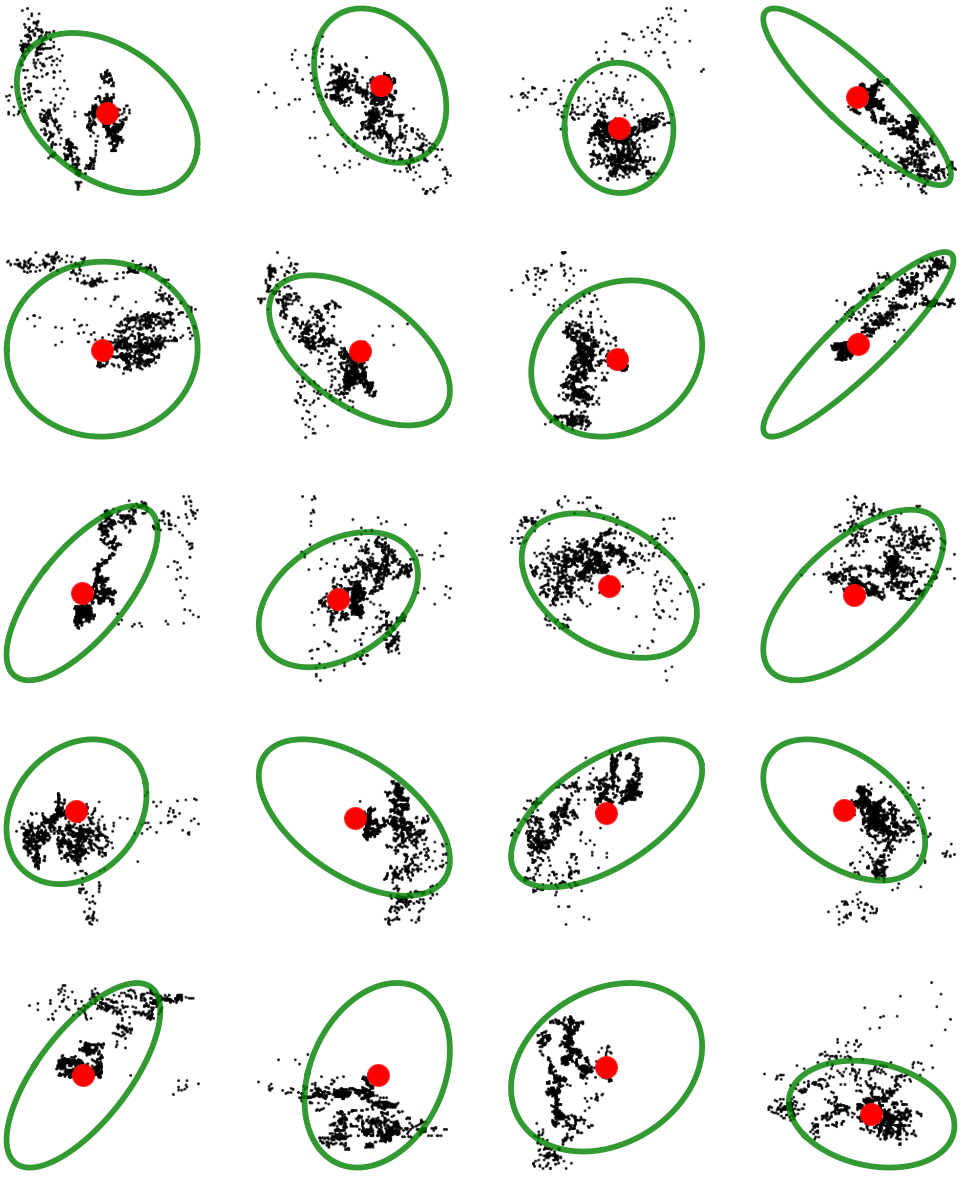

Figure 4.4: Tracked Brownian bridge for exponential kernel with $\lambda = 5$ and $c = 1000$. Red dot represent the point $(0, 0)$ and green ellipse given by equation (4.3) when $\kappa = 1$

where

$$\begin{aligned}\alpha =&4M_0(1)(M_1(1)-2M_2(1))-M_1^2(1)+4M_1(1)M_2(1)\\&+4\int_0^1 t\mu(t)(2M_2(t)-tM_1(t))dt\\&-2\int_0^1 tM_0^2(t)dt-2\int_0^1(M_1(t)-tM_0(t))^2dt\end{aligned}\tag{4.7}$$

and

$$\begin{aligned}\beta =&-4(M_1^2(1)-4M_1(1)M_2(1)+8M_2^2(1))\\&+8\int_0^1(1-t)tM_0^2(t)dt\\&+16\int_0^1(1-2t)M_0(t)(2M_2(t)-tM_1(t))dt\\&+8\int_0^1 M_1(t)((1-4t)M_1(t)+8M_2(t))dt.\end{aligned}\tag{4.8}$$

For the proof of Theorem 4.3.1 we refer the reader to the appendix. The next Proposition allow us to calculate the size of two dimension tracked Brownian bridge.

Proposition 4.3.1. *The average radius of gyration r^2 of two dimension tracked Brownian bridge defined in (4.1) as $c\to\infty$ is given by*

$$r^2=2M_1(1)-4M_2(1).\tag{4.9}$$

Proof. Recalt that $r^2=2\mathbb{E}\left[\int_0^1 X^2(t)\mu(t)dt\right]$. By using (A.31), we have

$$r^2=2M_1(1)-4M_2(1).\tag{4.10}$$

□

4.3.1 Examples

Here we are aiming to apply the asphericity formula derived in (4.6) on selected tracking kernels and compare the analytic Asphericity with simulation.

Uniform tracking strategy kernel

For the probability density function of a continuous uniform distribution on $[0, a]$ where $0 < a \leq 1$ as a tracking strategy kernel, that is, $\mu(t) = \frac{1}{a}\mathbf{1}_{\{0\leq t\leq a\}}$ and the corresponding CDF $M_0(t) = \int_0^t \mu(s)ds = \begin{cases} \frac{t}{a} & \text{if } 0 \leq t \leq a \\ 1 & \text{if } t \geq a \end{cases}$. Also we calculated the functions

$$M_1(t) = \begin{cases} \frac{t^2}{2a} & \text{if } 0 \leq t \leq a \\ t - \frac{a}{2} & \text{if } a \leq t \leq 1 \end{cases}$$

and

$$M_2(t) = \begin{cases} \frac{t^3}{6a} & \text{if } 0 \leq t \leq a \\ \frac{1}{2}\left(t^2 - at + \frac{1}{3}a^2\right) & \text{if } a \leq t \leq 1 \end{cases}$$

The formula in (4.6) in this case can be simplified to

$$\text{ego-}A_2(a) = 1 + \frac{12a - 15}{40a^2 - 108a + 75}. \tag{4.11}$$

The asphericity ego-$A_2(a)$ here is a decreasing function on the interval $[0, 1]$ and

$$\lim_{a\to 0^+} \text{ego-}A_2(a) = \frac{4}{5} = 0.8 \tag{4.12}$$

$$\lim_{a\to 1^-} \text{ego-}A_2(a) = \frac{4}{7} \approx 0.5714 \tag{4.13}$$

From figure 4.5 we see that the simulation consistent with analytic asphericity calculation by (4.11). The radius of gyration is given by

$$r^2(a) = a - \frac{2}{3}a^2. \tag{4.14}$$

The maximum value is $\frac{3}{8}$ obtained at $a = \frac{3}{4}$, and

$$\lim_{a\to 1^-} r^2(a) = \frac{1}{3}. \tag{4.15}$$

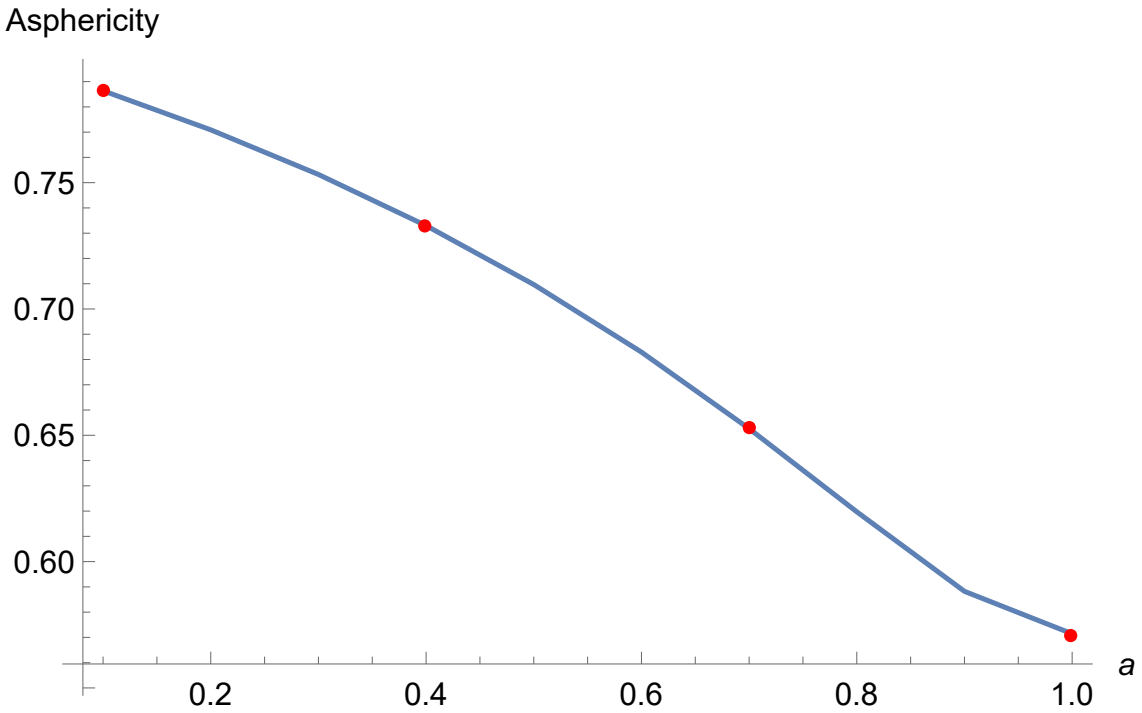

Figure 4.5: Asphericity for the uniform tracking kernel $\mu(t) = \frac{1}{a}\mathbf{1}_{\{0\leq t\leq a\}}$ for $0 \leq a \leq 1$. Red dots represent simulation when $c = 10^4$ and the blue graph represent the result obtained analytically by (4.11).

Exponential tracking strategy kernel

Consider a probability density function of an exponential distribution with parameter $\lambda > 0$ supported on $[0, 1]$, then $\mu(t) = \frac{\lambda e^{-\lambda t}}{1-e^{-\lambda}}$ and corresponding CDF

$$M_0(t) = \frac{e^{\lambda}}{1 - e^{\lambda}}(e^{-\lambda t} - 1)$$

also we calculate that

$$M_1(t) = \frac{e^{\lambda}(\lambda t + e^{-\lambda t} - 1)}{\lambda(e^{\lambda} - 1)}$$

and

$$M_2(t) = \frac{e^{\lambda}\left(\lambda t(\lambda t - 2) - 2e^{-\lambda t} + 2\right)}{2(e^{\lambda} - 1)\lambda^2}.$$

The formula in (4.11) can be simplified as follow

$$\text{ego-}A_2(\lambda) = \frac{2(8 - 16e^{\lambda} + 5\lambda + \lambda^2 + e^{2\lambda}(8 - 5\lambda + \lambda^2))}{16 + 13\lambda + 3\lambda^2 + 4e^{\lambda}(\lambda^2 - 8) + e^{2\lambda}(16 - 13\lambda + 3\lambda^2)}. \tag{4.16}$$

The asphericity for the exponential kernel is increasing function on $(0, \infty)$ and

$$\lim_{\lambda \to 0^+} \text{ego-}A_2(\lambda) = \frac{4}{7} \approx 0.5714$$
$$\lim_{\lambda \to \infty} \text{ego-}A_2(\lambda) = \frac{2}{3} \approx 0.6667.$$

Figure 4.6 illustrate that the analytic asphericity obtained by (4.16) is consistent with simulation. The radius of gyration of the exponential kernel is given by

$$r^2(\lambda) = \frac{2\left(e^{\lambda}(\lambda - 2) + \lambda + 2\right)}{(e^{\lambda} - 1)\,\lambda^2}. \tag{4.17}$$

The radius of gyration here is decreasing on the interval $(0, \infty)$ and we also observe that

$$\lim_{\lambda \to 0^+} r^2(\lambda) = \frac{1}{3} \text{ and } \lim_{\lambda \to \infty} r^2(\lambda) = 0.$$

Triangle tracking strategy kernel

For $a \in (0, 1)$, the tracking strategy kernel here taken to be the following PDF

$$\mu(t) = \begin{cases} \frac{2}{a}t & \text{if } 0 \le t \le a \\ \frac{2}{a-1}t + \frac{2}{1-a} & \text{if } a < t \le 1 \\ 0 & \text{otherewise} \end{cases} \tag{4.18}$$

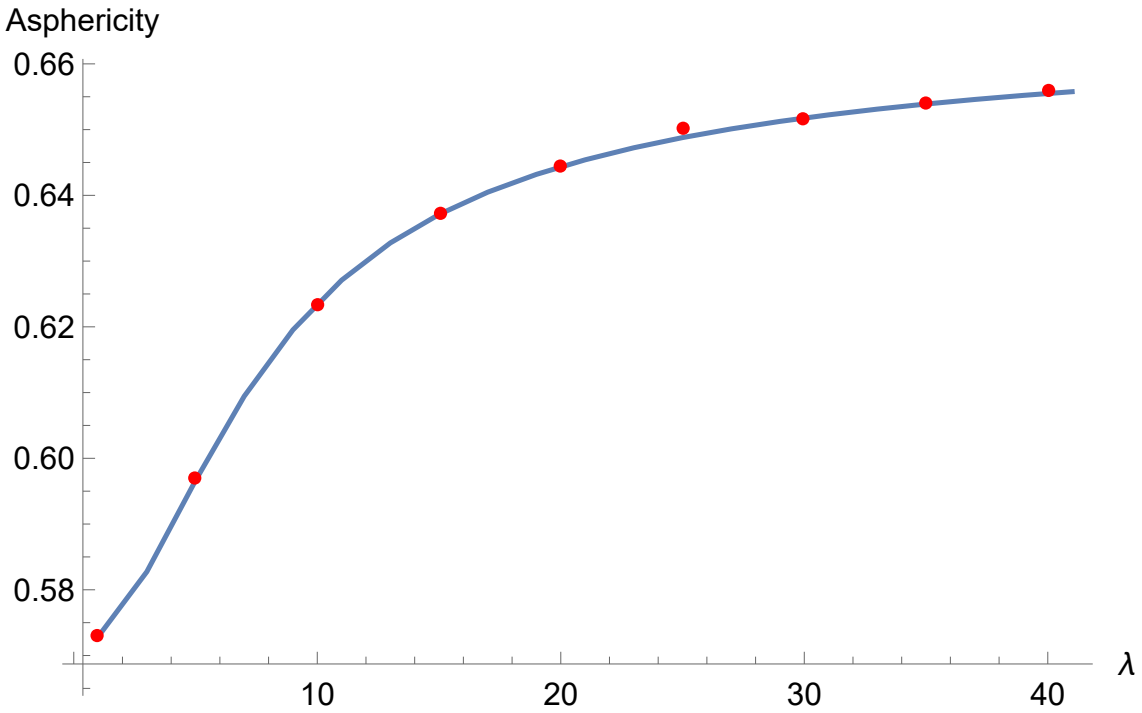

Figure 4.6: Asphericity for the exponential tracking kernel for $\lambda \geq 0$ $\mu(t) = \frac{\lambda e^{-\lambda t}}{1-e^{-\lambda}}$. Red dots represent simulation when $c = 10^4$ and the blue graph represent the result obtained analytically by (4.16) .

with the corresponding functions

$$M_0(t) = \begin{cases} \frac{t^2}{a} & \text{if } 0 \leq t \leq a \\ \frac{a+t^2-2t}{a-1} & \text{if } a < t \leq 1 \\ 0 & \text{otherwise} \end{cases},$$

$$M_1(t) = \begin{cases} \frac{t^3}{3a} & \text{if } 0 \leq t \leq a \\ \frac{a^2-3at-t^3+3t^2}{3(1-a)} & \text{if } a < t < 1 \\ 0 & \text{otherwise} \end{cases},$$

$$M_2(t) = \begin{cases} \frac{t^4}{12a} & \text{if } 0 \leq t \leq a \\ \frac{a^3-4a^2t+6at^2+t^4-4t^3}{12(a-1)} & \text{if } a < t < 1 \\ 0 & \text{otherwise} \end{cases}.$$

The asphericity is given by

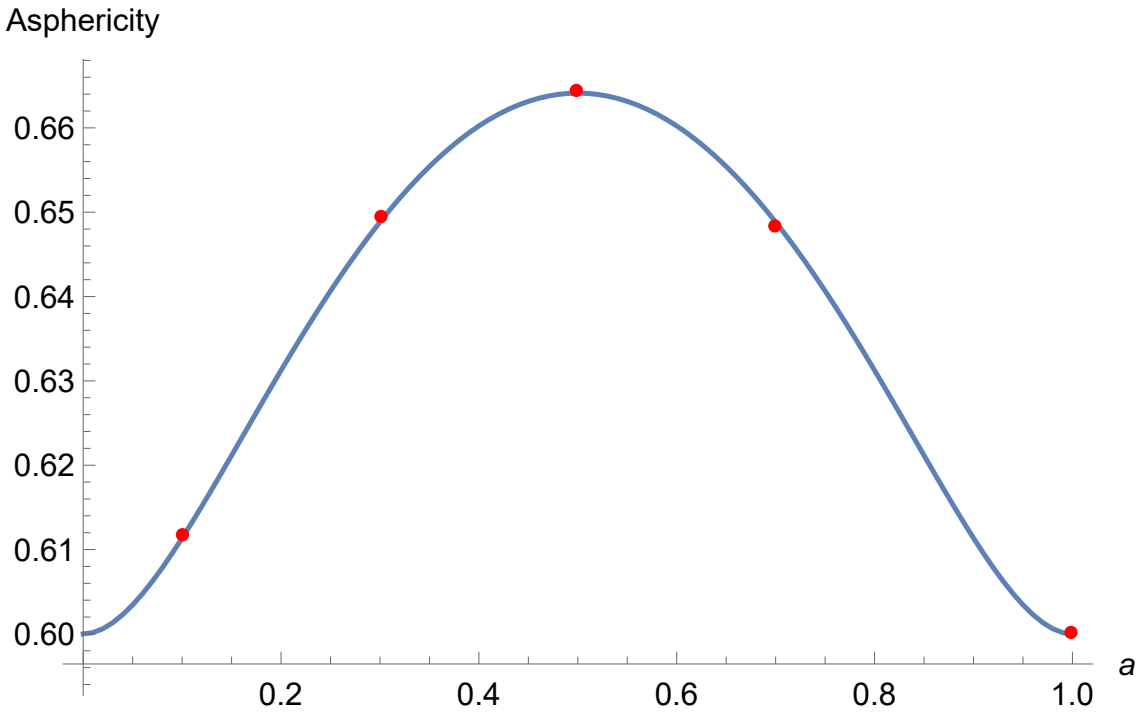

Figure 4.7: Egocentric Asphericity for the triangular tracking kernel for $0 < a < 1$. Red dots represent simulation when $c = 10^4$ and the blue graph represent the result obtained analytically by (4.19) .

$$\text{ego-}A_2(a) = \frac{15a^4 - 30a^3 + 9a^2 + 6a + 3}{11a^4 - 22a^3 + a^2 + 10a + 5}. \tag{4.19}$$

In particular, we have

$$\lim_{a\to 0^+} \text{ego-}A_2(a) = \lim_{a\to 1^-} \text{ego-}A_2(a) = \frac{3}{5} = 0.6.$$

The maximum asphericity is 0.664122 obtained at $a = \frac{1}{2}$ and the minimum asphericity value is 0.6 obtained at $a = 0$ and $a = 1$. Figure 4.7 shows asphericity for various values of parameter $0 < a < 1$.

The radius of gyration is given by

$$r^2(a) = \frac{1}{3}(1 + a - a^2).$$

Its maximum value is $\frac{5}{12}$ obtained at $a = \frac{1}{2}$ and

$$\lim_{a\to 0^+} r^2(a) = \lim_{a\to 1^-} r^2(a) = \frac{1}{3}.$$

Inverted triangle tracking strategy kernel

For $0 < a < 1$, consider the tracking strategy kernel

$$\mu(t) = \begin{cases} -\frac{2}{a}t + 2 & \text{if } 0 \le t \le a \\ \frac{2}{1-a}t + \frac{2a}{a-1} & \text{if } a \le t \le 1 \\ 0 & \text{otherwise,} \end{cases}$$

and the corresponding functions

$$M_0(t) = \begin{cases} -\frac{t^2}{a} + 2t & \text{if } 0 \le t \le a \\ \frac{-2at+a+t^2}{1-a} & \text{if } a \le t \le 1 \\ 0 & \text{otherwise} \end{cases}$$

$$M_1(t) = \begin{cases} -\frac{t^3}{3a} + t^2 & \text{if } 0 \le t \le a \\ \frac{a^2+3a(t-1)t-t^3}{3(a-1)} & \text{if } a \le t \le 1 \\ 0 & \text{otherwise} \end{cases}$$

$$M_2(t) = \begin{cases} \frac{t^3(4a-t)}{12a} & \text{if } 0 \le t \le a \\ \frac{a^3-4a^2t-4at^3+6at^2+t^4}{12-12a} & \text{if } a \le t \le 1 \\ 0 & \text{otherwise} \end{cases}$$

The asphericity is given by

$$\text{ego-}A_2(a) = \frac{37a^4 - 74a^3 + 11a^2 + 26a - 15}{a^4 - 2a^3 - 47a^2 + 48a - 25}, \tag{4.20}$$

and it has maximum at $a_1 = \frac{1}{2} \pm \frac{\sqrt{21}}{10}$ with value ego-$A_2(a_1) = 0.602329$ and has

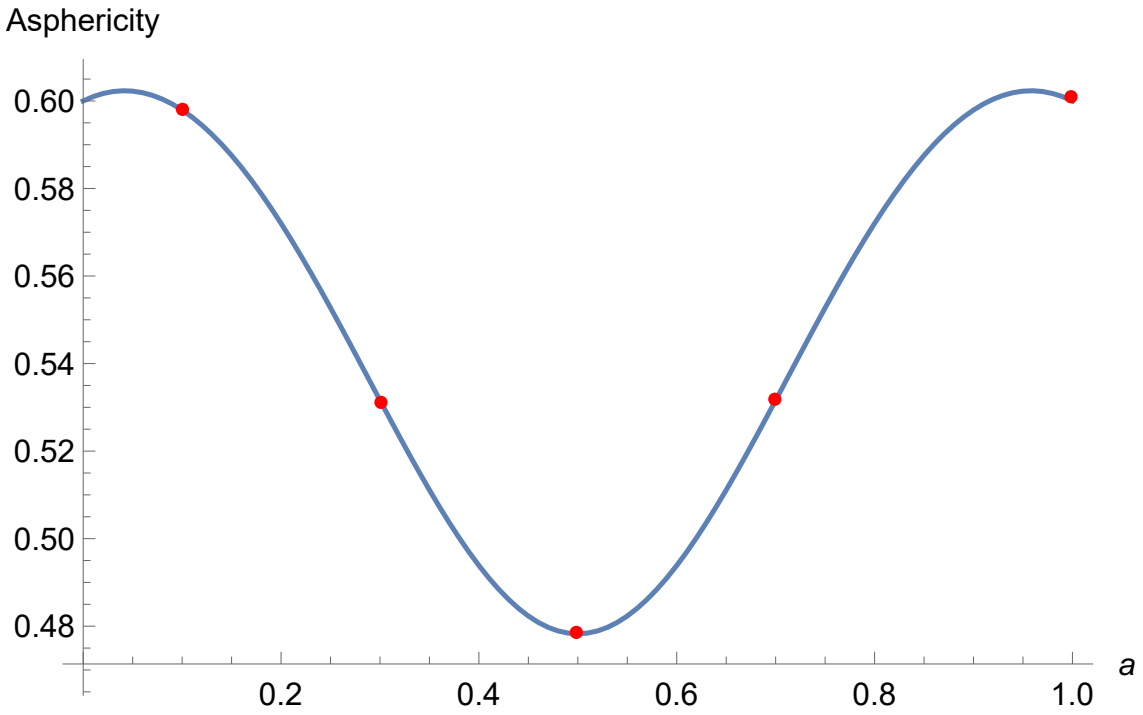

Figure 4.8: Asphericity for the Inverted triangle tracking kernel for $a \in (0,1)$. Red dots represent simulation when $c = 10^4$ and the blue graph represent the result obtained analytically by (4.20) .

minimum at $a_2 = \frac{1}{2}$ with value ego-$A_2(a_2) = \frac{11}{23} \approx 0.478261$. The asphericity ego-$A_2(a)$ is increasing on the intervals $(0, \frac{1}{2} - \frac{\sqrt{21}}{10})$ and $(\frac{1}{2}, \frac{1}{2} + \frac{\sqrt{21}}{10})$, and decreasing on the intervals $(\frac{1}{2} - \frac{\sqrt{21}}{10}, \frac{1}{2})$ and $(\frac{1}{2} + \frac{\sqrt{21}}{10}, 1)$. Figure 4.8 illustrate the asphericity calculated exactly by (4.20) against simulation for various values of parameter $0 < a < 1$. The radius of gyration is given by

$$r^2(a) = \frac{1}{3}\left(a^2 - a + 1\right),$$

with minimum value $\frac{1}{4}$ at $a = \frac{1}{2}$ and also

$$\lim_{a \to 0^+} r^2(a) = \lim_{a \to 1^-} r^2(a) = \frac{1}{3}.$$

U-Shaped tracking strategy kernel

Consider the tracking strategy kernel $\mu(t) = (2k+1)(2t-1)^{2k}$ for $t \in [0,1]$ and $k \in \mathbb{N}$, and the corresponding functions are

$$\begin{aligned} M_0(t) &= \frac{1}{2}[(2t-1)^{2k+1}+1], \\ M_1(t) &= \frac{1}{2}\left(\frac{(2t-1)^{2k+2}-1}{4(k+1)}+t\right), \\ M_2(t) &= \frac{1}{8}\left(-\frac{t}{k+1}+\frac{(2t-1)^{2k+3}+1}{(k+1)(4k+6)}+2t^2\right). \end{aligned}$$

The asphericity is given by

$$\text{ego-}A_2(k) = \frac{4\,(2k^2+4k+3)}{20k^2+40k+21}. \tag{4.21}$$

The asphericity here is decreasing with maximum value $\frac{4}{9} \approx 0.444$ at $k=1$ and also

$$\lim_{k\to\infty} \text{ego-}A_2(k) = \frac{2}{5} \approx 0.4. \tag{4.22}$$

Figure 4.9 illustrate the asphericity for various values of k. The radius of gyration is given by

$$r^2(k) = \frac{1}{2k+3}.$$

The radius of gyration here is decreasing with maximum value $\frac{1}{5}$ obtained at $k=1$ and also we have

$$\lim_{k\to\infty} r^2(k) = 0. \tag{4.23}$$

4.4 Simulation

The tracking Brownian bridge is constructed in similar way as the memorised Brownian motion in previous chapter. We first generate the set of tracking times S by

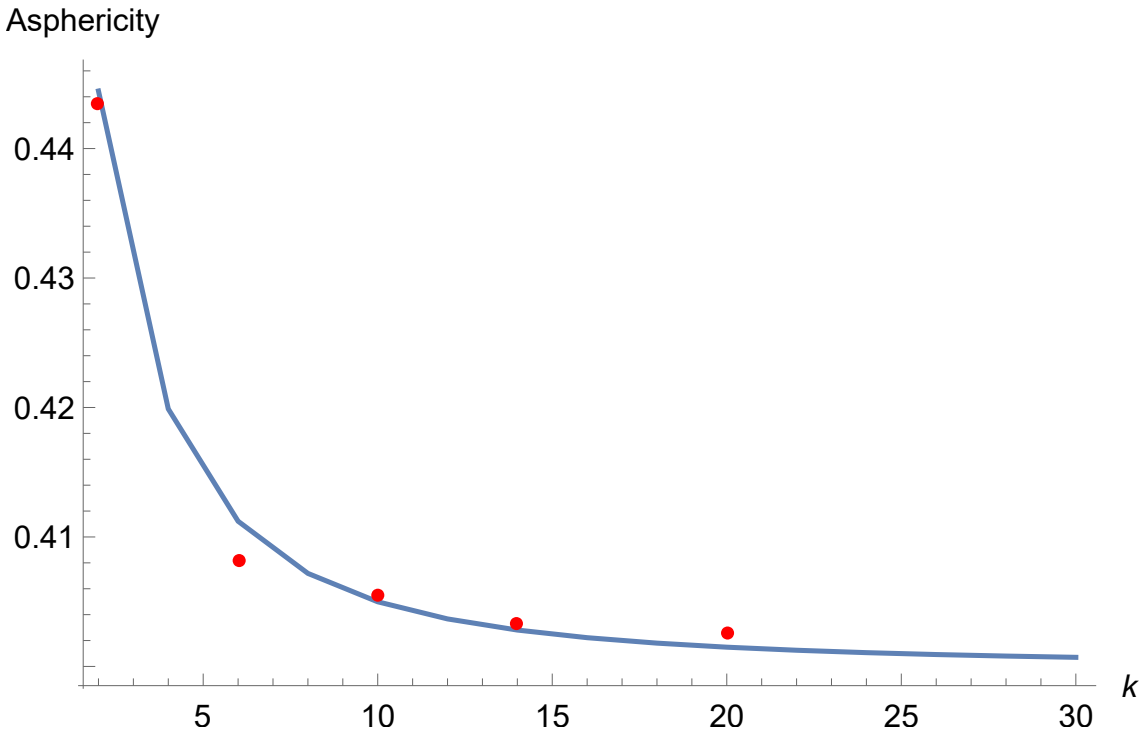

Figure 4.9: Asphericity for the tracking strategy kernel $\mu(t) = (2k+1)(2t-1)^{2k}$ for different value of k. Red dots represent the corresponding asphericity from simulation when $c = 10^4$.

modelling it as the arrival times of non-homogeneous Poisson point process on $[0,1]$ with intensity function $\lambda(t) = c\mu(t)$. At time $\tau \in [0,1]$, the cumulative distribution function (CDF) of the next arrival time Z is

$$\mathbb{P}[Z \leq t | Z > \tau] = F_\tau(t) = \begin{cases} 1 - \exp(-c\int_\tau^t \mu(s)ds) & \text{if } t \geq \tau \\ 0 & \text{otherwise} \end{cases}.$$

The inverse of the function $F_\tau(t)$ on the modified domain $[0,1]$ is given by

$$F_\tau^{-1}(u) = \begin{cases} M_0^{-1}\left(M_0(\tau) - \frac{\ln(1-u)}{c}\right) & \text{if } u \leq F_\tau(1) \\ 1 & \text{if } u > F_\tau(1), \end{cases} \tag{4.24}$$

where M_0 is the cumulative distribution function of the density function μ. If Z_k the kth arrival (tracking) time, then the next tracking time may be simulated by

$Z_{k+1} \stackrel{d}{=} F^{-1}_{Z_k}(U)$ where the notation $\stackrel{d}{=}$ indicate equality in distribution and U is a standard uniform random variable. After generating the set S we can now calculate the locations of two independent Brownian motion W_1 and W_2 at the tracking times $S \cup \{0, 1\}$ by knowing that

$$W_1(Z_{k+1}) - W_1(Z_k) \sim \mathcal{N}(0, Z_{k+1} - Z_k)$$
$$W_2(Z_{k+1}) - W_2(Z_k) \sim \mathcal{N}(0, Z_{k+1} - Z_k)$$

where $\mathcal{N}(\mu, \sigma^2)$ is the normal (Gaussian) distribution with expectation μ and variance σ^2. Now we can construct the two independent tracking Brownian bridge X and Y by

$$X(Z_k) = W_1(Z_k) - Z_k W_1(1)$$
$$Y(Z_k) = W_2(Z_k) - Z_k W_2(1)$$

Figure 4.2 illustrate an example of two dimensions Brownian bridge and the corresponding tracked brownian bridge.

4.4.1 Comparing exact results against simulation

In order to verify our analytic result (4.3.1) by simulation, we generate large number of the tracked Brownian bridge (the set L) for given tracking strategy $\mu(t)$ and rate c, then we extract the eigenvalues λ_1 and λ_2 from the egocentric gyration tensor (defined in (4.2)) for each L. the egocentric asphericity calculate by

$$\text{ego-}A_2 = \frac{\mathbb{E}[(\lambda_1 - \lambda_2)^2]}{\mathbb{E}[(\lambda_1 + \lambda_2)^2]}.$$

To compare our analytic results (as $c \to \infty$) with simulation and see the effect of intensity rate, we will consider closely the exponential and U-shaped kenel. Figure 4.10 and figure 4.11 illustrate the analytic asphericity for the exponential and U-shaped kernels against simulated asphericty for different values of intensity rates

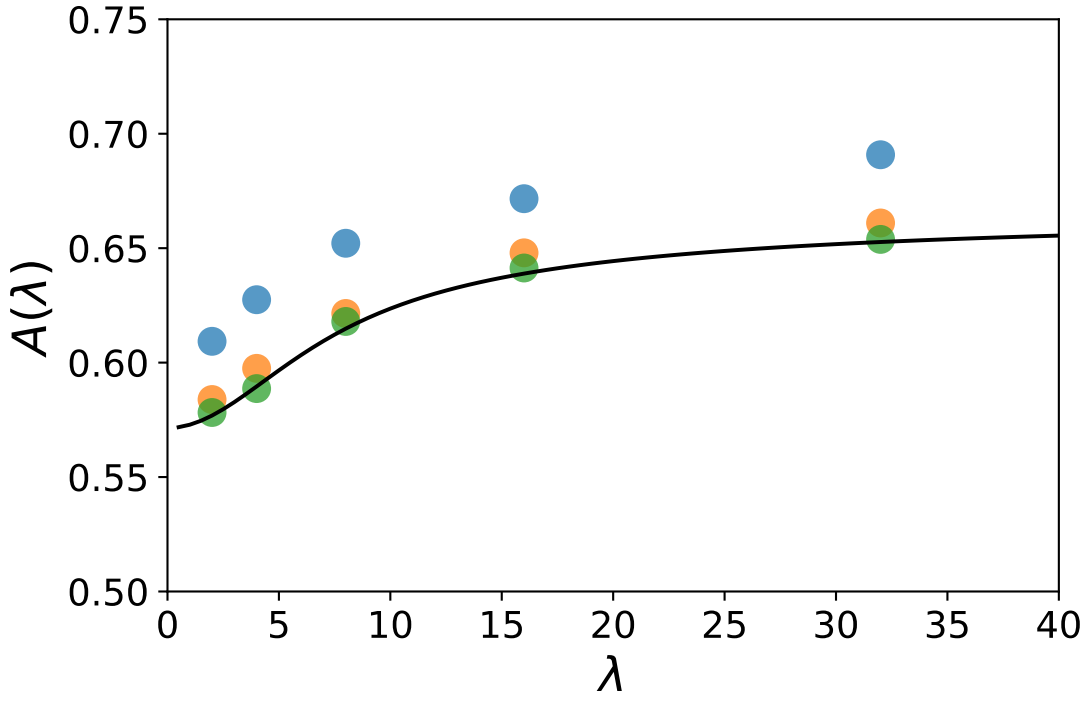

Figure 4.10: Asphericities of the tracked Brownian bridge for exponential kernel. Blue, orange and green dots represent simulated asphericities for intensity rate $c = 20, 100, 1000$ respectively. Black line respresent analytic asphericity obtained by equation (4.16).

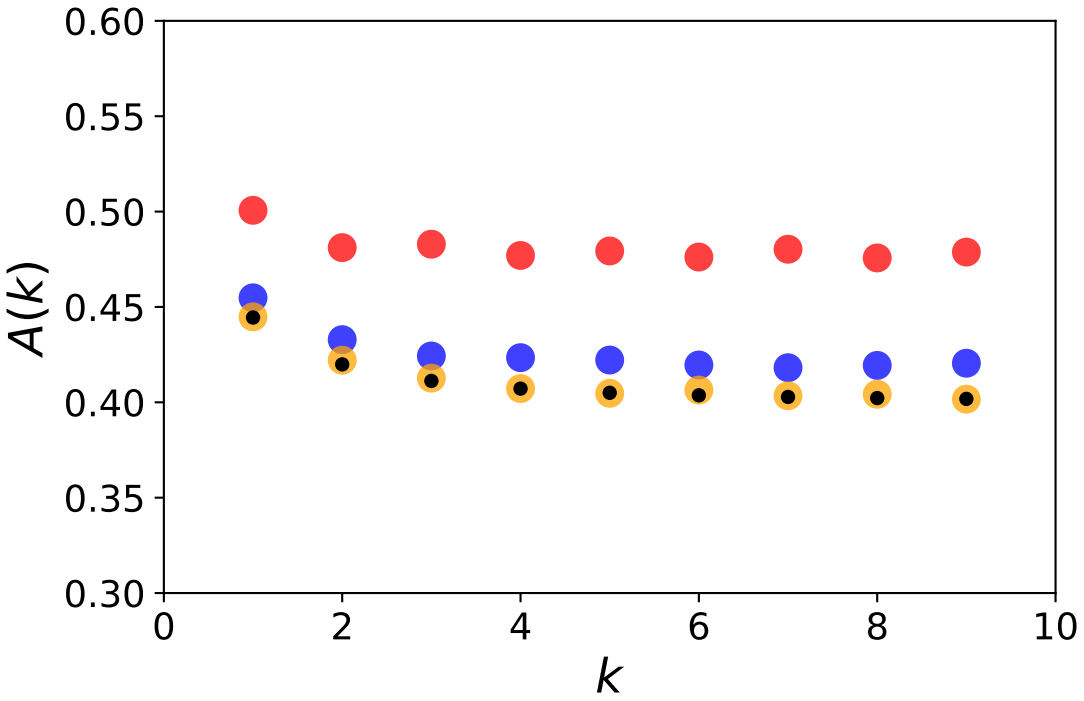

Figure 4.11: Asphericities of the tracked Brownian bridge for U-shaped kernel. Red, blue and orange represent simulated asphericities for intensity rate $c = 20, 100, 1000$ respectively. Black dots represent analytic asphericity obtained by equation (4.21). Simulation computed for 10^4 trials.

$c = 20, 100, 1000$. We observe that the our analytic asphericity underestimate the actual asphericity when $c < 100$ and as c approaches 100 the simulated asphericity converges rapidly to our analytic asphericty.

Figure 4.12 shows the analytic gyration radius $r^2(\lambda)$ of tracked Brownian bridge with the exponential kernel calculated by (4.17) in comparison with simulation for different values of the rates $c \in \{20, 100, 1000\}$. When c is small our analytic radius of gyration overestimate the actual radius by a small fraction. by increasing c the simulated radius of gyration converges rapidly to our analytic result. For a given intensity rate, the quantity of the variance is approximately proportional to the radius of gyration, so the relative error seems to be independent of the parameter λ. In order to visualise the average spatial distribution of the tracked Brownian bridge for given tracking kernel. We first generate large number of the tracked locations sets $\{L_1, L_2, ...\}$. Then we rotate each individual set so that its principal axis is horizontally aligned, and if necessary we apply a second rotation by π to ensure

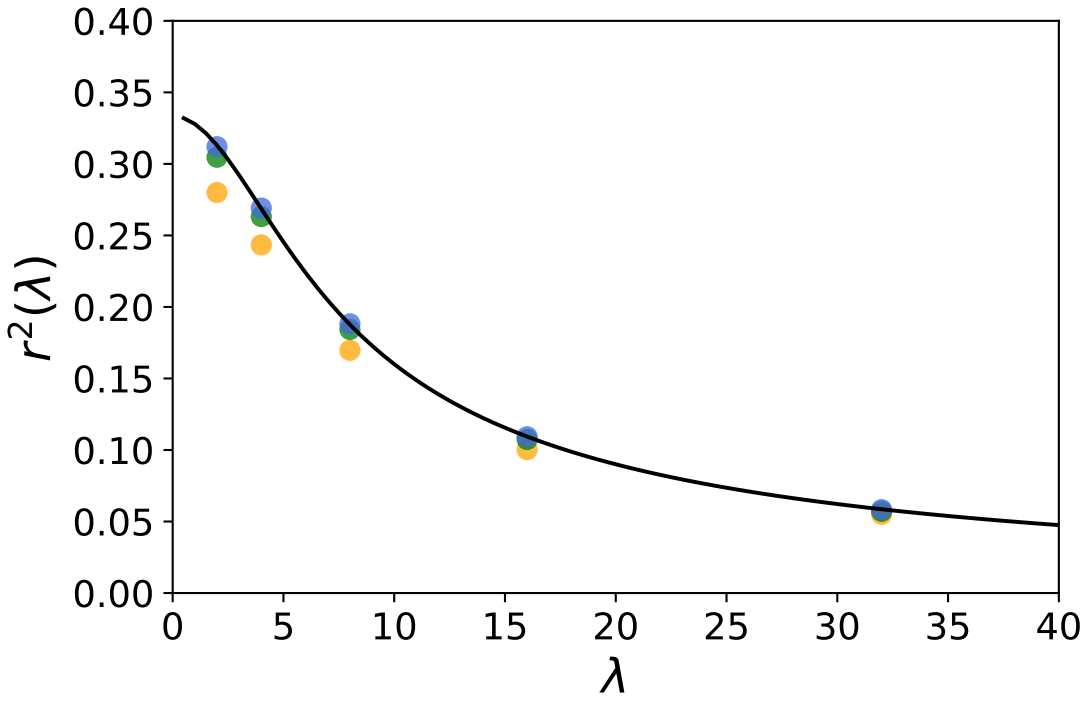

Figure 4.12: Radius of gyration, $r^2(\lambda)$, of the tracked Brownian bridge with the exponential kernel. Orange, green and blue dots represent radius of gyration corresponding to the intensity rates $c = 20, 100, 1000$ respectively. Black line shows our exact result given by equation (4.17)

the horizontal coordinate of its mass centre is positive. The probability density of the combined rotated sets $\{L_1, L_2, ...\}$ is calculated by applying Gaussian kernel density estimation [108]. Figure 4.13 we have two examples of the average spatial distribution of the tracked Brownian bridge generated from 400 tacked bridge. In figure 4.13 we can observe that the tracking kernel with higher asphericity produces a tracking bridge with more elongated density.

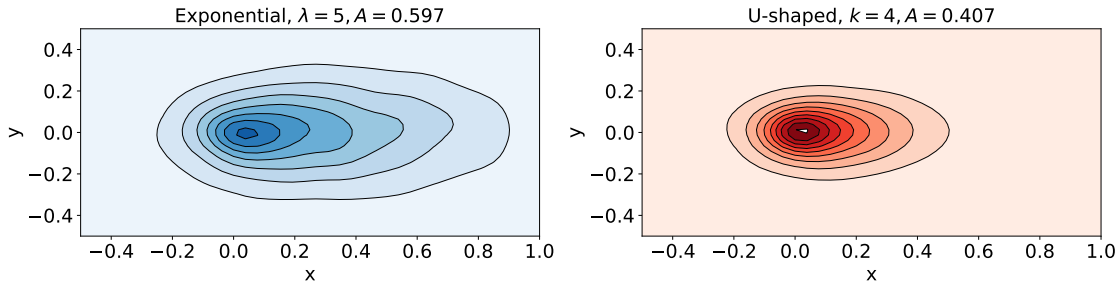

Figure 4.13: Probability density of the tracked bridge with $c = 1000$.

4.5 Discussion

Recent advances in tracking technology has prompted dramatic increase in movement data of human and animals [98, 60]. The tracking process might be the principal cause of distortion of the statistical properties of the tracked paths [99]. In this chapter we studied the effect of tracking strategy on the shape and the size of tracked Brownian bridge. By applying a method used to measure the shape of random walk [73, 109], we have derived an analytic expression to relate the shape and size of the tracked path to the tracking strategy μ. We have verified the analytic result by simulation, and we have investigated the impact of the tracking formation rate c on the shape and size of the tracked path. We observe that tracking few locations (reducing c), rise the asphericity and lessen the radius of gyration. The intensity rates c impact are relatively small, and by increasing the intensity rate c the asphericity and gyration radius converge rapidly to our analytic result.

Chapter 5

Conclusion

In this thesis we used techniques from statistical physics to investigate spatial effects in random walks, with applications in ecology and animal or human movement. We begin by studying a chase and capture [2] model for two agents; a predator and a prey animal. The movements of the two walkers are modelled as two dimensional random walks on a lattice with n hiding places for prey to shelter in. Our intent was to understand the effects of the shape of home range on the prey survival probability and investigate whether there is a optimal arrangement of the hiding places that maximizes the prey survival probability. We showed that changing the shape of the home range with the same area does not substantially affect the prey survival probability unless the home range is stretched until the ratio of the width to the length is less than $\frac{1}{n}$. We successfully attained an approximation of the optimal arrangements of three, four and five hiding places that maximizes the survival probability of the prey for different shapes of the home range. When the movements of the walkers are influenced by memory, we need to use a more sophisticated process.

In chapter 3, we investigated the effect of memory on the average shape of the mental map of a foraging animal for different memory kernels. The mental map was obtained from a two dimensional standard Brownian motion at the arrival times of a inhomogeneous Poisson point processes. We succeed in deriving an exact analytic expression linking the average elongation of spatial memory to the memory kernel. We confirm our exact result by simulation, and showed how the shape of the set of

memory locations depends on the way in which information is recalled. For slower decaying memory [14] kernel the shape of the memory locations is less elongated. The shape characteristics obtained with a range of different memory kernels are summarised in table 3.1. The results of this chapter were published in [110].

We extended the work presented in chapter 3 to study the case where the walker repeatedly returns to a certain location. We now think of the walk as being "tracked". We applied the same method used in chapter 3 to study the effect of tracking strategy on the shape and size of the set of observed (tracked) locations of a Brownian bridge. We derived an exact analytic expression relating the average size and shape of the tracked walk to tracking strategy. We verified our exact result by simulation. We investigated the influence of the tracking formation rate c on the size and the shape of the tracked path. We note that tracking fewer locations (by reducing c) results in more elongated shape and reduces the radius of gyration. The influence of the tracking formation rate c is relatively small, and as we increase c the asphericity and the radius of gyration converge rapidly to our analytic result. The results of this chapter have been submitted for publication, and having been reviewed, are being corrected for final submission.

Appendix A

Appendix title

A.1 Brownian motion

A.1.1 Random sums

This section is devoted to deal with random sums over a Poisson process and then we introduce corollary A.1.4 which is used to approximate the element of the matrix in (3.13) by integrals with stochastic integrands.

Lemma A.1.1. *For $N \in \mathbb{N}$ and $c > 0$, we have*

$$\lim_{c\to\infty} c^N e^{-c} \sum_{k=0}^{\infty} \frac{c^k}{k!(k+1)^N} = 1. \tag{A.1}$$

For the remaining of this section, for a continuous function $f : [0, \infty) \to \mathbb{R}, n \in \mathbb{N}$ and λ such that $\int_0^\infty \lambda(t)dt < \infty$, let denote

$$I(f, n, \lambda) = \int_0^\infty f^n(t)\lambda(t)dt, \tag{A.2}$$

provided that the integral converges. For the power of $I(f, n, \lambda)$ we use the following notation

$$I^k(f, n, \lambda) = \Big(I(f, n, \lambda)\Big)^k \text{ for } k \in \mathbb{N}. \tag{A.3}$$

The following theorem gives the characteristic function of the sum over a Poisson

process.

Theorem A.1.1 (Campbell's theorem [111, 112])**.** *Let S be a non-homogeneous Poisson point process on $[0,\infty)$ with intensity $\lambda(t)$. Let $f:[0,\infty)\to\mathbb{R}$ be a continuous function such that*

$$\int_0^\infty \min\{1,|f(t)|\}\lambda(t)<\infty, \tag{A.4}$$

the characteristic function of $\sum_{t\in S} f(t)$ is given by

$$\varphi(\theta)=\mathbb{E}\left[\exp\left(i\theta\sum_{t\in S}f(t)\right)\right]=\exp\left(\int_0^\infty (e^{i\theta f(t)}-1)\lambda(t)dt\right), \tag{A.5}$$

provided that the integral exist.

The following result is a simple consequences of Campbell's theorem.

Corollary A.1.1. *For any continuous functions $f,g:[0,\infty)\to\mathbb{R}$ satisfying (A.4), we have*

$$\begin{aligned}
\mathbb{E}\left[\sum_{t\in S}f(t)\right] &= I(f,1,\lambda),\\
\mathbb{E}\left[\left(\sum_{t\in S}f(t)\right)^2\right] &= I^2(f,1,\lambda)+I(f,2,\lambda),\\
\mathbb{E}\left[\left(\sum_{t\in S}f(t)\right)^4\right] &= I^4(f,1,\lambda)+6I^2(f,1,\lambda)I(f,2,\lambda)+3I^2(f,2,\lambda)\\
&\quad +4I(f,1,\lambda)I(f,3,\lambda)+I(f,4,\lambda),\\
\mathbb{E}\left[\sum_{t\in S}f(t)\sum_{s\in S}g(s)\right] &= I(f,1,\lambda)I(g,1,\lambda)+I(f\cdot g,1,\lambda).
\end{aligned}$$

In the following in section A.1.1, we let S to be a Posisson point process on $[0,\infty)$ with intensity $\lambda(t)=c\mu(t)$ where $c>0$ and $\mu(t)$ is a memory kernel. The function $\mu(t)$ is a non-increasing probability density function of a continuous probability distribution defined on $[0,\infty)$ with finite mean. The following result is consequences from the previous Corollary.

Corollary A.1.2. *For any two continuous functions $f, g : [0, \infty) \to \mathbb{R}$ satisfying (A.4), we have*

$$\begin{aligned}
\lim_{c\to\infty} \mathbb{E}\left[\frac{1}{c}\sum_{t\in S} f(t)\right] &= I(f, 1, \mu),\\
\lim_{c\to\infty} \mathbb{E}\left[\left(\frac{1}{c}\sum_{t\in S} f(t)\right)^2\right] &= I^2(f, 1, \mu),\\
\lim_{c\to\infty} \mathbb{E}\left[\left(\frac{1}{c}\sum_{t\in S} f(t)\right)^4\right] &= I^4(f, 1, \mu),\\
\lim_{c\to\infty} \mathbb{E}\left[\frac{1}{c}\sum_{t\in S} f(t)\frac{1}{c}\sum_{s\in S} g(s)\right] &= I(f, 1, \mu)I(g, 1, \mu).
\end{aligned}$$

Corollary A.1.3. *For any two continuous functions $f, g : [0, \infty) \to \mathbb{R}$ satisfying (A.4), we have*

1)

$$\lim_{c\to\infty} \mathbb{E}\left[\frac{1}{1+|S|}\sum_{t\in S} f(t)\right] = I(f, 1, \mu),$$

2)

$$\lim_{c\to\infty} \mathbb{E}\left[\left(\frac{1}{1+|S|}\sum_{t\in S} f(t)\right)^2\right] = I^2(f, 1, \mu),$$

3)

$$\lim_{c\to\infty} \mathbb{E}\left[\frac{1}{1+|S|}\sum_{t\in S} f(t)\frac{1}{1+|S|}\sum_{s\in S} g(s)\right] = I(f, 1, \mu)I(g, 1, \mu).$$

Proof. 1) To prove this identity we need to to show that

$$\mathbb{E}\left[\frac{1}{1+|S|}\sum_{t\in S} f(t)\right] - \mathbb{E}\left[\frac{1}{c}\sum_{t\in S} f(t)\right] \xrightarrow{c\to\infty} 0.$$

By employing the Jensen's inequality and the Cauchy–Schwarz inequality, we

have

$$\begin{aligned}
&\left|\mathbb{E}\left[\frac{1}{1+|S|}\sum_{t\in S} f(t)\right] - \mathbb{E}\left[\frac{1}{c}\sum_{t\in S} f(t)\right]\right| \\
&\quad\leq \mathbb{E}\left[\left|\frac{1}{1+|S|}\sum_{t\in S} f(t) - \frac{1}{c}\sum_{t\in S} f(t)\right|\right] \\
&\quad= \mathbb{E}\left[\left|\left(\frac{c}{1+|S|}-1\right)\right|\left|\frac{1}{c}\sum_{t\in S} f(t)\right|\right] \\
&\quad\leq \mathbb{E}\left[\left|\left(\frac{c}{1+|S|}-1\right)\right| \quad \frac{1}{c}\sum_{t\in S}|f(t)|\right] \\
&\quad\leq \sqrt{\mathbb{E}\left[\left(\frac{c}{1+|S|}-1\right)^2\right]}\sqrt{\mathbb{E}\left[\left(\frac{1}{c}\sum_{t\in S}|f(t)|\right)^2\right]}. \qquad \text{(A.6)}
\end{aligned}$$

By applying Corollary A.1.2, the second term of the product in (A.6) converges to $I(|f|, 1, \mu)$, therefore it is sufficient to show that the first term of the product converges to 0. By applying the law of total expectation and Lemma A.1.1 we have

$$\begin{aligned}
\mathbb{E}\left[\left(\frac{c}{1+|S|}-1\right)^2\right] =& \mathbb{E}\left[\frac{c^2}{(1+|S|)^2} - \frac{2c}{1+|S|} + 1\right] \\
=& 1 + c^2\mathbb{E}\left[\frac{1}{(1+|S|)^2}\right] - 2c\mathbb{E}\left[\frac{1}{1+|S|}\right] \text{ (by linearity of expectation)} \\
=& 1 + c^2\sum_{k=0}^{\infty}\mathbb{E}\left[\frac{1}{(1+|S|)^2}\middle||S|=k\right]\mathbb{P}(|S|=k) \\
& - 2c\sum_{k=0}^{\infty}\mathbb{E}\left[\frac{1}{(1+|S|)}\middle||S|=k\right]\mathbb{P}(|S|=k) \\
=& 1 + c^2\sum_{k=0}^{\infty}\frac{1}{(1+k)^2}\mathbb{P}(|S|=k) - 2c\sum_{k=0}^{\infty}\frac{1}{1+k}\mathbb{P}(|S|=k) \\
=& 1 + c^2e^{-c}\sum_{k=0}^{\infty}\frac{c^k}{k!(1+k)^2} - 2ce^{-c}\sum_{k=0}^{\infty}\frac{c^k}{k!(k+1)} \\
& \xrightarrow{c\to\infty} 0.
\end{aligned}$$

2) Similar way as in 1). We have

$$\begin{aligned}
&\left|\mathbb{E}\left[\left(\frac{1}{1+|S|}\sum_{t\in S} f(t)\right)^2\right] - \mathbb{E}\left[\left(\frac{1}{c}\sum_{t\in S} f(t)\right)^2\right]\right| \\
&\quad\leq \mathbb{E}\left[\left|\left(\frac{c^2}{(1+|S|)^2}-1\right)\right| \quad \frac{1}{c^2}\left(\sum_{t\in S} f(t)\right)^2\right] \text{ (by Jensen's inequality)} \\
&\quad\leq \sqrt{\mathbb{E}\left[\left(\frac{c^2}{(1+|S|)^2}-1\right)^2\right]}\sqrt{\mathbb{E}\left[\left(\frac{1}{c}\sum_{t\in S} f(t)\right)^4\right]} \text{ (by the Cauchy–Schwarz inequality)}
\end{aligned} \tag{A.7}$$

By applying Corollary A.1.2, the second term of the product in (A.7) converges to $I^2(f,1,\mu)$, so we need to show that the first term of the product converges to 0 as follow

$$\begin{aligned}
&\mathbb{E}\left[\left(\frac{c^2}{(1+|S|)^2}-1\right)^2\right] \\
&= c^4\mathbb{E}\left[\frac{1}{(1+|S|)^4}\right] - 2c^2\mathbb{E}\left[\frac{1}{(1+|S|)^2}\right] + 1 \\
&= 1 + c^4\sum_{k=0}^{\infty}\mathbb{E}\left[\frac{1}{(1+|S|)^4}\middle||S|=k\right]\mathbb{P}(|S|=k) \\
&\quad - 2c^2\sum_{k=0}^{\infty}\mathbb{E}\left[\frac{1}{(1+|S|)^2}\middle||S|=k\right]\mathbb{P}(|S|=k) \text{ (by the law of total expectation)} \\
&= 1 + c^4e^{-c}\sum_{k=0}^{\infty}\frac{c^k}{k!(k+1)^4} - 2c^2e^{-c}\sum_{k=0}^{\infty}\frac{c^k}{k!(k+1)^2},
\end{aligned}$$

by applying Lemma A.1.1, hence

$$\mathbb{E}\left[\left(\frac{c^2}{(1+|S|)^2}-1\right)^2\right] \xrightarrow{c\to\infty} 0. \tag{A.8}$$

3) In similar way as in 1) and 2), we have

$$
\begin{aligned}
&\left|\mathbb{E}\left[\frac{1}{1+|S|}\sum_{t\in S} f(t)\frac{1}{1+|S|}\sum_{s\in S} g(s)\right] - \mathbb{E}\left[\frac{1}{c}\sum_{t\in S} f(t)\frac{1}{c}\sum_{s\in S} g(s)\right]\right| \\
&\quad \leq \mathbb{E}\left[\left|\frac{1}{1+|S|}\sum_{t\in S} f(t)\frac{1}{1+|S|}\sum_{s\in S} g(s) - \frac{1}{c}\sum_{t\in S} f(t)\frac{1}{c}\sum_{s\in S} g(s)\right|\right] \text{ (by Jensen's inequality)} \\
&\quad = \mathbb{E}\left[\left|\frac{c^2}{(1+|S|)^2} - 1\right| \left|\frac{1}{c}\sum_{t\in S} f(t)\frac{1}{c}\sum_{s\in S} g(s)\right|\right] \\
&\quad \leq \mathbb{E}\left[\left|\frac{c^2}{(1+|S|)^2} - 1\right| \frac{1}{c}\sum_{t\in S} |f(t)|\frac{1}{c}\sum_{s\in S} |g(s)|\right] \text{ (by triangle inequality).}
\end{aligned}
$$

By applying the Cauchy–Schwarz inequality, we obtain

$$
\begin{aligned}
&\left|\mathbb{E}\left[\frac{1}{1+|S|}\sum_{t\in S} f(t)\frac{1}{1+|S|}\sum_{s\in S} g(s)\right] - \mathbb{E}\left[\frac{1}{c}\sum_{t\in S} f(t)\frac{1}{c}\sum_{s\in S} g(s)\right]\right| \\
&\quad \leq \sqrt{\mathbb{E}\left[\left(\frac{c^2}{(1+|S|)^2} - 1\right)^2 \frac{1}{c^2}\left(\sum_{t\in S} |f(t)|\right)^2\right]}\sqrt{\mathbb{E}\left[\left(\frac{1}{c}\sum_{s\in S} |g(s)|\right)^2\right]}.
\end{aligned} \tag{A.9}
$$

By Corollary A.1.2, the second term in the right hand side of (A.9) converges to $I(|g|, 1, \mu)$, therefore it is sufficient to show that the first term of the product converges to 0. By applying the Cauchy–Schwarz inequality, we have

$$
\begin{aligned}
&\mathbb{E}\left[\left(\frac{c^2}{(1+|S|)^2} - 1\right)^2 \frac{1}{c^2}\left(\sum_{t\in S} |f(t)|\right)^2\right] \\
&\quad \leq \sqrt{\mathbb{E}\left[\left(\frac{c^2}{(1+|S|)^2} - 1\right)^4\right]}\sqrt{\mathbb{E}\left[\left(\frac{1}{c}\sum_{t\in S} |f(t)|\right)^4\right]}.
\end{aligned} \tag{A.10}
$$

Again, by Corollary A.1.2 the second term in the right hand side of (A.10) converges to $I^2(|f|, 1, \mu)$, and the first term in the right hand side is

$$
\begin{aligned}
&\mathbb{E}\left[\left(\frac{c^2}{(1+|S|)^2}-1\right)^4\right] \\
&= \mathbb{E}\left[\frac{c^8}{(1+|S|)^8}-4\frac{c^6}{(1+|S|)}+6\frac{c^4}{(1+|S|)^4}-4\frac{c^2}{(1+|S|)^2}+1\right] \\
&= 1+c^8\sum_{k=0}^{\infty}\mathbb{E}\left[\frac{1}{(1+|S|)^8}\middle||S|=k\right]\mathbb{P}(|S|=k)-4c^6\sum_{k=0}^{\infty}\mathbb{E}\left[\frac{1}{(1+|S|)^6}\middle||S|=k\right]\mathbb{P}(|S|=k) \\
&\quad +6c^4\sum_{k=0}^{\infty}\mathbb{E}\left[\frac{1}{(1+|S|)^4}\middle||S|=k\right]\mathbb{P}(|S|=k)-4c^2\sum_{k=0}^{\infty}\mathbb{E}\left[\frac{1}{(1+|S|)^2}\middle||S|=k\right]\mathbb{P}(|S|=k) \\
&= 1+c^8e^{-c}\sum_{k=0}^{\infty}\frac{c^k}{k!(k+1)^8}-4c^6e^{-c}\sum_{k=0}^{\infty}\frac{c^k}{k!(k+1)^6}+6c^4e^{-c}\sum_{k=0}^{\infty}\frac{c^k}{k!(k+1)^4} \\
&\quad -4c^2e^{-c}\sum_{k=0}^{\infty}\frac{c^k}{k!(k+1)^2} \\
&\xrightarrow{c\to\infty} 0.
\end{aligned}
$$

□

Corollary A.1.4. *Let $(X(t), Y(t)$ be a two dimensions standard Brownian motion. For polynomials $p_1(x,y)=x^2, p_2(x,y)=y^2$ and $p_3(x,y)=xy$, as $c\to\infty$, we have*

$$
\mathbb{E}\left[\left(\frac{1}{1+|S|}\sum_{t\in S}p_i(X(t),Y(t))\right)^k\right]\to\mathbb{E}\left[\left(\int_0^{\infty}p_i(X(s),Y(s))\mu(s)ds\right)^k\right], \quad \text{(A.11)}
$$

$$
\mathbb{E}\left[\frac{1}{1+|S|}\sum_{t\in S}X^2(t)\frac{1}{1+|S|}\sum_{t\in S}Y^2(t)\right]\to\mathbb{E}\left[\int_0^{\infty}X^2(s)\mu(s)ds\right]\mathbb{E}\left[\int_0^{\infty}Y^2(s)\mu(s)ds\right], \quad \text{(A.12)}
$$

where $i\in\{1,2,3\}$ and $k\in\{1,2\}$. Since μ is a density function of a distribution with finite mean, then $\int_0^{\infty}p_i(X(s),Y(s))\mu(s)ds$ is well-defined.

Proof. 1) By employing tower property and Corollary A.1.3, we have

$$\begin{aligned}
&\mathbb{E}\left[\left(\frac{1}{1+|S|}\sum_{t\in S} p_i(X(t),Y(t))\right)^k\right] \\
&= \mathbb{E}\left[\mathbb{E}\left[\left(\frac{1}{1+|S|}\sum_{t\in S} p_i(X(t),Y(t))\right)^k \middle| \begin{array}{c}\text{Conditioning on}\\ \text{Brownian motion}\\ \text{path}\end{array}\right]\right] \\
&\xrightarrow{c\to\infty} \mathbb{E}\left[\left(\int_0^\infty p_i(X(s),Y(s))\mu(s)ds\right)^k\right].
\end{aligned}$$

2) Similarly

$$\begin{aligned}
&\mathbb{E}\left[\frac{1}{1+|S|}\sum_{t\in S} X^2(t)\frac{1}{1+|S|}\sum_{t\in S} Y^2(t)\right] \\
&= \mathbb{E}\left[\mathbb{E}\left[\frac{1}{1+|S|}\sum_{t\in S} X^2(t)\frac{1}{1+|S|}\sum_{t\in S} Y^2(t) \middle| \begin{array}{c}\text{Conditioning on}\\ \text{Brownian motion}\\ \text{path}\end{array}\right]\right] \\
&\xrightarrow{c\to\infty} \mathbb{E}\left[\left(\int_0^\infty X^2(s)\mu(s)ds\right)\left(\int_0^\infty Y^2(s)\mu(s)ds\right)\right]
\end{aligned}$$

Since X and Y are independent, then

$$\begin{aligned}
&\mathbb{E}\left[\frac{1}{1+|S|}\sum_{t\in S} X^2(t)\frac{1}{1+|S|}\sum_{t\in S} Y^2(t)\right] \\
&\xrightarrow{c\to\infty} \mathbb{E}\left[\int_0^\infty X^2(s)\mu(s)ds\right]\mathbb{E}\left[\int_0^\infty Y^2(s)\mu(s)ds\right].
\end{aligned}$$

□

A.2 Brownian bridge

Lemma A.2.1. *For $i \in \{1,2,3\}$, let $\{W_i(t)\}_{t\geq 0}$ be a standard Brownian motion and let $\rho_{(i,j)}$ is denoted the correlation coefficient of W_i and W_j. For any non-anticipating stochastic processes $\{X(t)\}_{t\geq 0}$, $\{Y(t)\}_{t\geq 0}$ and $\{Z(t)\}_{t\geq 0}$ to the given*

standard Brownian motion we have

$$\begin{aligned}\mathbb{E}\left[\int_0^t X(s)dW_1(s)\int_0^t Y(s)\,dW_2(s)\int_0^t Z(s)dW_3(s)\right]\\ &= \rho_{(2,3)}\int_0^t \mathbb{E}\left[Y(s)Z(s)\int_0^s X(r)dW_1(r)\right]ds\\ &+ \rho_{(1,3)}\int_0^t \mathbb{E}\left[X(s)Z(s)\int_0^s Y(r)\,dW_2(r)\right]ds\\ &+ \rho_{(1,2)}\mathbb{E}\left[\int_0^t X(s)Y(s)\,ds\int_0^t Z(s)\,dW_3(s)\right]. \qquad \text{(A.13)}\end{aligned}$$

Particularly, if X and Y are deterministic functions then it is simplified to

$$\begin{aligned}&\mathbb{E}\left[\int_0^t X(s)dW_1(s)\int_0^t Y(s)\,dW_2(s)\int_0^t Z(s)dW_3(s)\right]\\ &\quad= \rho_{(2,3)}\int_0^t Y(s)\,\mathbb{E}\left[Z(s)\int_0^s X(r)dW_1(r)\right]ds + \rho_{(1,3)}\int_0^t X(s)\,\mathbb{E}\left[Z(s)\int_0^s Y(r)\,dW_2(r)\right]ds. \qquad \text{(A.14)}\end{aligned}$$

Proof. By applying Ito's product formula we have

$$\begin{aligned}d\left(\int_0^t X(s)dW_1(s)\int_0^t Y(s)dW_2(s)\right) &= \int_0^t X(s)dW_1(s)\,d\left(\int_0^t Y(s)dW_2(s)\right)\\ &+ \int_0^t Y(s)dW_2(s)\,d\left(\int_0^t X(s)dW_1(s)\right)\\ &+ d\left(\int_0^t X(s)dW_1(s)\right)d\left(\int_0^t Y(s)dW_2(s)\right)\end{aligned}$$

By using Table 1.1, we obtain

$$\begin{aligned}d\left(\int_0^t X(s)dW_1(s)\int_0^t Y(s)dW_2(s)\right) &= \int_0^t X(s)dW_1(s)Y(t)dW_2(t)\\ &+ \int_0^t Y(s)dW_2(s)X(t)dW_1(t)\\ &+ X(t)Y(t)\rho_{(1,2)}dt\end{aligned}$$

By integrating both sides we arrive in

$$\int_0^t X(s)dW_1(s)\int_0^t Y(s)dW_2(s) = \int_0^t Y(s)\int_0^s X(r)dW_1(r)dW_2(s) + \int_0^t X(s)\int_0^s Y(r)dW_2(r)dW_1(s) + \rho_{(1,2)}\int_0^t X(s)Y(s)ds.$$

Hence

$$\begin{aligned}\mathbb{E}\left[\int_0^t X(s)dW_1(s)\int_0^t Y(s)dW_2(s)\int_0^t Z(s)dW_3(s)\right] &= \mathbb{E}\left[\int_0^t Y(s)\int_0^s X(r)dW_1(r)dW_2(s)\int_0^t Z(s)dW_3(s)\right] \\ &+ \mathbb{E}\left[\int_0^t X(s)\int_0^s Y(r)dW_2(r)dW_1(s)\int_0^t Z(s)dW_3(s)\right] \\ &+ \rho_{(1,2)}\mathbb{E}\left[\int_0^t X(s)Y(s)ds\int_0^t Z(s)dW_3(s)\right]. \end{aligned} \tag{A.15}$$

By applying Ito's isometry (Proposition 1.3.4) we have

$$\begin{aligned}\mathbb{E}\left[\int_0^t X(s)dW_1(s)\int_0^t Y(s)dW_2(s)\int_0^t Z(s)dW_3(s)\right] &= \mathbb{E}\left[\int_0^t Y(s)Z(s)\int_0^s X(r)dW_1(r)\rho_{(2,3)}ds\right] \\ &+ \mathbb{E}\left[\int_0^t X(s)Z(s)\int_0^s Y(r)dW_2(r)\rho_{(1,3)}ds\right] \\ &+ \rho_{(1,2)}\mathbb{E}\left[\int_0^t X(s)Y(s)ds\int_0^t Z(s)dW_3(s)\right]. \end{aligned} \tag{A.16}$$

Using Fubini's theorem gives

$$\begin{aligned}\mathbb{E}\left[\int_0^t X(s)dW_1(s)\int_0^t Y(s)dW_2(s)\int_0^t Z(s)dW_3(s)\right]\\ &= \rho_{(2,3)}\int_0^t \mathbb{E}\left[Y(s)Z(s)\int_0^s X(r)dW_1(r)\right]ds\\ &+ \rho_{(1,3)}\int_0^t \mathbb{E}\left[X(s)Z(s)\int_0^s Y(r)dW_2(r)\right]ds\\ &+ \rho_{(1,2)}\mathbb{E}\left[\int_0^t X(s)Y(s)ds\int_0^t Z(s)dW_3(s)\right]. \qquad \text{(A.17)}\end{aligned}$$

In our calculation the two processes $X(t)$ and $Y(t)$ are deterministic and form this the third expectation is

$$\begin{aligned}&\mathbb{E}\left[\int_0^t X(s)Y(s)ds\int_0^t Z(s)dW(s)\right]\\ &\quad= \int_0^t X(s)Y(s)ds\,\mathbb{E}\left[\int_0^t Z(s)dW(s)\right] \text{ (by Fubini's theorem)}\\ &\quad= 0 \qquad (\text{ by Proposition 1.3.4}) \qquad \text{(A.18)}\end{aligned}$$

and therefore (A.17) becomes

$$\begin{aligned}\mathbb{E}\left[\int_0^t X(s)dW_1(s)\int_0^t Y(s)dW_2(s)\int_0^t Z(s)dW_3(s)\right]\\ &= \rho_{(2,3)}\int_0^t Y(s)\mathbb{E}\left[Z(s)\int_0^s X(r)dW_1(r)\right]ds\\ &+ \rho_{(1,3)}\int_0^t X(s)\mathbb{E}\left[Z(s)\int_0^s Y(r)dW_2(r)\right]ds. \qquad \square\end{aligned}$$

In order to prove Theorem 4.3.1 we need to introduce and prove the following series of lemmas. Let μ be a tracking strategy kernel. For $N \in \mathbb{N}$ consider the sequence $\{M_k\}_{k=0}^N$ defined as

$$M_{-1}(t) = \mu(t) \text{ and } M_k(t) = \int_0^t M_{k-1}(s)ds \quad \text{for } k \in \{0,1,2,\ldots,N\}, \qquad \text{(A.19)}$$

Lemma A.2.2. *For the tracking strategy kernel μ and the sequence $\{M_k\}_{k=0}^N$, we have*

$$\int_0^t s^n \mu(s)\, ds = \sum_{k=0}^{n} (-1)^k \frac{n!}{(n-k)!} t^{n-k} M_k(t), \tag{A.20}$$

$$\int_0^t s^n M_j(s)\, ds = \sum_{k=0}^{n} (-1)^k \frac{n!}{(n-k)!} t^{n-k} M_{j+k+1}(t), \tag{A.21}$$

for $j \in \{0, 1, ..., N-2\}$ and $n \in \{0, 1, ..., N-j-1\}$.

Proof. By mathematical induction and integration by parts. □

Lemma A.2.3. *Let $\{B(t)\}_{t\in[0,1]}$ be a standard Brownian bridge and $\{W(t)\}_{t\geq 0}$ is a standard Brownian motion then for any $k \in \{-1, 0, 1, ..., N-2\}$ we have*

1)

$$W^3(t) = 3\int_0^t (W^2(s) - s) dW(s) + 3tW(t), \text{ for } t \geq 0. \tag{A.22}$$

2)

$$\int_0^1 B(t) M_k(t)\, dt = \int_0^1 W(t) M_k\, dt + W(1)\Big(M_{k+2}(1) - M_{k+1}(1)\Big). \tag{A.23}$$

3)

$$\int_0^1 W(t) M_{k+1}(t)\, dt = W(1) M_{k+2}(1) - \int_0^1 M_{k+2}(t)\, dW(t). \tag{A.24}$$

4)

$$\int_0^1 t M_k(t) W(t)\, dt = W(1)\Big(M_{k+1}(1) - M_{k+2}(1)\Big) + \int_0^1 M_{k+2}(t)\, dW(t) - \int_0^1 t M_{k+1}(t)\, dW(t). \tag{A.25}$$

5)

$$\int_0^1 B^2(t)M_k(t)\,dt = 2W^2(1)\Big(M_{k+1}(1) - M_{k+2}(1) + M_{k+3}(1)\Big) - M_{k+2}(1) - 2\int_0^1 W(t)M_{k+1}(t)dW(t) - 2W(1)\int_0^1 tW(t)M_k(t)\,dt. \tag{A.26}$$

Proof. 1) By applying Ito's lemma with $f(t, W(t)) = W^3(t)$.

2) Substituting $B(t) = W(t) - tW(1)$ (see Lemma 1.3.4), gives us

$$\int_0^1 B(t)M_k(t)dt = \int_0^1 W(t)M_k(t)dt - W(1)\int_0^1 tM_k(t)dt. \tag{A.27}$$

By applying Lemma A.2.2 we obtain

$$\int_0^1 B(t)M_k(t)dt = \int_0^1 W(t)M_k(t)dt + W(1)\Big(M_{k+2}(1) - M_{k+1}(1)\Big). \qquad \square$$

3) Proved by using Ito's lemma with $f(t, W(t)) = M_{k+2}(t)W(t)$.

4) By applying Ito's lemma with $f(t, W(t)) = tM_{k+1}(t)W(t)$, we have

$$\int_0^1 tM_k(t)W(t)\,dt = W(1)M_{k+1}(1) - \int_0^1 W(t)M_{k+1}(t)\,dt - \int_0^1 tM_{k+1}(t)\,dW(t),$$

then we substituting (A.24) to obtain the desired result.

5) Substituting $B(t) = W(t) - tW(1)$ (see Lemma 1.3.4), gives us

$$\int_0^1 B^2(t)M_k(t)\,dt = \int_0^1 W^2(t)M_k(t)dt - 2W(1)\int_0^1 tW(t)M_k(t)dt + W^2(1)\int_0^1 t^2M_k(t)dt \tag{A.28}$$

By applying Ito's lemma with $f(t, W(t)) = M_{k+1}(t)W^2(t)$ and then Lemma A.2.2

to the first term in the right hand side (RHS) of (A.28), we have

$$\int_0^1 W^2(t)M_k(t)\,dt = W^2(1)M_{k+1}(1) - M_{k+2}(1) - 2\int_0^1 W(t)M_{k+1}(t)dW(t) \quad \text{(A.29)}$$

The integral $\int_0^1 t^2 M_k(t)\,dt$ in the third term in the RHS of (A.28) may be calculated by applying Lemma A.2.2 to obtain

$$\int_0^1 t^2 M_k(t)\,dt = M_{k+1}(1) - 2M_{k+2}(1) + 2M_{k+3}(1) \quad \text{(A.30)}$$

By substituting (A.29) and (A.30) in (A.28) and rearranging we obtain the desired result.

Lemma A.2.4. *Let $\{B(t)\}_{t\in[0,1]}$ be a standard Brownian bridge and $\{W(t)\}_{t\geq 0}$ is a standard Brownian motion then for any $k \in \{-1, 0, 1, ..., N-2\}$ we have*

1)

$$\mathbb{E}\left[\int_0^1 B^2(t)M_k(t)dt\right] = M_{k+2}(1) - 2M_{k+3}(1). \quad \text{(A.31)}$$

2)

$$\mathbb{E}\left[W(1)\int_0^1 tW(t)M_k(t)\,dt\right] = M_{k+1}(1) - 2M_{k+2}(1) + 2M_{k+3}(1). \quad \text{(A.32)}$$

Proof. 1) By applying (A.26) we obtain

$$\begin{aligned}\mathbb{E}\left[\int_0^1 B^2(t)M_k(t)dt\right] &= 2\mathbb{E}[W^2(1)]\Big(M_{k+1}(1) - M_{k+2}(1) + M_{k+3}(1)\Big)\\ &\quad - M_{k+2}(1) - 2\mathbb{E}\left[\int_0^1 M_{k+1}(t)W(t)dW(t)\right]\\ &\quad - 2\mathbb{E}\left[W(1)\int_0^1 tW(t)M_k(t)dt\right]\end{aligned}$$

Using the fact $\mathbb{E}[W^2(1)] = 1$ and Ito's properties (Proposition 1.3.4), gives us

$$\mathbb{E}\left[\int_0^1 B^2(t)M_k dt\right] = 2M_{k+1}(1) - 3M_{k+2}(1) + 2M_{k+3}(1) - 2\mathbb{E}\left[W(1)\int_0^1 tW(t)M_k(t)dt\right]$$

By applying (A.25) and using the fact that $\mathbb{E}[W^2(1)] = 1$ we have

$$\mathbb{E}\left[\int_0^1 B^2(t)M_k(t)dt\right] = 2M_{k+3}(1) - M_{k+2}(1) - 2\mathbb{E}\left[W(1)\int_0^1 M_{k+2}(t)dW(t)\right] + 2\mathbb{E}\left[W(1)\int_0^1 tM_{k+1}(t)dW(t)\right]$$

By substituting $W(1) = \int_0^1 dW(t)$ and then apply Ito Isometry we have

$$\mathbb{E}\left[\int_0^1 B^2(t)M_k(t)dt\right] = 2M_{k+3}(1) - M_{k+2}(1) - 2\int_0^1 M_{k+2}(t)dt + 2\int_0^1 tM_{k+1}(t)dt$$

Employing Lemma A.2.2 result in

$$\mathbb{E}\left[\int_0^1 B^2(t)M_k(t)dt\right] = M_{k+2}(1) - 2M_{k+3}(1).$$

2) In order to prove (A.32) we use (A.25) to obtain

$$\mathbb{E}\left[W(1)\int_0^1 tW(t)M_k(t)dt\right] = \mathbb{E}[W^2(1)]\Big(M_{k+1}(1) - M_{k+2}(1)\Big) + \mathbb{E}\left[W(1)\int_0^1 M_{k+2}(t)dW(t)\right] - \mathbb{E}\left[W(1)\int_0^1 tM_{k+1}(t)dW(t)\right].$$

By using the fact $\mathbb{E}[W^2(1)] = 1$ and substituting $W(1) = \int_0^1 dW(t)$ and then apply

Ito Isometry we have

$$\mathbb{E}\left[W(1)\int_0^1 tW(t)M_k(t)dt\right] = M_{k+1}(1) - M_{k+2}(1) + \int_0^1 M_{k+2}(t)dt - \int_0^1 tM_{k+1}(t)dt$$

Applying Lemma A.2.2 gives us

$$\mathbb{E}\left[W(1)\int_0^1 tW(t)M_k(t)dt\right] = M_{k+1}(1) - 2M_{k+2}(1) + 2M_{k+3}(1). \qquad \square$$

Lemma A.2.5. *Let W be a standard Brownian motion, then*

$$\begin{aligned}\mathbb{E}\left[\left(W(1)\int_0^1 tW(t)M_k(t)dt\right)^2\right] &= 3\left(M_{k+1}(1) - M_{k+2}(1)\right)^2 \\ &\quad + 6\left(M_{k+1}(1) - M_{k+2}(1)\right)\left(2M_{k+3}(1) - M_{k+2}(1)\right) \\ &\quad + \int_0^1 \left(M_{k+2}(t) - tM_{k+1}(t)\right)^2 dt \\ &\quad + 8\int_0^1 \left(M_{k+2}(t) - tM_{k+1}(t)\right) M_{k+3}(t)dt \\ &\quad + 4\int_0^1 tM_{k+2}(t)\left(tM_{k+1}(t) - M_{k+2}(t)\right)dt, \quad \text{(A.33)}\end{aligned}$$

for $k \in \{-1, 0, ..., N-2\}$.

Proof. By substituting the fact that $W^2(1) = 2\int_0^1 W(t)dW(t) + 1$, we have

$$\begin{aligned}\mathbb{E}\left[\left(W(1)\int_0^1 tW(t)M_k(t)dt\right)^2\right] &= \mathbb{E}\left[W^2(1)\left(\int_0^1 tW(t)M_k(t)dt\right)^2\right] \\ &= \mathbb{E}\left[2\int_0^1 W(t)dW(t)\left(\int_0^1 tW(t)M_k(t)dt\right)^2\right] + \mathbb{E}\left[\left(\int_0^1 tW(t)M_k(t)dt\right)^2\right].\end{aligned}$$

We apply (A.25) to obtain

$$
\begin{aligned}
&\mathbb{E}\left[\left(W(1)\int_0^1 tW(t)M_k(t)dt\right)^2\right] \\
&\quad= 2\big(M_{k+1}(1)-M_{k+2}(1)\big)^2\mathbb{E}\left[W^2(1)\int_0^1 W(t)dW(t)\right] \\
&\quad+ 2\mathbb{E}\left[\left(\int_0^1 M_{k+2}(t)dW(t)\right)^2\int_0^1 W(t)dW(t)\right]+2\mathbb{E}\left[\left(\int_0^1 tM_{k+1}(t)dW(t)\right)^2\int_0^1 W(t)dW(t)\right] \\
&\quad+ 4\big(M_{k+1}(1)-M_{k+2}(1)\big)\mathbb{E}\left[W(1)\int_0^1 M_{k+2}(t)dW(t)\int_0^1 W(t)dW(t)\right] \\
&\quad- 4\big(M_{k+1}(1)-M_{k+2}(1)\big)\mathbb{E}\left[W(1)\int_0^1 tM_{k+1}(t)dW(t)\int_0^1 W(t)dW(t)\right] \\
&\quad- 4\mathbb{E}\left[\int_0^1 M_{k+2}(t)dW(t)\int_0^1 tM_{k+1}(t)dW(t)\int_0^1 W(t)dW(t)\right] \\
&\quad+ \big(M_{k+1}(1)-M_{k+2}(1)\big)^2\mathbb{E}\left[W^2(1)\right]+\mathbb{E}\left[\left(\int_0^1 M_{k+2}(t)dW(t)\right)^2\right] \\
&\quad+ \mathbb{E}\left[\left(\int_0^1 tM_{k+1}(t)dW(t)\right)^2\right]+2\big(M_{k+1}(1)-M_{k+2}(1)\big)\mathbb{E}\left[W(1)\int_0^1 M_{k+2}(t)dW(t)\right] \\
&\quad- 2\big(M_{k+1}(1)-M_{k+2}(1)\big)\mathbb{E}\left[W(1)\int_0^1 tM_{k+1}(t)dW(t)\right] \\
&\quad- \mathbb{E}\left[\int_0^1 M_{k+2}(t)dW(t)\int_0^1 tM_{k+1}(t)dW(t)\right] \qquad \text{(A.34)}
\end{aligned}
$$

Let $\mathbf{e}[i]$ indicates the expectation in ith term of right hand side of equation (A.34). The first expectation,$\mathbf{e}[1]$ by substituting the fact that $W^2(1)=2\int_0^1 W(t)dW(t)+1$ and using (1.88) we have

$$
\mathbf{e}[1]=\mathbb{E}\left[W^2(1)\int_0^1 W(t)dW(t)\right]=2\mathbb{E}\left[\int_0^1 W(t)dW(t)\int_0^1 W(t)dW(t)\right]
$$

We employ Itô Isometry (equation (1.89)) and Fubini's Theorem to obtain

$$
\begin{aligned}
\mathbf{e}[1] &= 2\int_0^1 \mathbb{E}[W^2(t)]dt \\
&= 2\int_0^1 tdt=1. \quad \text{(we used the fact that } \mathbb{E}[W^2(t)]=1) \qquad \text{(A.35)}
\end{aligned}
$$

The second expectation,$\mathbf{e}[2]$, by applying (A.14) we have

$$\begin{aligned}\mathbf{e}[2] &= \mathbb{E}\left[\left(\int_0^1 M_{k+2}(t)dW(t)\right)^2 \int_0^1 W(t)dW(t)\right] \\ &= 2\int_0^1 M_{k+2}(t)\mathbb{E}\left[W(t)\int_0^t M_{k+2}(s)dW(s)\right]dt\end{aligned}$$

By substituting $W(t) = \int_0^t dW(s)$ and applying Itô Isometry (equation (1.89)) we obtain

$$\begin{aligned}\mathbf{e}[2] &= 2\int_0^1 M_{k+2}(t)\int_0^t M_{k+2}(s)dsdt \\ &= 2\int_0^1 M_{k+2}(t)M_{k+3}(t)dt \quad \text{(by Lemma A.2.2)} \end{aligned} \tag{A.36}$$

Similarly, the third expectation, $\mathbf{e}[3]$, is

$$\mathbf{e}[3] = 2\int_0^1 tM_{k+1}(t)\big(tM_{k+2}(t) - M_{k+3}\big)dt. \tag{A.37}$$

The fourth expectation, $\mathbf{e}[4]$, by substituting $W(1) = \int_0^1 dW(t)$ and using (A.14) we have

$$\begin{aligned}\mathbf{e}[4] &= \mathbb{E}\left[W(1)\int_0^1 M_{k+2}(t)dW(t)\int_0^1 W(t)dW(t)\right] \\ &= \int_0^1 \mathbb{E}\left[W(t)\int_0^t M_{k+2}(s)dW(s)\right]dt \\ &\quad + \int_0^1 M_{k+2}(t)\mathbb{E}\left[W(t)\int_0^t dW(s)\right]dt\end{aligned} \tag{A.38}$$

We substitute $W(t) = \int_0^t dW(s)$ and apply Itô Isometry (equation (1.89)) to obtain

$$\begin{aligned}\mathbf{e}[4] &= \int_0^1\int_0^t M_{k+2}(s)dsdt + \int_0^1 tM_{k+2}(t)dt \\ &= M_{k+3}(1) \quad \text{(by Lemma A.2.2)}\end{aligned} \tag{A.39}$$

In the similar way as in $\mathbf{e}[4]$, the fifth expectation, $\mathbf{e}[5]$ is

$$\begin{aligned}\mathbf{e}[5] &= \mathbb{E}\left[W(1)\int_0^1 tM_{k+1}(t)dW(t)\int_0^1 W(t)dW(t)\right] \\ &= M_{k+2}(1) - M_{k+3}(1). \end{aligned} \tag{A.40}$$

The sixth expectation, $\mathbf{e}[6]$ by applying (A.14) we obtain

$$\begin{aligned}\mathbf{e}[6] &= \mathbb{E}\left[\int_0^1 M_{k+2}(t)dW(t)\int_0^1 tM_{k+1}(t)dW(t)\int_0^1 W(t)dW(t)\right] \\ &= \int_0^1 M_{k+2}(t)\mathbb{E}\left[W(t)\int_0^t sM_{k+1}(s)dW(s)\right]dt \\ &\quad + \int_0^1 tM_{k+1}(t)\mathbb{E}\left[W(t)\int_0^t M_{k+2}(s)dW(s)\right]dt\end{aligned}$$

By substituting $W(t) = \int_0^t dW(s)$ and applying Itô Isometry (equation (1.89)) we obtain

$$\begin{aligned}\mathbf{e}[6] &= \int_0^1 M_{k+2}(t)\int_0^t sM_{k+1}(s)dsdt + \int_0^t tM_{k+1}(t)\int_0^t sM_{k+2}(s)dsdt \\ &= \int_0^1 tM_{k+2}^2(t)dt - \int_0^1 M_{k+2}(t)M_{k+3}(t)dt \\ &\quad + \int_0^1 tM_{k+1}(t)M_{k+3}(t)dt \qquad \text{(by Lemma A.2.2)}\end{aligned} \tag{A.41}$$

The seventh expectation is obviously $\mathbf{e}[7] = \mathbb{E}[W^2(1)] = 1$. The eighth and ninth expectations are calculated by applying Itô Isometry (equation (1.89)) as follow

$$\begin{aligned}\mathbf{e}[8] &= \mathbb{E}\left[\left(\int_0^1 M_{k+2}(t)dW(t)\right)^2\right] \\ &= \int_0^1 M_{k+2}^2(t)dt\end{aligned} \tag{A.42}$$

and

$$\begin{aligned}\mathbf{e}[9] &= \mathbb{E}\left[\left(\int_0^1 tM_{k+1}(t)dW(t)\right)^2\right] \\ &= \int_0^1 tM_{k+1}^2(t)dt \end{aligned} \tag{A.43}$$

The tenth expectation by substituting the fact that $W(1) = \int_0^1 dW(t)$ and applying Itô Isometry (equation (1.89)) to obtain

$$\begin{aligned}\mathbf{e}[10] &= \mathbb{E}\left[W(1)\int_0^1 M_{k+2}(t)dW(t)\right] \\ &= \mathbb{E}\left[\int_0^1 dW(t)\int_0^1 M_{k+2}(t)dW(t)\right] \\ &= \int_0^1 M_{k+2}(t)dt \end{aligned} \tag{A.44}$$

Similarly, $\mathbf{e}[11]$ is

$$\begin{aligned}\mathbf{e}[11] &= \mathbb{E}\left[W(1)\int_0^1 tM_{k+1}(t)dW(t)\right] \\ &= \mathbb{E}\left[\int_0^1 dW(t)\int_0^1 tM_{k+1}(t)dW(t)\right] \\ &= \int_0^1 M_{k+2}(t)dt \end{aligned} \tag{A.45}$$

The last expectation, $\mathbf{e}[11]$, is calculated by Itô Isometry (equation (1.89)) to obtain

$$\begin{aligned}\mathbf{e}[12] &= \mathbb{E}\left[\int_0^1 M_{k+2}(t)dW(t)\int_0^1 tM_{k+1}(t)dW(t)\right] \\ &= \int_0^1 tM_{k+1}(t)M_{k+2}(t)dt. \end{aligned} \tag{A.46}$$

By substituting $\mathbf{e}[k]$ for $k \in \{1, 2, ..., 12\}$ in equation (A.34) we obtain the result in (A.33). □

Lemma A.2.6. *Let B be a standard Brownian bridge and W be Standard Brownian*

motion, then

$$\mathbb{E}\left[\left(\int_0^1 B^2(t)M_k(t)\,dt\right)^2\right] = -3M_{k+2}^2(1) + 12M_{k+2}(1)M_{k+3}(1) - 20M_{k+3}^2(1) + 8\int_0^1 (1-2t)M_{k+1}(t)\big(2M_{k+3}(t) - tM_{k+2}(t)\big)dt + 4\int_0^1 M_{k+2}(t)\big((1-4t)M_{k+2}(t) + 8M_{k+3}(t)\big)dt + 4\int_0^1 (1-t)tM_{k+1}^2(t)dt, \tag{A.47}$$

for $k \in \{-1, 0, 1, ..., N-2\}$.

Proof. By applying (A.26), and then using the facts that $\mathbb{E}[W^2(t)] = t$ and $\mathbb{E}[W^4(t)] = 3t^2$ we obtain

$$\begin{aligned}
&\mathbb{E}\left[\left(\int_0^1 B^2(t)M_k(t)\,dt\right)^2\right] \\
&= 12\Big(M_{k+1}(1) - M_{k+2}(1) + M_{k+3}(1)\Big)^2 + M_{k+2}^2(1) + 4\mathbb{E}\left[\left(\int_0^1 W(t)M_{k+1}(t)dW(t)\right)^2\right] \\
&+ 4\mathbb{E}\left[\left(W(1)\int_0^1 tW(t)M_k(t)dW(t)\right)^2\right] - 4M_{k+2}(1)\Big(M_{k+1}(1) - M_{k+2}(1) + M_{k+3}(1)\Big) \\
&- 8\Big(M_{k+1}(1) - M_{k+2}(1) + M_{k+3}(1)\Big)\mathbb{E}\left[W^2(1)\int_0^1 W(t)M_{k+1}(t)dW(t)\right] \\
&- 8\Big(M_{k+1}(1) - M_{k+2}(1) + M_{k+3}(1)\Big)\mathbb{E}\left[W^3(1)\int_0^1 tW(t)M_k(t)dt\right] \\
&+ 4M_{k+2}(1)\mathbb{E}\left[\int_0^1 W(t)M_{k+1}(t)dW(t)\right] + 4M_{k+2}(1)\mathbb{E}\left[W(1)\int_0^1 tW(t)M_k(t)dt\right] \\
&+ 8\mathbb{E}\left[W(1)\int_0^1 tW(t)M_k(t)dt\int_0^1 W(t)M_{k+1}(t)dW(t)\right]
\end{aligned} \tag{A.48}$$

Let $\mathbf{e}[i]$ indicates the ith expectation term of right hand side of equation (A.48). The first expectation term $\mathbf{e}[1]$ is calculated by using Itô Isometry (equation (1.89))

and using Fubini's theorem and the fact that $\mathbb{E}[W^2(t)] = t$ as follow

$$\begin{aligned}
\mathbf{e}[1] &= \mathbb{E}\left[\left(\int_0^1 W(t)M_{k+1}(t)dW(t)\right)^2\right] \\
&= \mathbb{E}\left[\int_0^1 W^2(t)M_{k+1}^2(t)dt\right] \\
&= \int_0^1 \mathbb{E}[W^2(t)]M_{k+1}^2(t)dt = \int_0^1 tM_{k+1}^2(t)dt. \qquad \text{(A.49)}
\end{aligned}$$

The second expectation term $\mathbf{e}[2]$ is calculated previously and given in (A.33). In order to calculated the expectation term $\mathbf{e}[3]$ we need to apply Lemma 3.21 to gives us

$$\begin{aligned}
\mathbf{e}[3] &= \mathbb{E}\left[W^2(1)\int_0^1 W(t)M_{k+1}(t)dW(t)\right] \\
&= 2\mathbb{E}\left[\int_0^1 W(t)dW(t)\int_0^1 W(t)M_{k+1}(t)dW(t)\right] \\
&\quad + \mathbb{E}\left[\int_0^1 W(t)M_{k+1}(t)dW(t)\right]
\end{aligned}$$

By using (1.88) and Itô Isometry (equation (1.89)) we have

$$\begin{aligned}
\mathbf{e}[3] &= 2\mathbb{E}\left[\int_0^1 W_2(t)M_{k+1}(t)dt\right] \\
&= 2\int_0^1 \mathbb{E}\left[W_2(t)\right]M_{k+1}(t)dt \quad \text{(by Fubini's theorm)} \\
&= 2\int_0^1 tM_{k+1}(t)dt \\
&= 2\Big(M_{k+2}(1) - M_{k+3}(1)\Big). \quad \text{(by Lemma A.2.2)} \qquad \text{(A.50)}
\end{aligned}$$

The fourth expectation,$\mathbf{e}[4]$, by substituting (A.22) becomes

$$\begin{aligned}
\mathbf{e}[4] &= \mathbb{E}\left[W^3(1)\int_0^1 tW(t)M_k(t)dt\right] \\
&= 3\mathbb{E}\left[\int_0^1 \Big(W^2(t) - t\Big)dW(t)\int_0^1 tW(t)M_k(t)dt\right] + 3\mathbb{E}\left[W(1)\int_0^1 tW(t)M_k(t)dt\right] \qquad \text{(A.51)}
\end{aligned}$$

By substituting (A.32) and then (A.25) in right hand side we obtain

$$\mathbf{e}[4] = 3\Big(M_{k+1}(1) - 2M_{k+2}(1) + 2M_{k+3}(1)\Big). \tag{A.52}$$

The five expectation term by (1.88) is

$$\mathbf{e}[5] = \mathbb{E}\left[\int_0^1 W(t)M_{k+1}(t)dW(t)\right] = 0. \tag{A.53}$$

The expectation $\mathbf{e}[6] = \mathbb{E}\left[W(1)\int_0^1 tW(t)M_k(t)dt\right]$ is calculated previously in (A.32). In order to calculated the seventh expectation,$\mathbf{e}[7]$, we substitute (A.25) to obtain

$$\begin{aligned}
\mathbf{e}[7] &= \mathbb{E}\left[W(1)\int_0^1 tW(t)M_k(t)dt\int_0^1 W(t)M_{k+1}(t)dW(t)\right] \\
&= \Big(M_{k+1}(1) - M_{k+2}(1)\Big)\mathbb{E}\left[W^2(1)\int_0^1 W(t)M_{k+1}(t)dW(t)\right] \\
&+ \mathbb{E}\left[W(1)\int_0^1 M_{k+2}(t)dW(t)\int_0^1 W(t)M_{k+1}(t)dW(t)\right] \\
&- \mathbb{E}\left[W(1)\int_0^1 tM_{k+1}(t)dW(t)\int_0^1 W(t)M_{k+1}(t)dW(t)\right]
\end{aligned} \tag{A.54}$$

Let $\mathbf{e}[7,k]$ indicates the k-th expectation in the right hand side of (A.54). The expectation $\mathbf{e}[7,1]$ is calculated by using (3.21) and then applying (1.88) and Itô Isometry (equation (1.89)) as follow

$$\begin{aligned}
\mathbf{e}[7,1] &= \mathbb{E}\left[W^2(1)\int_0^1 W(t)M_{k+1}(t)dW(t)\right] \\
&= \mathbb{E}\left[\Big(2\int_0^1 W(t)dW(t) + 1\Big)\int_0^1 W(t)M_{k+1}(t)dW(t)\right] \\
&= 2\mathbb{E}\left[\int_0^1 W(t)dW(t)\int_0^1 W(t)M_{k+1}(t)dW(t)\right] + \mathbb{E}\left[\int_0^1 W(t)M_{k+1}(t)dW(t)\right] \\
&= 2\int_0^1 \mathbb{E}[W^2(t)]M_{k+1}(t)dt \quad (\text{ by Fubini's theorem}) \\
&= 2\int_0^1 tM_{k+1}(t)dt = 2\Big(M_{k+2}(1) - M_{k+3}(1)\Big) \quad (\text{ by Lemma A.2.2})
\end{aligned} \tag{A.55}$$

The expectation $\mathbf{e}[7,2]$ is calculated by using A.2.1 and then applying Itô Isometry (equation (1.89)) as follow

$$\begin{aligned}\mathbf{e}[7,2] &= \mathbb{E}\left[W(1)\int_0^1 M_{k+2}(t)dW(t)\int_0^1 W(t)M_{k+1}(t)dW(t)\right]\\ &= \int_0^1 M_{K+1}(t)M_{K+2}(t)\mathbb{E}\left[W(t)\int_0^t dW(s)\right]dt\\ &\quad + \int_0^1 M_{k+1}(t)\mathbb{E}\left[W(t)\int_0^t M_{k+2}(s)dW(s)\right]dt\end{aligned}$$

$$\begin{aligned}\mathbf{e}[7,2] &= \int_0^1 tM_{k+1}(t)M_{k+2}(t)dt + \int_0^1 M_{k+1}(t)\int_0^t M_{k+2}(s)dsdt\\ &= \int_0^1 tM_{k+1}(t)M_{k+2}(t)dt + \int_0^1 M_{k+1}(t)M_{k+3}(t)dt \quad (\text{ by Lemma A.2.2})\end{aligned}$$

Similarly,

$$\mathbf{e}[7,3] = \mathbb{E}\left[W(1)\int_0^1 tM_{k+1}(t)dW(t)\int_0^1 W(t)M_{k+1}(t)dW(t)\right] \tag{A.56}$$

$$= \int_0^1 t^2M_{k+1}^2(t)dt + \int_0^1 M_{k+1}(t)\big(tM_{k+2}(t) - M_{k+3}(t)\big)dt \quad (\text{ by Lemma A.2.2}) \tag{A.57}$$

Substituting $\mathbf{e}[7,1]$,$\mathbf{e}[7,2]$ and $\mathbf{e}[7,3]$ in (A.54) gives

$$\begin{aligned}\mathbf{e}[7] &= 2\Big(M_{k+1}(1) - M_{k+2}(1)\Big)\Big(M_{k+2}(1) - M_{k+3}(1)\Big)\\ &\quad + 2\int_0^1 M_{k+1}(t)M_{k+3}(t)dt - \int_0^1 t^2M_{k+1}^2(t)dt.\end{aligned} \tag{A.58}$$

By substituting $\mathbf{e}[k]$ for $k \in \{1,2,...,7\}$ in equation (A.48) we obtain the result in (A.47). □

Lemma A.2.7. *Let B_1 and B_2 be two independent standard Brownian bridges and W be a standard Brownian motion, then*

$$\mathbb{E}\left[\left(\int_0^1 B_1(t)B_2(t)M_k(t)\,dt\right)^2\right] = 2M_{k+2}^2(1) + 4M_{k+3}^2(1) - 8M_{k+2}(1)M_{k+3}(1) - 4\int_0^1 tM_{k+1}(t)M_{k+2}(t)dt + 8\int_0^1 M_{k+1}(t)M_{k+3}(t)dt + 2\int_0^1 tM_{k+1}^2(t)dt - 2\int_0^1 t^2M_{k+1}^2(t)dt + 2\int_0^1 M_{k+2}^2(t)dt \tag{A.59}$$

Proof. By substituting $B_1(t) = W_1(t) - tW_1(1)$, $B_2(t) = W_2(t) - tW_2(1)$ and using the expectation's properties, we have

$$\begin{aligned}
&\mathbb{E}\left[\left(\int_0^1 B_1(t)B_2(t)M_k(t)\,dt\right)^2\right] \\
&= \mathbb{E}\left[\left(\int_0^1 W_1(t)W_2(t)M_k(t)dt\right)^2\right] + \mathbb{E}\left[\left(W_2(1)\int_0^1 tW_1(t)M_k(t)dt\right)^2\right] \\
&+ \mathbb{E}\left[\left(W_1(1)\int_0^1 tW_2(t)M_k(t)dt\right)^2\right] + \mathbb{E}\left[\left(W_1(1)W_2(1)\int_0^1 t^2M_k(t)dt\right)^2\right] \\
&- 2\mathbb{E}\left[W_2(1)\int_0^1 W_1(t)W_2(t)M_k(t)dt\int_0^1 tW_1(t)M_k(t)dt\right] \\
&- 2\mathbb{E}\left[W_1(1)\int_0^1 W_1(t)W_2(t)M_k(t)dt\int_0^1 tW_2(t)M_k(t)dt\right] \\
&+ 2\mathbb{E}\left[W_1(1)W_2(1)\int_0^1 W_1(t)W_2(t)M_k(t)dt\right]\int_0^1 t^2M_k(t)dt \\
&+ 2\mathbb{E}\left[W_1(1)W_2(1)\int_0^1 tW_1(t)M_k(t)dt\int_0^1 tW_2(t)M_k(t)dt\right] \\
&- 2\mathbb{E}\left[W_1(1)W_2^2(1)\int_0^1 tW_1(t)M_k(t)dt\right]\int_0^1 t^2M_k(t)dt \\
&- 2\mathbb{E}\left[W_1^2(1)W_2(1)\int_0^1 tW_2(t)M_k(t)dt\right]\int_0^1 t^2M_k(t)dt
\end{aligned} \tag{A.60}$$

Let $\mathbf{e}[i]$ indicates the expectation in ith term of right hand side of equation (A.60) and let the correlation coefficient of $W_i(t)$ and $W_j(t)$ for $i, j \in \{1, 2, 3\}$ is denoted by $\rho_{(i,j)}$. The first expectation $\mathbf{e}[1]$ is obtained by applying Lemma 3.3.6

$$\mathbf{e}[1] = \mathbb{E}\left[\left(\int_0^1 W_1(t)W_2(t)M_k(t)dt\right)^2\right] = \frac{1}{2}\left(\int_0^1 tM_k(t)dt\right)^2 + \frac{1}{2}M_{k+1}^2(1) + 2\int_0^1 tM_{k+1}^2(t)dt$$
$$- \frac{1}{2}\left(\int_0^1 M_{k+1}(t)dt\right)^2 - 4M_{k+1}(1)\int_0^1 tM_{k+1}(t)dt$$
$$+ M_{k+1}(1)\int_0^1 M_{k+1}(t)dt.$$

By applying Lemma A.2.2 and rearranging we have

$$\mathbf{e}[1] = M_{k+1}^2(1) - 4M_{k+1}(1)M_{k+2}(1)$$
$$+ 4M_{k+1}(1)M_{k+3}(1) + 2\int_0^1 tM_{k+1}^2(t)dt \qquad \text{(A.61)}$$

The second expectation, $\mathbf{e}[2]$, in (A.60) by using the independence of W_1 and W_2 can be written as

$$\mathbf{e}[2] = \mathbb{E}\left[W_2^2(1)\right]\mathbb{E}\left[\left(\int_0^1 tW_1(t)M_k(t)dt\right)^2\right]$$
$$= \mathbb{E}\left[\left(\int_0^1 tW_1(t)M_k(t)dt\right)^2\right] \qquad (\text{ by using the fact } \mathbb{E}\left[W_2^2(1)\right] = 1)$$

Using (A.25) to obtain

$$\mathbf{e}[2] = \mathbb{E}\left[\left(\Big(M_{k+1}(1) - M_{k+2}(1)\Big)W_1(1) + \int_0^1 M_{k+2}(t)dW_1(t) - \int_0^1 tM_{k+1}dW_1(t)\right)^2\right]$$
$$= \Big(M_{k+1}(1) - M_{k+2}(1)\Big)^2\mathbb{E}\left[W_1^2(1)\right] + \mathbb{E}\left[\Big(\int_0^1 M_{k+2}(t)dW_1(t)\Big)^2\right]$$
$$+ \mathbb{E}\left[\Big(\int_0^1 tM_{k+1}(t)dW_1(t)\Big)^2\right] + 2\Big(M_{k+1}(1) - M_{k+2}(1)\Big)\mathbb{E}\left[W_1(1)\int_0^1 M_{k+2}(t)dW_1(t)\right]$$
$$- 2\Big(M_{k+1}(1) - M_{k+2}(1)\Big)\mathbb{E}\left[W_1(1)\int_0^1 tM_{k+1}(t)dW_1(t)\right]$$
$$- 2\mathbb{E}\left[\int_0^1 M_{k+2}(t)dW_1(t)\int_0^1 tM_{k+1}(t)dW_1(t)\right] \qquad \text{(A.62)}$$

Using the fact that $\mathbb{E}[W_1^2(1)] = 1$ and substituting $W_1(1) = \int_0^1 dW_1(t)$ and then

applying Ito isometry gives us

$$\mathbf{e}[2] = \Big(M_{k+1}(1) - M_{k+2}(1)\Big)^2 + \int_0^1 M_{k+2}^2(t)dt + \int_0^1 t^2 M_{k+1}^2(t)dt - 2\int_0^1 tM_{k+1}(t)M_{k+2}(t)dt$$
$$+ 2\Big(M_{k+1}(1) - M_{k+2}(1)\Big)\int_0^1 M_{k+2}(t)dt - 2\Big(M_{k+1}(1) - M_{k+2}(1)\Big)\int_0^1 tM_{k+1}(t)dt$$

By employing Lemma A.2.2 and rearranging we have

$$\mathbf{e}[2] = M_{k+1}^2(1) + 3M_{k+2}^2(1) - 4M_{k+1}(1)M_{k+2}(1) + 4M_{k+1}(1)M_{k+3}(1) - 4M_{k+2}(1)M_{k+3}(1)$$
$$- 2\int_0^1 tM_{k+1}(t)M_{k+2}(t)dt + \int_0^1 t^2 M_{k+1}^2(t)dt + \int_0^1 M_{k+2}^2(t)dt \qquad \text{(A.63)}$$

The third expectation, $\mathbf{e}[3]$, in (A.60) is

$$\mathbf{e}[3] = \mathbf{e}[2]$$
$$= M_{k+1}^2(1) + 3M_{k+2}^2(1) - 4M_{k+1}(1)M_{k+2}(1) + 4M_{k+1}(1)M_{k+3}(1) - 4M_{k+2}(1)M_{k+3}(1)$$
$$- 2\int_0^1 tM_{k+1}(t)M_{k+2}(t)dt + \int_0^1 t^2 M_{k+1}^2(t)dt + \int_0^1 M_{k+2}^2(t)dt \qquad \text{(A.64)}$$

The fourth expectation, $\mathbf{e}[4]$, in (A.60) is simply calculated by using the independence of W_1 and W_2 and then substituting the fact that $\mathbb{E}\left[W_1^2(1)\right] = \mathbb{E}\left[W_2^2(1)\right] = 1$ as follow

$$\mathbf{e}[4] = \mathbb{E}\left[\left(W_1(1)W_2(1)\int_0^1 t^2 M_k(t)dt\right)^2\right]$$
$$= \mathbb{E}\left[W_1^2(1)\right]\left[W_2^2(1)\right]\left(\int_0^1 t^2 M_k(t)dt\right)^2 = \left(\int_0^1 t^2 M_k(t)dt\right)^2$$

By using Lemma A.2.2, we obtain

$$\mathbf{e}[4] = \Big(M_{k+1}(1) - 2M_{k+2}(1) + 2M_{k+3}(1)\Big)^2 \qquad \text{(A.65)}$$

In order to calculate the fifth expectation term, $\mathbf{e}[5]$, in equation (A.60), we use a generalised form of Lemma 3.3.4 by replacing the notation $\mu(t)$ by $M_k(t)$, that is, we substitute

$$\int_0^1 W_1(t)W_2(t)M_k(t)dt = \int_0^1 W_3^2(t)M_k(t)dt - \frac{1}{2}\int_0^1 W_1^2(t)M_k(t)dt - \frac{1}{2}\int_0^1 W_2^2(t)M_k(t)dt. \tag{A.66}$$

where W_1 and W_2 are independent and $W_3(t) = \frac{W_1(t)+W_2(t)}{\sqrt{2}}$, the correlation coefficient of W_3 and W_i for $i \in \{1,2\}$ is $\rho_{(3,1)} = \rho_{(3,2)} = \frac{1}{\sqrt{2}}$, therefore

$$\begin{aligned}
\mathbf{e}[5] &= \mathbb{E}\left[W_2(1)\int_0^1 W_1(t)W_2(t)M_k(t)dt \int_0^1 tW_1(t)M_k(t)dt\right] \\
&= \mathbb{E}\left[W_2(1)\int_0^1 W_3^2(t)M_k(t)dt \int_0^1 tW_1(t)M_k(t)dt\right] \\
&- \frac{1}{2}\mathbb{E}\left[W_2(1)\int_0^1 W_1^2(t)M_k(t)dt \int_0^1 tW_1(t)M_k(t)dt\right] \\
&- \frac{1}{2}\mathbb{E}\left[W_2(1)\int_0^1 W_2^2(t)M_k(t)dt \int_0^1 tW_1(t)M_k(t)dt\right]
\end{aligned}$$

The last two terms are zero due to the independence of W_1 and W_2 and by using Fubini's theorem and the fact that $\mathbb{E}[W_2(t)] = \mathbb{E}[W_2(t)] = 0$. Thus

$$\mathbf{e}[5] = \mathbb{E}\left[W_2(1)\int_0^1 W_3^2(t)M_k(t)dt \int_0^1 tW_1(t)M_k(t)dt\right]$$

By substituting (A.25) , we have

$$\begin{aligned}
\mathbf{e}[5] =& \big(M_{k+1}(1) - M_{k+2}(1)\big)\,\mathbb{E}\left[W_1(1)W_2(1)\int_0^1 W_3^2(t)M_k(t)dt\right] \\
&- \mathbb{E}\left[W_2(1)\int_0^1 tM_{k+1}(t)dW_1(t)\int_0^1 W_3^2(t)M_k(t)dt\right] \\
&+ \mathbb{E}\left[W_2(1)\int_0^1 M_{k+2}(t)dW_1(t)\int_0^1 W_3^2(t)M_k(t)dt\right]
\end{aligned} \tag{A.67}$$

Let $\mathbf{e}[5,k]$ refer to the kth expectation in the right hand side of equation (A.67). By using a modified version of lemma 3.3.2 by replacing $\mu(t)$ with $M_k(t)$, that is, we substitute

$$\int_0^1 W_3^2(t)M_k(t)dt = M_{k+1}(1)W_3^2(1) - 2\int_0^1 M_{k+1}(t)W_3(t)dW_3(t) - \int_0^1 M_{k+1}(t)dt, \tag{A.68}$$

in the first expectation in (A.67) to obtain

$$\begin{aligned}\mathbf{e}[5,1] = \mathbb{E}\left[W_1(1)W_2(1)\int_0^1 W_3^2(t)M_k(t)dt\right] =& M_{k+1}(1)\mathbb{E}\left[W_1(1)W_2(1)W_3^2(1)\right] \\ &- 2\mathbb{E}\left[W_1(1)W_2(1)\int_0^1 M_{k+1}(t)W_3(t)dW_3(t)\right] \\ &- \mathbb{E}\left[W_1(1)W_2(1)\right]\int_0^1 M_{k+1}(t)dt.\end{aligned}$$

By substituting $W_3(t) = \frac{W_1(t)+W_2(t)}{\sqrt{2}}$ in the first term in the right hand side and by using the independence of W_1 and W_2 we have

$$\begin{aligned}\mathbf{e}[5,1] = \mathbb{E}\left[W_1(1)W_2(1)\int_0^1 W_3^2(t)M_k(t)dt\right] =& \frac{1}{2}M_{k+1}(1)\mathbb{E}[W_1^3(1)]\mathbb{E}[W_2(1)] \\ &+ \frac{1}{2}M_{k+1}(1)\mathbb{E}[W_1(1)]\mathbb{E}[W_2^3(1)] \\ &+ M_{k+1}(1)\mathbb{E}[W_1^2(1)]\mathbb{E}[W_2^2(1)] \\ &- 2\mathbb{E}\left[W_1(1)W_2(1)\int_0^1 M_{k+1}(t)W_3(t)dW_3(t)\right] \\ &- \mathbb{E}\left[W_1(1)\right]\left[W_2(1)\right]\int_0^1 M_{k+1}(t)dt.\end{aligned}$$

Since $\mathbb{E}[W(1)] = 0$ and $\mathbb{E}[W^2(1)] = 1$, then

$$\mathbf{e}[5,1] = M_{k+1}(1) - 2\mathbb{E}\left[W_1(1)W_2(1)\int_0^1 M_{k+1}(t)W_3(t)dW_3(t)\right]$$

Substituting $W(1) = \int_0^1 dW(t)$ and then using Lemma A.2.1 yield

$$\mathbf{e}[5,1] = \mathbb{E}\left[W_1(1)W_2(1)\int_0^1 W_3^2(t)M_k(t)dt\right] = M_{k+1}(1) - 2\int_0^1 tM_{k+1}(t)dt \tag{A.69}$$

The second expectation , $\mathbf{e}[5,2]$, in equation (A.67) is calculated by substituting equation (A.68) to obtain

$$\begin{aligned}\mathbf{e}[5,2] = & M_{k+1}(1)\mathbb{E}\left[W_2(1)W_3^2(1)\int_0^1 tM_{k+1}(t)dW_1(t)\right] \\ & - 2\mathbb{E}\left[W_2(1)\int_0^1 tM_{k+1}(t)dW_1(t)\int_0^1 M_{k+1}(t)W_3(t)dW_3(t)\right] \\ & - \mathbb{E}\left[W_2(1)\int_0^1 tM_{k+1}(t)dW_1(t)\right]\int_0^1 M_{k+1}(t)dt.\end{aligned}$$

By substituting $W_3(t) = \frac{W_1(t)+W_2(t)}{\sqrt{2}}$ in the first term and then use the independence of W_1 and W_2 we have

$$\begin{aligned}\mathbf{e}[5,2] = & \frac{1}{2}M_{k+1}(1)\mathbb{E}\left[W_2(1)\right]\mathbb{E}\left[W_1^2(1)\int_0^1 tM_{k+1}(t)dW_1(t)\right] \\ & + \frac{1}{2}M_{k+1}(1)\mathbb{E}\left[W_2^3(1)\right]\mathbb{E}\left[\int_0^1 tM_{k+1}(t)dW_1(t)\right] \\ & + M_{k+1}(1)\mathbb{E}\left[W_2^2(1)\right]\mathbb{E}\left[W_1(1)\int_0^1 tM_{k+1}(t)dW_1(t)\right] \\ & - 2\mathbb{E}\left[W_2(1)\int_0^1 tM_{k+1}(t)dW_1(t)\int_0^1 M_{k+1}(t)W_3(t)dW_3(t)\right] \\ & - \mathbb{E}\left[W_2(1)\right]\mathbb{E}\left[\int_0^1 tM_{k+1}(t)dW_1(t)\right]\int_0^1 M_{k+1}(t)dt.\end{aligned}$$

Due to the facts $\mathbb{E}\left[W_2(1)\right] = \mathbb{E}\left[W_2^3(1)\right] = 0$, and $\mathbb{E}\left[W_2^2(1)\right] = 1$ we have

$$\begin{aligned}\mathbf{e}[5,2] = & + M_{k+1}(1)\mathbb{E}\left[W_1(1)\int_0^1 tM_{k+1}(t)dW_1(t)\right] \\ & - 2\mathbb{E}\left[W_2(1)\int_0^1 tM_{k+1}(t)dW_1(t)\int_0^1 M_{k+1}(t)W_3(t)dW_3(t)\right].\end{aligned}$$

By substituting $W_1(1) = \int_0^1 dW_1(t)$ and $W_2(1) = \int_0^1 dW_2(t)$, we have

$$\begin{aligned}\mathbf{e}[5,2] = & M_{k+1}(1)\mathbb{E}\left[\int_0^1 dW_1(t)\int_0^1 tM_{k+1}(t)dW_1(t)\right] \\ & - 2\mathbb{E}\left[\int_0^1 dW_2(t)\int_0^1 tM_{k+1}(t)dW_1(t)\int_0^1 M_{k+1}(t)W_3(t)dW_3(t)\right].\end{aligned} \tag{A.70}$$

Let $\mathbf{e}[5,2,k]$ refer to the kth expectation in the right hand side of equation (A.70).

The expectation $\mathbf{e}[5,2,1]$ is calculated by applying Ito isometry as follow

$$\begin{aligned}\mathbf{e}[5,2,1] = \mathbb{E}\left[\int_0^1 dW_1(t)\int_0^1 tM_{k+1}(t)dW_1(t)\right] &= \mathbb{E}\left[\int_0^1 tM_{k+1}(t)dt\right] \\ &= \int_0^1 tM_{k+1}(t)dt.\end{aligned} \tag{A.71}$$

By applying Lemma A.2.1, the second expectation $\mathbf{e}[5,2,2]$ in (A.70) becomes

$$\begin{aligned}\mathbf{e}[5,2,2] = &\mathbb{E}\left[\int_0^1\int_0^t sM_{k+1}(s)dW_1(s)dW_2(t)\int_0^1 M_{k+1}(t)W_3(t)dW_3(t)\right] \\ &+\mathbb{E}\left[\int_0^1 tM_{k+1}(t)\int_0^t dW_2(s)dW_1(t)\int_0^1 M_{k+1}(t)W_3(t)dW_3(t)\right] \\ &+\mathbb{E}\left[\int_0^1 tM_{k+1}(t)\rho_{(1,2)}dt\int_0^1 M_{k+1}(t)W_3(t)dW_3(t)\right]\end{aligned}$$

Applying Ito isometry and then Fubini's theorem give us

$$\begin{aligned}\mathbf{e}[5,2,2] = &\int_0^1 M_{k+1}(t)\mathbb{E}\left[W_3(t)\int_0^t sM_{k+1}(s)dW_1(s)\right]\rho_{(2,3)}dt \\ &+\int_0^1 tM^2(t)\mathbb{E}\left[W_3(t)\int_0^t dW_2(s)\right]\rho_{(1,3)}dt \\ &+0 \qquad (\text{ by the independence of } W_1(t) \text{ and } W_2(t))\end{aligned}$$

By substituting $W_3(t) = \int_0^t dW_3(s)$ and applying Ito isometry again we have

$$\begin{aligned}\mathbf{e}[5,2,2] = &\int_0^1 M_{k+1}(t)\mathbb{E}\left[\int_0^t sM_{k+1}(s)\rho_{(1,3)}ds\right]\rho_{(2,3)}dt \\ &+\int_0^1 tM_{k+1}^2(t)\mathbb{E}\left[\int_0^t \rho_{(2,3)}ds\right]\rho_{(1,3)}dt\end{aligned}$$

By knowing that $\rho_{(1,3)} = \rho_{(2,3)} = \frac{1}{\sqrt{2}}$ then

$$\mathbf{e}[5,2,2] = \frac{1}{2}\int_0^1 M_{k+1}(t)\int_0^t sM_{k+1}(s)dsdt + \frac{1}{2}\int_0^1 t^2M_{k+1}^2(t)dt \tag{A.72}$$

By substituting (A.71) and (A.72) in (A.70) we have

$$\begin{aligned}\mathbf{e}[5,2] &= \mathbb{E}\left[W_2(1)\int_0^1 tM_{k+1}(t)dW_1(t)\int_0^1 W_3^2(t)M_k(t)dt\right] \\ &= M_{k+1}(1)\int_0^1 tM_{k+1}(t)dt - \int_0^1 M_{k+1}(t)\int_0^t sM_{k+1}(s)dsdt - \int_0^1 t^2M_{k+1}^2(t)dt.\end{aligned} \tag{A.73}$$

The third expectation, $\mathbf{e}[5,3]$, in equation (A.67) calculated in similar way as $\mathbf{e}[5,2]$ and we have

$$\begin{aligned}\mathbf{e}[5,3] &= \mathbb{E}\left[W_2(1)\int_0^1 M_{k+2}(t)dW_1(t)\int_0^1 W_3^2(t)M_k(t)dt\right] \\ &= M_{k+1}(1)\int_0^1 M_{k+2}(t)dt - \int_0^1 M_{k+1}(t)\int_0^t M_{k+2}(s)dsdt \\ &\quad - \int_0^1 tM_{k+1}(t)M_{k+2}(t)dt.\end{aligned} \tag{A.74}$$

By substituting $\mathbf{e}[5,1]$, $\mathbf{e}[5,2]$ and $\mathbf{e}[5,3]$ in equation (A.67) we have

$$\begin{aligned}\mathbf{e}[5] =& \mathbb{E}\left[W_2(1)\int_0^1 W_1(t)W_2(t)M_k(t)dt\int_0^1 tW_1(t)M_k(t)dt\right] \\ =& M^2(1) - M_{k+2}(1)M_{k+1}(1) - 3M_{k+1}(1)\int_0^1 tM_{k+1}(t)dt + 2M_{k+2}(1)\int_0^1 tM_{k+1}(t)dt \\ &+ \int_0^1 M_{k+1}(t)\int_0^t sM_{k+1}(s)dsdt + \int_0^1 t^2M^2(t)dt + M_{k+1}(1)\int_0^1 M_{k+2}(t)dt \\ &- \int_0^1 M_{k+1}(t)\int_0^t M_{k+2}(s)dsdt - \int_0^1 tM_{k+1}(t)M_{k+2}(t)dt.\end{aligned}$$

We employ Lemma A.2.2 and rearrange to obtain

$$\begin{aligned}\mathbf{e}[5] &= M_{k+1}^2(1) + 2M_{k+2}^2(1) - 4M_{k+1}(1)M_{k+2}(1) + 4M_{k+1}(1)M_{k+3}(1) - 2M_{k+2}(1)M_{k+3}(1) \\ &\quad + \int_0^1 M_{k+1}(t)\int_0^t sM_{k+1}(s)dsdt - \int_0^1 M_{k+1}(t)\int_0^t M_{k+2}(s)dsdt \\ &\quad + \int_0^1 t^2M_{k+1}^2(t)dt - \int_0^1 tM_{k+1}(t)M_{k+2}(t)dt.\end{aligned} \tag{A.75}$$

It is clear that $\mathbf{e}[6] = \mathbf{e}[5]$, that is

$$\begin{aligned}\mathbf{e}[6] = & M_{k+1}^2(1) + 2M_{k+2}^2(1) - 4M_{k+1}(1)M_{k+2}(1) + 4M_{k+1}(1)M_{k+3}(1) - 2M_{k+2}(1)M_{k+3}(1) \\ & + \int_0^1 M_{k+1}(t) \int_0^t sM_{k+1}(s)dsdt - \int_0^1 M_{k+1}(t) \int_0^t M_{k+2}(s)dsdt \\ & + \int_0^1 t^2 M_{k+1}^2(t)dt - \int_0^1 tM_{k+1}(t)M_{k+2}(t)dt. \end{aligned} \tag{A.76}$$

The seventh expectation term, $\mathbf{e}[7]$, in equation (A.60), calculated by using the independence of W_1 and W_2, and substituting equation (A.66) to obtain

$$\begin{aligned}\mathbf{e}[7] &= \mathbb{E}\left[W_1(1)W_2(1)\int_0^1 W_1(t)W_2(t)M_k(t)dt\right] \\ &= \mathbb{E}\left[W_1(1)W_2(1)\int_0^1 W_3^2(t)\mu(t)dt\right] \\ &\quad - \frac{1}{2}\mathbb{E}\left[W_1(1)\int_0^1 W_1^2(t)\mu(t)dt\right]\mathbb{E}\left[W_2(1)\right] \\ &\quad - \frac{1}{2}\mathbb{E}\left[W_1(1)\right]\mathbb{E}\left[W_2(1)\int_0^1 W_2^2(t)\mu(t)dt\right]\end{aligned}$$

Since $\mathbb{E}\left[W_1(1)\right] = \mathbb{E}\left[W_1(1)\right] = 0$, then the last two term is zero, therefore,

$$\begin{aligned}\mathbf{e}[7] =& \mathbb{E}\left[W_1(1)W_2(1)\int_0^1 W_3^2(t)\mu(t)dt\right] = \mathbf{e}[5,1] \\ &= M_{k+1}(1) - 2\int_0^1 tM_{k+1}(t)dt. \qquad (\text{ from equation (A.69)}) \\ &= M_{k+1}(1) - 2M_{k+2}(1) + 2M_{k+3}(1) \quad (\text{ by Lemma A.2.2 })\end{aligned} \tag{A.77}$$

By using the independence of W_1 and W_2, the eighth expectation, $\mathbf{e}[8]$, can be written as

$$\mathbf{e}[8] = \mathbb{E}\left[W_1(1)\int_0^1 tW_1(t)M_k(t)dt\right]\mathbb{E}\left[W_2(1)\int_0^1 tW_2(t)M_k(t)dt\right] \tag{A.78}$$

By using (A.32) we have

$$\mathbf{e}[8] = \Big(M_{k+1}(1) - 2M_{k+2}(1) + 2M_{k+3}(1)\Big)^2. \tag{A.79}$$

The ninth expectation, $\mathbf{e}[9]$, in equation (A.60) is calculated as follow

$$\begin{aligned}
\mathbf{e}[9] &= \mathbb{E}\left[W_1(1)W_2^2(1)\int_0^1 tW_1(t)M_k(t)dt\right] \\
&= \mathbb{E}[W_2^2(1)]\mathbb{E}\left[W_1(1)\int_0^1 tW_1(t)M_k(t)dt\right] \quad (\text{ by the independence of } W_1 \text{ and } W_2) \\
&= \mathbb{E}\left[W_1(1)\int_0^1 tW_1(t)M_k(t)dt\right] \quad (\text{ by using the fact that } \mathbb{E}[W_2^2(1)] = 1) \\
&= M_{k+1}(1) - 2M_{k+2}(1) + 2M_{k+3}(1). \quad (\text{ from equation (A.32)})
\end{aligned} \tag{A.80}$$

The tenth expectation, $\mathbf{e}[10]$, in equation (A.60) is

$$\begin{aligned}
\mathbf{e}[10] &= \mathbb{E}\left[W_1^2(1)W_2(1)\int_0^1 tW_2(t)M_k(t)dt\right] = \mathbf{e}[9] \\
&= M_{k+1}(1) - 2M_{k+2}(1) + 2M_{k+3}(1) \quad (\text{ from equation (A.80)})
\end{aligned} \tag{A.81}$$

By substituting $\mathbf{e}[k]$ for $k \in \{1, 2, ..., 10\}$ in equation (A.60) we obtain the result in (A.59). □

Proof. Theorem 4.3.1 is proved in similar way as Theorem 3.3.1. From (3.47) recall that

$$\text{ego-}A_2 = 1 - 4\frac{\mathbb{E}[T_{11}T_{22}] - \mathbb{E}[T_{12}^2]}{\mathbb{E}[T_{11}^2] + 2\mathbb{E}[T_{11}T_{22}] + \mathbb{E}[T_{22}^2]}. \tag{A.82}$$

For high memory formation rate (as $c \to \infty$) and by applying A.1.4 , we can approximate the elements of T in equation (4.2) as follow

$$T_{11} = \frac{1}{2 + |S|}\sum_{t\in S} X^2(t) = \int_0^1 X^2(t)M_k(t)\,dt,$$

$$T_{22} = \frac{1}{2+|S|}\sum_{t\in S} Y^2(t) = \int_0^1 Y^2(t)M_k(t)\,dt,$$

$$T_{12} = \frac{1}{2+|S|}\sum_{t\in S} X(t)Y(t) = \int_0^1 X(t)Y(t)M_k(t)\,dt.$$

The first expectation term in the numerator of equation (A.82) is

$$\begin{aligned}\mathbb{E}\left[T_{11}T_{22}\right] =& \mathbb{E}\left[\int_0^1 X^2(t)M_k(t)\,dt \int_0^1 Y^2(t)M_k(t)\,dt\right] \\ =& \mathbb{E}\left[\int_0^1 X^2(t)M_k(t)\,dt\right]\mathbb{E}\left[\int_0^1 Y^2(t)M_k(t)\,dt\right] \text{ (by the independence of } X(t) \text{ and } Y(t)) \\ =& \left(M_{k+2}(1) - 2M_{k+3}(1)\right)^2 \qquad \text{(by equation (A.31))} \qquad (A.83)\end{aligned}$$

By applying Lemma A.2.7 the remaining expectation term in the numerator of (A.82) is

$$\begin{aligned}\mathbb{E}[T_{12}^2] = \mathbb{E}\left[\left(\int_0^1 X(t)Y(t)M_k(t)\,dt\right)^2\right] =& 2M_{k+2}^2(1) + 4M_{k+3}^2(1) - 8M_{k+2}(1)M_{k+3}(1) \\ & - 4\int_0^1 tM_{k+1}(t)M_{k+2}(t)dt + 8\int_0^1 M_{k+1}(t)M_{k+3}(t)dt \\ & + 2\int_0^1 tM_{k+1}^2(t)dt - 2\int_0^1 t^2M_{k+1}^2(t)dt \\ & + 2\int_0^1 M_{k+2}^2(t)dt. \qquad (A.84)\end{aligned}$$

The first expectation term in the denominator of (A.82) is obtained by applying Lemma A.2.6 as follow

$$\begin{aligned}\mathbb{E}\left[T_{11}^2\right] =& \mathbb{E}\left[\left(\int_0^1 X(t)^2 M_k(t)\,dt\right)^2\right] \\ &= -3M_{k+2}^2(1) + 12M_{k+2}(1)M_{k+3}(1) - 20M_{k+3}^2(1) \\ &\quad + 8\int_0^1 (1-2t)M_{k+1}(t)\big(2M_{k+3}(t) - tM_{k+2}(t)\big)dt \\ &\quad + 4\int_0^1 M_{k+2}(t)\big((1-4t)M_{k+2}(t) + 8M_{k+3}(t)\big)dt \\ &\quad + 4\int_0^1 (1-t)tM_{k+1}^2(t)dt, \end{aligned} \tag{A.85}$$

Clearly,

$$\begin{aligned}\mathbb{E}\left[T_{22}^2\right] &= \mathbb{E}\left[\left(\int_0^1 Y(t)^2 M_k(t)\,dt\right)^2\right] \\ &= \mathbb{E}\left[T_{11}^2\right] \end{aligned} \tag{A.86}$$

By substituting the results from equations (A.83)-(A.86) in equation (A.82) when $k = -1$ and simplifying we obtain the result in (4.6). □

Bibliography

[1] E. Rady, W. Hassanein, and T. Elhaddad. The power Lomax distribution with an application to bladder cancer data. *SpringerPlus*, 5, 2016.

[2] G. Oshanin, O. Vasilyev, P. L. Krapivsky, and J. Klafter. Survival of an evasive prey. *Proceedings of the National Academy of Sciences*, 106(33):13696–13701, 2009.

[3] T. L. Wilson et al. Spatial ecology of refuge selection by an herbivore under risk of predation. *Ecosphere*, 3(1):1, 2012.

[4] G. Romanes. Mental evolution in animals. *Nature*.

[5] PH Harvey and JR Krebs. Comparing brains. *Science*, 249(4965):140–146, 1990.

[6] A. DeCasien, S. Williams, and J. Higham. Primate brain size is predicted by diet but not sociality. *Nature Ecology and Evolution*, 1(112), 2017.

[7] K. Janmaat. What animals do not do or fail to find: A novel observational approach for studying cognition in the wild. *Evolutionary Anthropology: Issues, News, and Reviews*, 28(6):303–320, 2019.

[8] P. A. Garber. Role of spatial memory in primate foraging patterns: Saguinus mystax and saguinus fuscicollis. *American Journal of Primatology*, 19(4):203–216, 1989.

[9] C. Janson. Experimental evidence for route integration and strategic planning in wild capuchin monkeys. *Animal Cognition*, 10:341–356, 2007.

[10] Karline R. L. Janmaat, Richard W. Byrne, and Klaus Zuberbuhler. Primates take weather into account when searching for fruits. *CURRENT BIOLOGY*, 16(12):1232–1237, JUN 2006.

[11] E. Normand and C. Boesch. Sophisticated euclidean maps in forest chimpanzees. *Animal Behaviour*, 77(05):1095–1201, 2009.

[12] E. C. Tolman. Cognitive maps in rats and men. *Psychological Review*, 55:189–208, 1948.

[13] J. O'Keefe and L. Nadel. *The Hippocampus as a Cognitive Map*. Oxford: Clarendon Press, 1978.

[14] L. Averell and A. Heathcote. The form of the forgetting curve and the fate of memories. *Journal of Mathematical Psychology*, 55(1):25 – 35, 2011.

[15] BK Briscoe, MA Lewis, and SE Parrish. Home range formation in wolves due to scent marking. *BULLETIN OF MATHEMATICAL BIOLOGY*, 64(2):261–284, MAR 2002.

[16] S. Towers and et al. Quantifying the relative effects of environmental and direct transmission of norovirus. *Royal Society Open Science*, 5(3):170602, 2018.

[17] S. Boone and C. Gerba. Significance of fomites in the spread of respiratory and enteric viral disease. 73(6):1687–1696, 2007.

[18] G. Grimmett and D. Welsh. *Probability: An Introduction*. Oxford University Press, United Kingdom, 2014.

[19] G. F. Lawler. *Introduction to Stochastic Processes*. Chapman and Hall/CRC, United States of America, 2006.

[20] G. R. Grimmett and D. R. Stirzaker. *Probability and Random Processes*. Oxford University Press Inc., New York, 2001.

[21] R. P. Dobrow. *Introduction to Stochastic processes with R.* John Wiley and Sons, Inc., United States of America, 2016.

[22] P. L. Krapivsky and S Redner. Kinetics of a diffusive capture process: Lamb besieged by a pride of lions. *Journal of Physics A: Mathematical and General*, 29(17):5347–5357, 1996.

[23] S Redner and P. L. Krapivsky. Capture of the lamb: Diffusing predators seeking a diffusing prey. *American Journal of Physics*, 67(12):1277–1283, 1999.

[24] C. Pu, S. Li, and J. Yang. Epidemic spreading driven by biased random walks. *Physica A: Statistical Mechanics and its Applications*, 432:230–239, 2015.

[25] M. Draief and A. Ganesh. A random walk model for infection on graphs: spread of epidemics and rumours with mobile agents. *Discrete Event Dynamic Systems-Theory and Applications*, 21(1, SI):41–61, 2011.

[26] M. et al. Auger-Methe. Evaluating random search strategies in three mammals from distinct feeding guilds. *Journal of Animal Ecology*, 85(5):1411–1421, 2016.

[27] N. Privault. *Understanding Markov chains.* Springer, Singapore, 2018.

[28] O. Calin. *An Informal Introduction To Stochastic Calculus With Applications.* World Scientific Publishing Co. Pte. Ltd., United States of America, 2015.

[29] O. Ibe. *Markov Processes for Stochastic Modeling.* Elsevier, United States of America, 2013.

[30] Kiyosi ITO. 109. stochastic integral. *Proceedings of the Imperial Academy*, 20(8):519–524, 1944.

[31] Kiyosi ITO. On a stochastic integral equation. *Proceedings of the Japan Academy*, 22(1-4):32–35, 1946.

[32] C. Mungan. A classic chase problem solved from a physics perspective. *European Journal of Physics*, 26(6):985–990, aug 2005.

[33] R. Escobedo, C. Muro, L. Spector, and R. P. Coppinger. Group size, individual role differentiation and effectiveness of cooperation in a homogeneous group of hunters. *Journal of The Royal Society Interface*, 11(95):20140204, 2014.

[34] M. Schwarzl. A single predator charging a herd of prey: effects of self volume and predator–prey decision-making. *Journal of Physics A: Mathematical and Theoretical*, 49(22):225601, 2016.

[35] A. Kamimura and T. Ohira. Group chase and escape. *New Journal of Physics*, 12(5):053013, 2010.

[36] H. Wang, W. Han, and J. Yang. Group chase and escape with sight-limited chasers. *Physica A: Statistical Mechanics and its Applications*, 465:34 – 39, 2017.

[37] J. Šćepanović et al. Group chase and escape in the presence of obstacles. *Physica A: Statistical Mechanics and its Applications*, 525:450 – 465, 2019.

[38] A Sih, G Englund, and D Wooster. Emergent impacts of multiple predators on prey. *Trends in Ecology and Evolution*, 13(9):350 – 355, 1998.

[39] P. Nahinh. *Chases and escapes: the mathematics of pursuit and evasion*. Princeton University Press, Princeton, 2007.

[40] D. Weihs and P.W. Webb. Optimal avoidance and evasion tactics in predator-prey interactions. *Journal of Theoretical Biology*, 106(2):189 – 206, 1984.

[41] A. Nair, C. Nguyen, and M. McHenry. A faster escape does not enhance survival in zebrafish larvae. *Proceedings of the Royal Society B: Biological Sciences*, 284(1852):20170359, 2017.

[42] S. Gal and J. Casas. Succession of hide-seek and pursuit-evasion at heterogeneous locations. *Journal of the royal society interface*, 11(94), 2014.

[43] M. Broom and G. Ruxton. You can run—or you can hide: optimal strategies for cryptic prey against pursuit predators. *Behavioral Ecology*, 16(3):534–540, 2005.

[44] S. Zhang, M. Liu, X. Lei, and Y. Huang. Stay-eat or run-away: Two alternative escape behaviors. *Physics letters A*, 383(7):593–599, 2019.

[45] D. Humphries and P. Driver. Protean defence by prey animals. *Oecologia*, 5(4):285–302, Dec 1970.

[46] H. C. Howland. Optimal strategies for predator avoidance: The relative importance of speed and manoeuvrability. *Journal of Theoretical Biology*, 47(2):333 – 350, 1974.

[47] T Liesenjohann and J Eccard. Foraging under uniform risk from different types of predators. *BMC Ecology*, 19(8), 2008.

[48] A. Gabel, S. Majumdar, N. Panduranga, and S. Redner. Can a lamb reach a haven before being eaten by diffusing lions? *Journal of statistical mechanics-theory and experiment*, 2012.

[49] C. T. Kelley. *Iterative Methods for Optimization*. Society for Industrial and Applied Mathematics, 1999.

[50] R. Dukas. Costs of memory: Ideas and predictions. *Journal of Theoretical Biology*, 197(1):41–50, 1999.

[51] L. Guo and et al. Influence maximization in trajectory databases. *IEEE Transactions on Knowledge and Data Engineering*, 29(3):627–641, March 2017.

[52] Y. Li, J. Bao, Y. Li, Y. Wu, Z. Gong, and Y. Zheng. Mining the most influential k -location set from massive trajectories. *IEEE Transactions on Big Data*, 4(4):556–570, Dec 2018.

[53] S. Mitra, P. Saraf, and A. Bhattacharya. Tips: Mining top-k locations to minimize user-inconvenience for trajectory-aware services. *IEEE Transactions on Knowledge and Data Engineering*, pages 1–1, 2019.

[54] Zhixin Qi and et al. TAILOR: time-aware facility location recommendation based on massive trajectories. *KNOWLEDGE AND INFORMATION SYSTEMS*.

[55] P. M. Kareiva and N. Shigesada. Analyzing insect movement as a correlated random walk. *Oecologia*, 56(2):234–238, Feb 1983.

[56] W. et al. Fagan. Spatial memory and animal movement. *Ecology Letters*, 16(10):1316–1329, 2013.

[57] W. F. Fagan and J. M. Calabrese. The correlated random walk and the rise of movement ecology. *The Bulletin of the Ecological Society of America*, 95(3):204–206, 2014.

[58] P. Turchin. *Quantitative Analysis of Movement*. Sinauer Associates, United States of America, 1998.

[59] E. A. Codling, M. J. Plank, and S. Benhamou. Random walk models in biology. *Journal of The Royal Society Interface*, 5(25):813–834, 2008.

[60] S. et al. Collins. New opportunities in ecological sensing using wireless sensor networks. *Frontiers in Ecology and the Environment*, 4(8):402–407, 2006.

[61] E. P. et al. Raposo. Dynamical robustness of lévy search strategies. *Phys. Rev. Lett.*, 91:240601, 2003.

[62] A. James, M. J. Plank, and A. M. Edwards. Assessing lévy walks as models of animal foraging. *Journal of The Royal Society Interface*, 8(62):1233–1247, 2011.

[63] G.M.Viswanathan, E. P. Raposo, and M. G. da Luz. Lévy flights and superdiffusion in the context of biological encounters and random searches. *Physics of Life Reviews*, 5:133–150, 2008.

[64] G.M.Viswanathan et al. Optimizing the success of random searches. *Nature*, 401:911–914, 1999.

[65] N. E. Humphries et al. Environmental context explains lévy and brownian movement patterns of marine predators. *Nature*, 465:1066–1069, 2010.

[66] F. B. Gill. Trapline foraging by hermit hummingbirds: competition for an undefended, renewable resource. *Ecology*, 69(6):1933–1942, 1988.

[67] J. D. Thomson. Trapline foraging by bumblebees: I. Persistence of flight-path geometry. *Behavioral Ecology*, 7(2):158–164, 1996.

[68] K. Ohashi and J. D. Thomson. Efficient harvesting of renewing resources. *Behavioral Ecology*, 16(3):592–605, 2005.

[69] D. Boyer and C. Solis-Salas. Random walks with preferential relocations to places visited in the past and their application to biology. *Phys. Rev. Lett.*, 112:240601, 2014.

[70] D. Boyer, M. C. Crofoot, and P. D. Walsh. Non-random walks in monkeys and humans. *Journal of The Royal Society Interface*, 9(70):842–847, 2012.

[71] T. C. Roth, N. C. Rattenborg, and V. V. Pravosudov. The ecological relevance of sleep: the trade-off between sleep, memory and energy conservation. *Philosophical Transactions of the Royal Society B: Biological Sciences*, 365(1542):945–959, 2010.

[72] T. Avgar, A. Mosser, G. S. Brown, and J. M. Fryxell. Environmental and individual drivers of animal movement patterns across a wide geographical gradient. *Journal of Animal Ecology*, 82(1):96–106, 2013.

[73] J. Rudnick and G. Gaspari. The asphericity of random walks. *Journal of Physics A: Mathematical and General*, 19(4):L191–L193, 1986.

[74] G. Claussen, A. K. Hartmann, and S. N. Majumdar. Convex hulls of random walks: Large-deviation properties. *Phys. Rev. E*, 91:052104, 2015.

[75] D. S. Grebenkov, Y. Lanoiselée, and S. .N Majumdar. Mean perimeter and mean area of the convex hull over planar random walks. *Journal of Statistical Mechanics: Theory and Experiment*, 2017(10):103203, 2017.

[76] D. Zhang and G. Lu. Review of shape representation and description techniques. *Pattern Recognition*, 37(1):1–19, 2004.

[77] N. Ritter and J. Cooper. New resolution independent measures of circularity. *Journal of Mathematical Imaging and Vision*, 35:117–127, 2009.

[78] K. Solc and W. H. Stockmayer. Shape of a random flight chain. *Journal of chemical physics*, 54(6):2756+, 1971.

[79] J. Rudnick and G. Gaspari. *Elements of the Random Walk: An introduction for Advanced Students and Researchers*. Cambridge University Press, Cambridge, 2004.

[80] S J Sciutto. Study of the shape of random walks. *Journal of Physics A: Mathematical and General*, 27(21):7015–7034, nov 1994.

[81] J. M. et al. Morales. Extracting more out of relocation data: building movement models as mixtures of random walks. *Ecology*, 85(9):2436–2445, 2004.

[82] T. A. Patterson et al. State–space models of individual animal movement. *Trends in Ecology and Evolution*, 23(2):87 – 94, 2008.

[83] C. A. Shaffer. Spatial foraging in free ranging bearded sakis: Traveling salesmen or lévy walkers? *American Journal of Primatology*, 76(5):472–484, 2014.

[84] G. M. Viswanathan, M. G. da Luz, E. P. Raposo, and H. E. Stanley. *The Physics of Foraging: An Introduction to Random Searches and Biological Encounters*. Cambridge University Press, Cambridge, 2011.

[85] P. Turchin. Translating foraging movements in heterogeneous environments into the spatial distribution of foragers. *Ecology*, 72(4):1253–1266, 1991.

[86] A. Reynolds. Liberating lévy walk research from the shackles of optimal foraging. *Physics of Life Reviews*, 14:59 – 83, 2015.

[87] M. Andersson. Optimal foraging area: Size and allocation of search effort. *Theoretical Population Biology*, 13(3):397 – 409, 1978.

[88] O. et al. Bénichou. Optimally frugal foraging. *Phys. Rev. E*, 97:022110, 2018.

[89] S. Minta. Tests of spatial and temporal interaction among animals. *Ecological Applications*, 2(2):178–188, 1992.

[90] M. Lewis, K. White, and J. D. Murray. Analysis of a model for wolf territories. *Journal of Mathematical Biology*, 35:749–774, 1997.

[91] J. Potts and M. Lewis. How do animal territories form and change? lessons from 20 years of mechanistic modelling. *Proceedings of the Royal Society B: Biological Sciences*, 281(1784):20140231, 2014.

[92] D. Brockmann, L. Hufnagel, and T. Geisel. The scaling laws of human travel. *Nature*, 439:462–465, 2006.

[93] M. González, C. Hidalgo, and A. Barabási. Understanding individual human mobility patterns. *Nature*, 453:779–782, 2008.

[94] D. Balcan and et al. Multiscale mobility networks and the spatial spreading of infectious diseases. *Proceedings of the National Academy of Sciences*.

[95] J. Burridge. Spatial evolution of human dialects. *Phys. Rev. X*, 7:031008, 2017.

[96] J. Burridge, B. Vaux, M. Gnacik, and Y. Grudeva. Statistical physics of language maps in the usa. *Phys. Rev. E*, 99:032305, 2019.

[97] J. Fort and J. Pérez-Losada. Can a linguistic serial founder effect originating in africa explain the worldwide phonemic cline? *Journal of The Royal Society Interface*, 13(117):20160185, 2016.

[98] Y. Zheng. Trajectory data mining: An overview. *ACM Trans. Intell. Syst. Technol.*, 6(3):20160185, 2015.

[99] R. Gallotti, R. Louf, J. Luck, and M. Barthelemy. Tracking random walks. *Journal of The Royal Society Interface*, 15(139):20170776, 2018.

[100] M. Plank and E. Codling. Sampling rate and misidentification of lévy and non-lévy movement paths. *Ecology*, 90(12):3546–3553, 2009.

[101] G. Mosetti, G. Jug, and E. Scalas. Power laws from randomly sampled continuous-time random walks. *Physica A: Statistical Mechanics and its Applications*, 375(1):233 – 238, 2007.

[102] M. et al. Karsai. Small but slow world: How network topology and burstiness slow down spreading. *Phys. Rev. E*, 83:025102, 2011.

[103] R. Lambiotte, L. Tabourier, and J. Delvenne. Burstiness and spreading on temporal networks. *The European Physical Journal B*, 86(7):320, Jul 2013.

[104] B. Oksendal. *Stochastic Differential Equations: An Introduction with Applications*. Springer, Berlin, 2010.

[105] J. Horne, E. Garton, S. Krone, and J. S. Lewis. Analyzing animal movements using brownian bridges. *Ecology*, 88(9):2354–2363, 2007.

[106] I. Silva and et al. Using dynamic brownian bridge movement models to identify home range size and movement patterns in king cobras. *PLOS ONE*, 13(9):1–20, 2018.

[107] J. Fischer, W. Walter, and M. Avery. Brownian Bridge Movement Models to Characterize Birds' Home Ranges. *The Condor*, 115(2):298–305, 2013.

[108] F. Pedregosa and et al. Scikit-learn: machine learning in python. *Journal of Machine Learning Research,*, 12(0):00, oct 2011.

[109] J. Rudnick, A. Beldjenna, and G. Gaspari. The shapes of high-dimensional random walks. *Journal of Physics A: Mathematical and General*, 20(4):971–984, 1987.

[110] Michał Gnacik, Abdulrahman Alsolami, and James Burridge. The shape of a memorised random walk. *Journal of Statistical Mechanics: Theory and Experiment*, 2018(8):083207, aug 2018.

[111] R. L. Streit. *Poisson Point Processes. Imaging, Tracking, and Sensing.* Springer US, United States of America, 2010.

[112] J. F. Kingman. *Poisson Processes.* Oxford University press, United States of America, 2002.